

Murat Gökçek, Editor



## **Mechanical Engineering**

Edited by Murat Gökçek

#### Published by InTech

Janeza Trdine 9, 51000 Rijeka, Croatia

# Copyright © 2012 InTech

All chapters are Open Access distributed under the Creative Commons Attribution 3.0 license, which allows users to download, copy and build upon published articles even for commercial purposes, as long as the author and publisher are properly credited, which ensures maximum dissemination and a wider impact of our publications. After this work has been published by InTech, authors have the right to republish it, in whole or part, in any publication of which they are the author, and to make other personal use of the work. Any republication, referencing or personal use of the work must explicitly identify the original source.

As for readers, this license allows users to download, copy and build upon published chapters even for commercial purposes, as long as the author and publisher are properly credited, which ensures maximum dissemination and a wider impact of our publications.

#### Notice

Statements and opinions expressed in the chapters are these of the individual contributors and not necessarily those of the editors or publisher. No responsibility is accepted for the accuracy of information contained in the published chapters. The publisher assumes no responsibility for any damage or injury to persons or property arising out of the use of any materials, instructions, methods or ideas contained in the book.

Publishing Process Manager Danijela Duric Technical Editor Teodora Smiljanic Cover Designer InTech Design Team

First published April, 2012 Printed in Croatia

A free online edition of this book is available at www.intechopen.com Additional hard copies can be obtained from orders@intechopen.com

Mechanical Engineering, Edited by Murat Gökçek p. cm. ISBN 978-953-51-0505-3

# Part 1

# **Power Transmission Systems**

# **Mechanical Transmissions Parameter Modelling**

Isad Saric, Nedzad Repcic and Adil Muminovic University of Sarajevo, Faculty of Mechanical Engineering, Department of Mechanical Design, Bosnia and Herzegovina

#### 1. Introduction

In mechanical technique, transmission means appliance which is used as intermediary mechanism between driving machine (e.g. of engine) and working (consumed) machine. The role of transmission is transmitting of mechanical energy from main shaft of driving machine to main shaft of working machine. The selection of transmission is limited by the price of complete appliance, by working environment, by dimensions of the appliance, technical regulations, etc. In mechanical engineering, so as in technique generally, mechanical transmissions are broadly used. Mechanical transmissions are mechanisms which are used for mechanical energy transmitting with the change of angle speed and appropriate change of forces and rotary torques. According to the type of transmitting, mechanical transmissions could be divided into: transmissions gear (sprocket pair), belt transmissions (belt pulleys and belt), friction transmissions (friction wheels) and chain transmissions (chain pulleys and chain). (Repcic & Muminovic, 2007)

In this chapter, the results of the research of three-dimensional (3D) geometric parameter modelling of the two frequently used types of mechanical transmissions, transmissions gear (different types of standard catalogue gears: spur gears, bevel gears and worms) and belt transmissions (belt pulley with cylindrical external surface, or more exactly, with pulley rim) using CATIA V5 software system (modules: *Sketcher, Part Design, Generative Shape Design, Wireframe and Surface Design* and *Assembly Design*), is shown.

Modelling by computers are based on geometric and perspective transformation which is not more detail examined in the chapter because of their large scope.

It is advisable to make the parameterisation of mechanical transmissions for the purpose of automatization of its designing. Parameter modelling application makes possible the control of created geometry of 3D model through parameters integrated in some relations (formulas, parameter laws, tables and so on). All dimensions, or more precisely, geometric changeable parameter of gear and belt pulley, can be expressed through few characteristic fixed parameters (m, z,  $z_1$ ,  $z_2$  and N for the selected gear; d,  $B_k$ ,  $d_v$  and s for the selected belt pulley). Geometry of 3D mechanical transmission model is changed by changes of these parameters values. Designer could generate more designing solutions by mechanical transmission parameterisation.

Because AutoCAD does not support parameter modelling, and command system, that it has, does not make possible simple realization of changes on finished model, parameter

oriented software systems (CATIA V5, SolidWorks, Mechanical Desktop, and so on) which used analytical expressions for variable connection through parameters are used. CATIA V5 (Computer-Aided Three-dimensional Interactive Application) is the product of the highest technological level and represents standard in the scope of designing (Dassault Systemes, IBM, 2011). Currently, it is the most modern integrated CAD/CAM/CAE software system that can be find on the market for commercial use and scientific-research work. The biggest and well-known world companies and their subcontractors use them. It is the most spread in the car industry (Daimler Chrysler, VW, BMW, Audi, Renault, Peugeot, Citroen, etc.), airplane industry (Airbus, Boeing, etc.), and production of machinery and industry of consumer goods. The system has mathematical models and programs for graphical shapes presentation, however users have no input about this process. As a solution, it is written independently from operative computer system and it provides the possibility for program module structuring and their adaptation to a user. In the "heart" of the system is the integrated associational data structure for parameter modelling, which enables the changes on the model to be reflected through all related phases of the product development. Therefore, time needed for manual models remodelling is saved. The system makes possible all geometric objects parametering, including solids, surfaces, wireframe models and constructive elements. (Karam & Kleismit, 2004; Saric et al., 2010) Whole model, or part of model, can parameterise in the view of providing of more flexibility in the development of new variants designing solutions. Intelligent elements interdependence is given to a part or assembly by parameterising. The main characteristic of parameter modelling in CATIA V5 system is the great flexibility, because of the fact that parameters can be, but do not have to be, defined in any moment. Not only changing of parameter value, but their erasing, adding and reconnecting, too, are always possible. (Karam & Kleismit, 2004) Total Graphical User Interface (GUI) programmed in C++ program is designed like tools palette and icons that can be find in Windows interface. Although it was primarily written for Windows and Windows 64-bit, the system was written for AIX, AIX 64-bit, HP-UX, IRIX and Solaris operative system. To obtain the maximum during the work with CATIA V5 system, optimized certificated hardware configurations are recommended (Certified hardware configurations for CATIA V5 systems, 2011).

Parameter modelling in CATIA V5 system is based on the concept of knowledge, creating and use of parameter modelled parts and assemblies. (Saric et al., 2009) Creating of 3D parameter solid models is the most frequently realized by combining of the approach based on *Features Based Design* – FBD and the approach based on Bool's operations (*Constructive Solid Geometry* – CSG). (Amirouche, 2004; Shigley et al. 2004; Spotts at el., 2004) The most frequent parameter types in modelling are: *Real, Integer, String, Length, Angle, Mass*, etc. They are devided into two types:

- internal parameters which are generated during geometry creating and which define its interior features (depth, distance, activity, etc.) and
- user parameters (with one fixed or complex variables) which user specially created and which define additional information on the: *Assembly Level, Part Level* or *Feature Level*.

So, parameter is a variable we use to control geometry of component, we influence its value through set relations. It is possible to do a control of geometry by use of tools palette *Knowledge* in different ways:

- by creating of user parameters set and by their values changing,
- by use of defined formulas and parameter laws that join parameters,
- by joining of parameters in designed tables and by selection of appropriate configured set.

The recommendation is, before components parameterising, to:

- 1. check the component complexity,
- 2. notice possible ways of component making,
- 3. notice dimensions which are going to change and
- 4. select the best way for component parameterising.

# 2. Mechanical transmissions parameter modelling

Modelling of selected mechanical transmissions was done in *Sketcher*, *Part Design* and *Generative Shape Design* modules of CATIA V5 system. As prerequisite for this way of modelling, it is necessary to know modelling methodology in modules *Wireframe and Surface Design* and *Assembly Design* of CATIA V5 system. (Karam & Kleismit, 2004; Dassault Systemes, 2007a, 2007b; Zamani & Weaver, 2007)

After finished modelling procedure, mechanical transmissions can be independently used in assemblies in complex way.

Parameter marks and conventional formulas (Table 1. and 5.) used in mechanical transmissions modelling can be found in references (Repcic & et al., 1998; Repcic & Muminovic, 2007, pgs. 139, 154-155, 160-161). Clear explanations for transmissions gear and belt transmissions can be found in references (Repcic & et al., 1998, pgs. 54-106, 118-151).

#### 2.1 Transmissions gear parameter modelling

Next paragraph is shows 3D geometric parameter modelling of characteristic standard catalogue gears: spur gears, bevel gears and worms.

Gears were selected as characteristic example, either because of their frequency as mechanical elements or because exceptionally complex geometry of cog side for modelling.

Every user of software system for designing is interested in creation of complex plane curve *Spline* which defined geometry of cog side profile.

The control of 3D parameterised model geometry is done by created parameters, formulas and parameter laws shown in the tree in Fig. 1. (Cozzens, 2006) Parameters review, formulas and parameter laws in the *Part* documents tree activating is done through the main select menu ( $Tools \rightarrow Options \rightarrow Part\ Infrastructure \rightarrow Display$ ).

Spur gear	Bevel gear	Worm
z	<i>z</i> 1, <i>z</i> 2	z1=1
т		m=1,5
a=20 deg		
p=m*PI		
$r=(z^*m)/2$	r=(z1*m)/2	<i>d</i> =20 mm
$rb=r*\cos(a)$	$rb=rc*\cos(a)$	

Spur gear	Bevel gear	Worm
rf=r-1.2*m		
ra=r+m		ra=d/2+ha
rr=0.38*m		
ha=m		
hf=1.2*m		
$xd=rb^*(\cos(t^*PI)+\sin(t^*))$	PI)*t*PI)	N=6,5
$yd=rb*(\sin(t*PI)-\cos(t*I))$	PI)*t*PI)	L=(N+1)*p
0≤ <i>t</i> ≤1		gama=atan(m*z1/d)
	delta = a tan(z1/z2)	dZ=-L/2
	$rc=r/\cos(delta)$	
	lc=rc/sin(delta)	
	tc=-atan(Relations\yd.Evaluate(a/180deg)/	
	Relations\xd.Evaluate(a/180deg))	
	b=0.3*rc	
	ratio=1-b/lc/cos(delta)	
	dZ=0  mm	

Table 1. Parameters and formulas

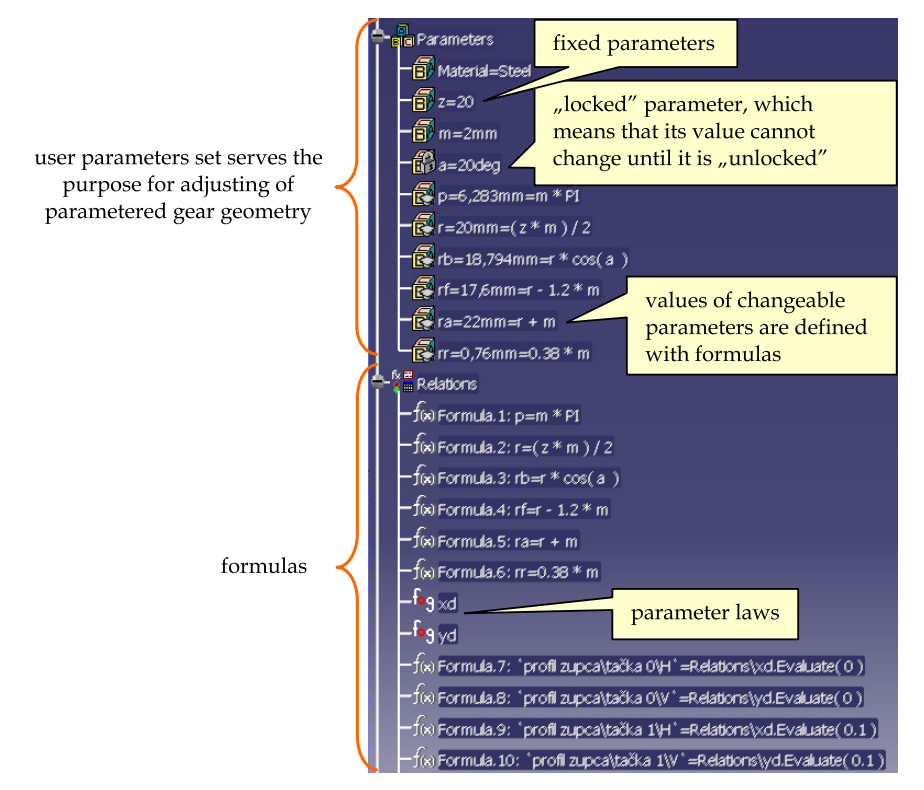


Fig. 1. Gear geometry control

## 2.1.1 Spur gears parameter modelling

To define fixed parameters (Fig. 2.), we select command *Formula* from tools palette *Knowledge* or from main select menu. Then, we:

- 1. choose desired parameter type (*Real, Integer, Length, Angle*) and press the button *New Parameter of type*,
- 2. type in a new parameter name,
- 3. assign a parameter value (only in the case if parameter has fixed value) and
- 4. press the button *Apply* to confirm a new parameter creation.

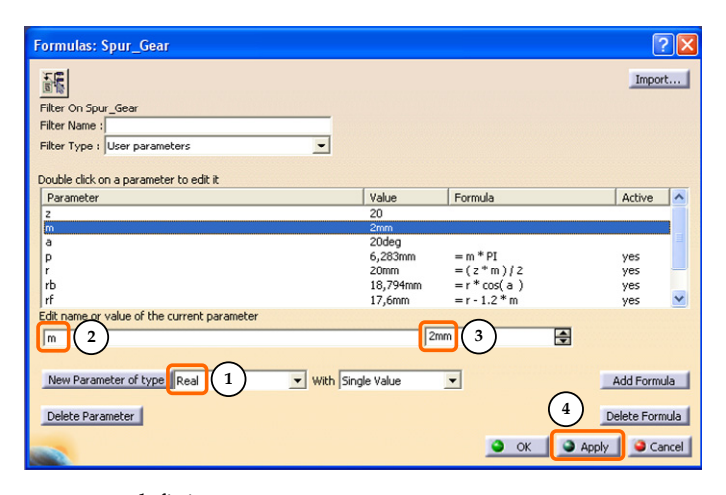


Fig. 2. Fixed parameters defining

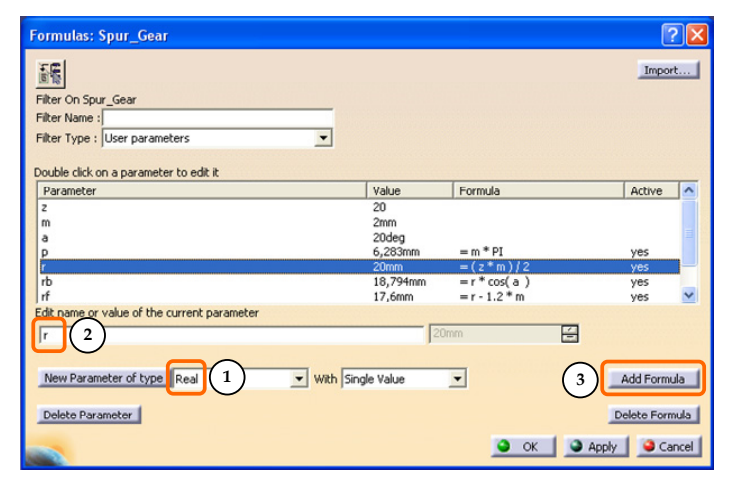


Fig. 3. Changeable parameters defining

Most geometrical gear parameters are changeable and are in the function of fixed parameters m and z (Fig. 3.). We do not need to set values for these parameters, because CATIA V5 system calculates them itself. So, instead of values setting, formulas are defined by choosing the command Formula for (Fig. 4.). When formula has been created, it is possible to manipulate with it by the tree, similar as with any other model feature.

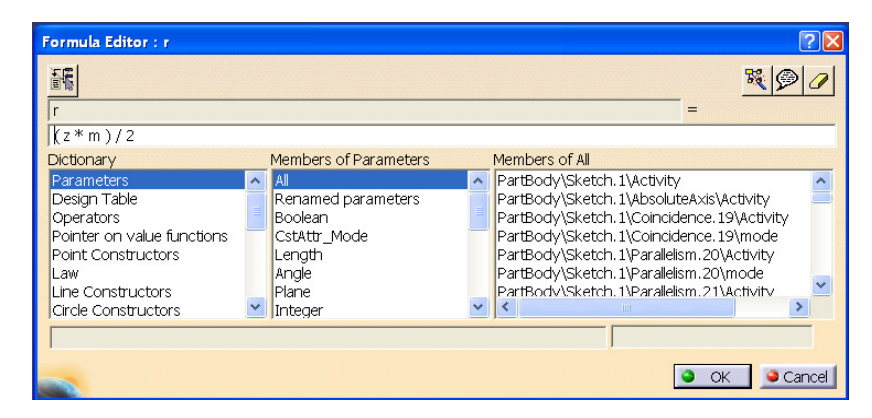


Fig. 4. Formula setting

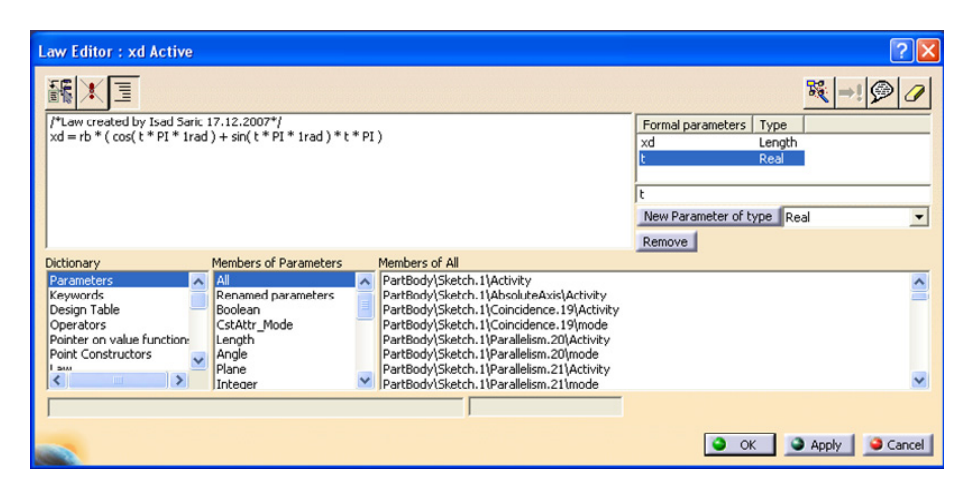


Fig. 5. Setting of parameter laws for calculation of x and y coordinates of involute points

Position of the points on involutes profile of cog side is defined in the form of parameter laws (Fig. 5.). For coordinate points of involute (x0,y0), (x1,y1), ...., (x4,y4) we most frequently define a set of parameters. To create parameter laws, we choose the command Law from tools palette Knowledge. Then, we give two laws in parameter form, which we are going to be used for calculation of x and y coordinate points of involute

$$xd = rb * (\cos(t * PI * 1rad) + \sin(t * PI * 1rad) * t * PI)$$
 (1)

$$yd = rb * (\sin(t * PI * 1rad) - \cos(t * PI * 1rad) * t * PI)$$
 (2)

While we use law editor, we have to take into account the following:

- trigonometric functions, specially angles, are not considered as numbers, and because of that angle constants like 1*rad* or 1deg must be used,
- PI is the value of the number  $\pi$ .

For the purpose of accuracy checking of previously conducted activities, review of formulas, parameter laws and values of all defined fixed and changeable parameters is activated in the tree of Part document ( $Tools \rightarrow Options \rightarrow Knowledge$ ).

The example of spur gear parameter modelling is shown in the next paragraph. All dimensions, or more precisely, geometric changeable parameters of spur gear are in the function of fixed parameters m and z. We can generate any spur gear by changing parameters m and z.

Part Number	m	Z	$d_g$	d	$b_z$	$b_g$	$b_k$	$t_k$
G2-20	2	20	30	15	20	35	5	2,35
G3-40	3	40	60	25	30	50	8	3,34
G4-60	4	60	120	30	40	60	10	3,34

Table 2. Selected spur gears parameters

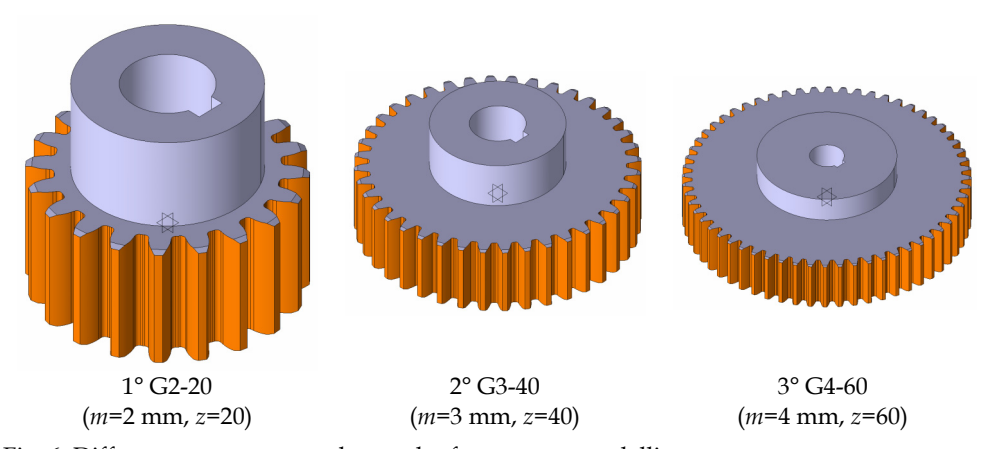


Fig. 6. Different spur gears are the result of parameter modelling

Fig. 6. shows three different standard catalogue spur gears made from the same CATIA V5 file, by changing parameters *m* and *z*. (Saric et al., 2009, 2010)

#### 2.1.2 Bevel gears parameter modelling

The example of bevel gear parameter modelling is shown in the next paragraph. All dimensions, or more precisely, geometric changeable parameters of bevel gear are in the function of fixed parameters m,  $z_1$  and  $z_2$ . We can generate any bevel gear by changing parameters m,  $z_1$  and  $z_2$ .

Part Number	m	$z_1$	$z_2$	$d_g$	d	$b_z$	$b_g$	Connection between hub and shaft
B2-25	2	25	25	40	12	10,6	25,52	M5
DB3-15	3	15	30	36	18	17	36,26	M6
FB4-15	4	15	60	48	20	34	59,9	M8

Table 3. Selected bevel gears parameters

Fig. 7. shows three different standard catalogue bevel gears made from the same CATIA V5 file, by changing parameters m,  $z_1$  and  $z_2$ . (Saric et al., 2009, 2010)

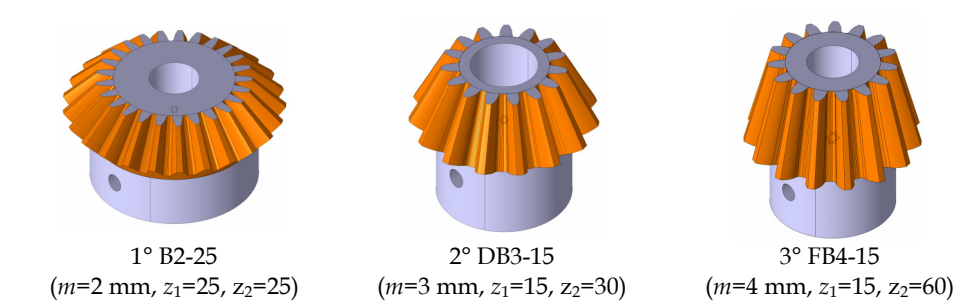


Fig. 7. Different bevel gears are the result of parameter modelling

# 2.1.3 Worms parameter modelling

The example of worm parameter modelling is shown in the next paragraph. All dimensions, or more precisely, geometric changeable parameters of worm are in the function of fixed parameters m,  $z_1$  and N. We can generate any worm by changing parameters m,  $z_1$  and N.

Part Number	m	$z_1$	$d_g$	d	L	$L_g$	Connection between hub and shaft
W1,5-1	1,5	1	23	10	35	45	M5
W2,5-2	2,5	2	35	15	45	60	M6
W3-3	3	3	41	20	55	70	M8

Table 4. Selected worms parameters

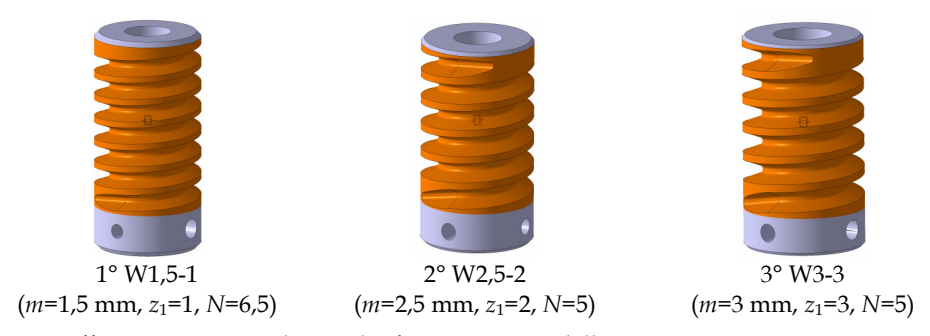


Fig. 8. Different worms are the result of parameter modelling

Fig. 8. shows three different standard catalogue worms made from the same CATIA V5 file, by changing parameters m,  $z_1$  and N. (Saric et al., 2009, 2010)

#### 2.2 Belt transmissions parameter modelling

This application includes wide area of the industry for the fact that belt transmitting is often required. Generally, belt transmitting designing process consists of needed drive power estimate, choice of belt pulley, length and width of belt, factor of safety, etc. Final design quality can be estimated by efficiency, compactness and possibilities of service. If engineer does not use parameter modelling, he/she must pass through exhausting phase of design, based on learning from the previous done mistakes, in order to have standard parts like belt pulleys and belts, mounted on preferred construction. This process is automatized by parameter modelling. In such process, characteristics that registered distance between belt pulleys, belts length, etc., are also created. Such characteristics, also, register links, belt angle speeds and exit angle speed. The results for given belts length can be obtained by the feasibility study. Few independent feasibility studies for the different belts lengths are compared with demands for compactness. In such a way, several constructions of belt transmitting can be tested, and then it is possible to find the best final construction solution.

The example of belt pulley parameter modelling is shown in the next paragraph. The belt pulley K is shown in the Fig. 9., and it consists of several mutual welded components: hub G, pulley rim V, plate P and twelve side ribs BR. All dimensions, or more precisely, geometric changeable parameters of belt pulley are in function of fixed parameters d,  $B_k$ ,  $d_v$  and s. We can generate any belt pulley with cylindrical external surface by changing parameters d,  $B_k$ ,  $d_v$  and s.

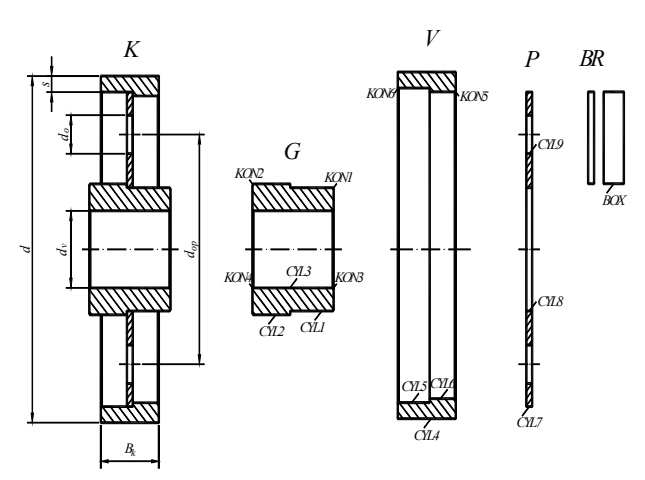


Fig. 9. Modelling of belt pulley parts with cylindrical external surface

Dimensions of hub depends from diameter of shaft  $d_v$ , on which hub is set. Shaft diameter is the input value through which the other hub dimension are expressed.

Hub shape can be obtained by adding and subtraction of cylinders and cones shown in the Fig. 9.

$$G = CYL1 + CYL2 - CYL3 - KON1 - KON2 - KON3 - KON4$$
(3)

Pulley rim of belt pulley depends from diameter of belt pulley d, pulley rim width  $B_k$ , diameter of shaft  $d_v$  and minimal pulley rim thickness s.

$$V = CYL4 - CYL5 - CYL6 - KON5 - KON6$$

$$\tag{4}$$

Plate dimensions depend from diameter of belt pulley d, minimal pulley rim thickness s and diameter of shaft  $d_v$ .

$$P = CYL7 - CYL8 - 6 \cdot CYL9 \tag{5}$$

Side ribs are side set rectangular plates which can be shown by primitive in the form of prism.

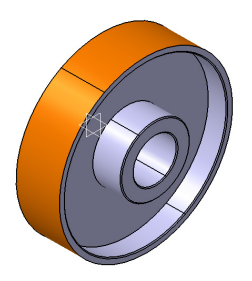
$$BR = BOX (6)$$

Whole belt pulley is obtained by adding of formed forms.

$$K = G + V + P + 6 \cdot BR \tag{7}$$

Belt pulley with cylindrical external surface								
CYL1: $D=1,6 \cdot d_v$ , $H=0,75 \cdot d_v$	$CYL9: H= 0.1 \cdot d_v$							
CYL2: $D=1.7 \cdot d_v$ , $H=0.65 \cdot d_v+2 \text{ mm}$	$KON1: D=1,6 \cdot d_v$ , $H=1$ mm, angle $45^{\circ}$							
CYL3: $D=d_v$ , $H=1,4 \cdot d_v+2 \text{ mm}$	KON2: $D=1,7 \cdot d_v$ , $H=1$ mm, angle $45^\circ$							
$CYL4: D=d, H=B_k$	KON3: $D=d_v$ , $H=1$ mm, angle $45^\circ$							
CYL5: $D=d-2$ s, $H=B_k/2+0.05$ $d_v+1$ mm	$KON4: D=d_v$ , $H=1$ mm, angle $45^{\circ}$							
CYL6: $D=d-2$ s-0,1 $d_v$ , $H=B_k/2-0,05$ $d_v-1$ mm	<i>KON5</i> : $D=d-2 \cdot s-0,1 \cdot d_v$ , $H=1 \text{ mm}$ , angle $45^{\circ}$							
CYL7: $D=d-2$ s, $H=0.1 \cdot d_v$	<i>KON6</i> : <i>D=d-2 ⋅ s, H=</i> 1 mm, angle 45°							
CYL8: $D=1,6 d_v, H=0,1 d_v$	BOX: $A=[(d-2 \cdot s)-1,8 \cdot d_v]/2$ , $B=0,35 \cdot B_k$ , $C=0,1 \cdot d_v$							

Table 5. Parameters and formulas



1° K200 (*d*=200 mm, *B<sub>k</sub>*=50 mm, *d<sub>v</sub>*=50 mm, *s*=4 mm)



2° K315 (d=315 mm,  $B_k$ =63 mm,  $d_v$ =60 mm, s=4,5 mm,  $d_{ov}$ =204 mm,  $d_o$ =60 mm)



3° K400 (d=400 mm,  $B_k$ =71 mm,  $d_v$ =70 mm, s=5 mm,  $d_{op}$ =250 mm,  $d_o$ =70 mm)

Fig. 10. Different belt pulleys with cylindrical external surface are the results of parameter modelling

Fig. 10. shows three different standard belt pulleys with cylindrical external surface made from the same CATIA V5 file, by changing parameters d,  $B_k$ ,  $d_v$  and s. (Saric et al., 2009)

Use of side ribs that are posed between holes on the plate is recommended during modelling of belt pulleys with longer diameter (Fig. 10.).

Rotary parts of belt pulley shown in the Fig. 9., can be modelled in a much more easier way. More complex contours, instead of their forming by adding and subtraction, they can be formed by rotation. In the first case, computer is loaded with data about points inside primitive which, in total sum, do not belong inside volume of component. In the second case, rotary contour (bolded line in the Fig. 11.) is first defined, and, then, primitive of desired shape is obtained by rotation around rotate axis.

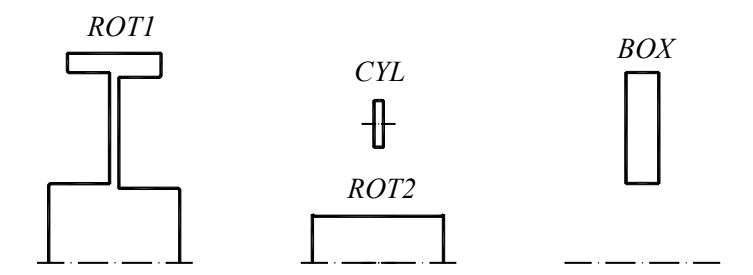


Fig. 11. Modelling of rotary forms

For primitives, shown in the Fig. 11., final form is obtained after the following operations

$$K = (ROT1 - ROT2 - 6 \cdot CYL) \cup 6 \cdot BOX$$
 (8)

#### 3. Conclusion

Designer must be significantly engaged into the forming of the component shape. Because of that reason, once formed algorithm for the modelling of the component shape is saved in computer memory and it is used when there is need for the modelling of the same or similar shape with similar dimensions. (Saric et al., 2009)

Parts which are not suitable for interactive modelling are modelled by parameters. In the process of geometric mechanical transmission modelling in CATIA V5 system, we do not have to create shape directly, but, instead of that, we can put parameters integrated in geometric and/or dimensional constraints. Changing of characteristic fixed parameters gives us a 3D solid model of mechanical transmission. This way, designer can generate more alternative designing samples, concentrating his attention on design functional aspects, without special focus on details of elements shape. (Saric et al., 2010)

For the purpose of final goal achieving and faster presentation of the product on the market, time spent for the development of the product is marked as the key factor for more profit gaining. Time spent for process of mechanical transmissions designing can be reduced even by 50% by parameter modelling use with focus on the preparatory phase (Fig. 12.).

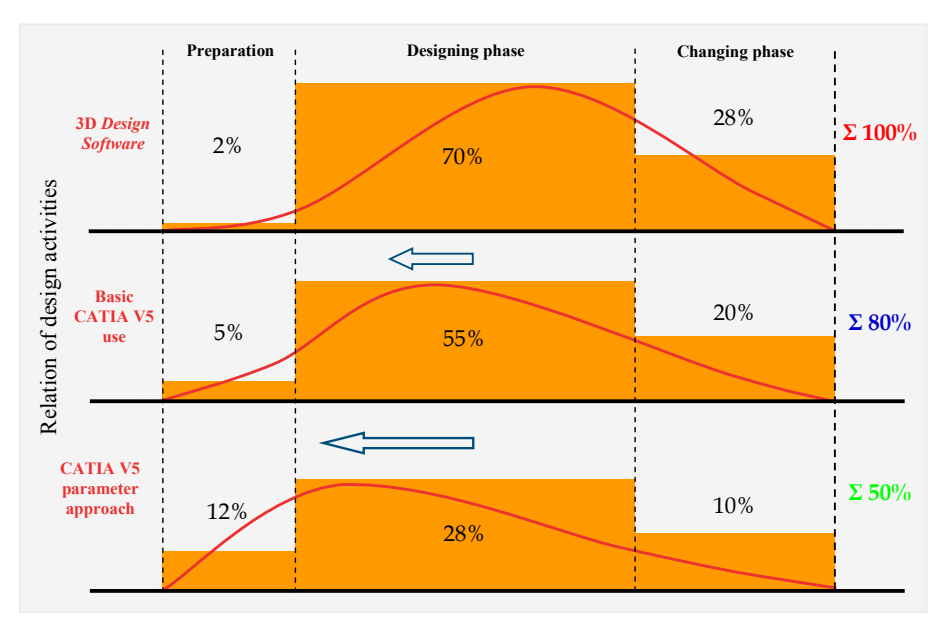


Fig. 12. Relation of design activities and reducing of time spent for design by parameter modelling

These are the advantages of parameter modelling use:

- possibility to make family of parts with the same shape based on one created model,
- forming of libraries basis of standard mechanical elements which take up computer memory, similar to the classic approach of 3D geometric modelling, is not necessary,
- use of parameters enables global modification of whole assembly (automatic reconfiguration),
- development of the product is faster, etc. (Saric et al., 2009)

We can conclude that CATIA V5 system offers possibility of geometric association creation defined by relations established between parameters. Therefore, components parameterisation must obligatory apply in combination with today's traditional geometric modelling approach. Direct financial effects can be seen in production costs reduction, which increases the productivity. Therefore profit is bigger and price of products are lower. (Saric et al., 2010)

Obtained 3D model from CATIA V5 system is used as the base for technical documentation making, analysis of stress and deformation by *Finite Element Method* (FEM), generating of NC/CNC programs for production of the parts on machine (CAM/NC), *Rapid Prototyping* (RP), etc.

# 4. Acknowledgment

Researches were partially financed by WUS Austria under supervision of Austrian Ministry of foreign affairs as the part of CDP+ project (No. project: 43-SA-04).

# 5. Nomenclature

A	mm	side rib length
a	0	line of contact angle
В	mm	side rib width
$B_k$	mm	pulley rim width
BR	-	side rib
b	mm	cog width
bg	mm	hub width
$b_k$	mm	keyway width
b <sub>z</sub>	mm	gear width
C	mm	side rib thickness
CYL	-	cylinder
D	mm	appropriate diameter of belt pulley components
d	mm	gear pitch circle; diameter of the hole for shaft; diameter of belt pulley
dg	mm	interior diameter of hub
$d_{o}$	mm	diameter of the hole on the plate
dop	mm	diameter on which holes on plate are set
$d_{v}$	mm	diameter of shaft
delta	0	a half of an angle of front cone
dΖ	mm	translation of geometry over z axis; translation of worm surface over z axis
G	-	hub
gama	0	angle of helix
Н	mm	appropriate length of belt pulley components
ha	mm	addendum part of cog height
hf	mm	root part of cog height
K	-	belt pulley
KON	-	cone
L	mm	helix length
$L_{g}$	mm	hub length
lc	mm	cone axis length
m	mm	module
N	-	number of helix
P	-	plate
PI	-	value of number $\pi$
р	mm	step on pitch circle
ROT	-	rotation
r	mm	pitch radius
ra	mm	addendum radius
ratio	-	factor of scaling exterior to interior cog profile
rb	mm	basic radius
rc	mm	length of generating line of back (additional) cone
rf	mm	root radius
rr	mm	radius of profile root radius
S	mm	minimal pulley rim thickness

t	-	involutes function parameter
$t_{k}$	mm	keyway depth
tc	0	cutting angle used for contact point putting in zx plane
V	-	pulley rim
xd	mm	x coordinate of involutes cog profile generated on the base of parameter t
yd	mm	y coordinate of involutes cog profile generated on the base of parameter t
(x,y)	mm	coordinates of involute points
Z	-	cog number
$z_1$	-	cog number of driver gear; number of turn of a worm
$\mathbf{z}_2$	-	cog number of following gear

#### 6. References

- Amirouche, F. (2004). *Principles of Computer-Aided Design and Manufacturing* (2nd edition), Prentice Hall, ISBN 0-13-064631-8, Upper Saddle River, New Jersey
- Certified hardware configurations for CATIA V5 systems. (May 2011). Available from: <a href="http://www.3ds.com/support/certified-hardware/overview/">http://www.3ds.com/support/certified-hardware/overview/</a>
- Cozzens, R. (2006). *Advanced CATIA V5 Workbook: Knowledgeware and Workbenches Release* 16. Schroff Development Corporation (SDC Publications), ISBN 978-1-58503-321-8, Southern Utah University
- Dassault Systemes. (2007a). CATIA Solutions Version V5 Release 18 English Documentation
- Dassault Systemes. (2007b). CATIA Web-based Learning Solutions Version V5 Release 18 Windows
- Dassault Systemes PLM solutions, 3D CAD and simulation software. (May 2011). Available from: <a href="http://www.3ds.com/home/">http://www.3ds.com/home/</a>
- International Business Machines Corp. (IBM). (May 2011). Available from: <a href="http://www.ibm.com/us/en/">http://www.ibm.com/us/en/</a>
- Karam, F. & Kleismit, C. (2004). *Using Catia V5*, Computer library, ISBN 86-7310-307-X, Cacak
- Repcic, N. et al. (1998). Mechanical Elements II Part, Svjetlost, ISBN 9958-10-157-7 (ISBN 9958-11-075-X), Sarajevo
- Repcic, N. & Muminovic, A. (2007). *Mechanical Elements II*, Faculty of Mechanical Engineering, Sarajevo
- Saric, I., Repcic, N. & Muminovic, A. (2006). 3D Geometric parameter modelling of belt transmissions and transmissions gear. *Technics Technologies Education Management TTEM*, Vol. 4, No. 2, (2009), pp. 181-188, ISSN 1840-1503
- Saric, I., Repcic, N. & Muminovic, A. (1996). Parameter Modelling of Gears, *Proceedings of the* 14th International Research/Expert Conference "Trends in the Development of Machinery and Associated Technology TMT 2010", pp. 557-560, ISSN 1840-4944, Mediterranean Cruise, September 11-18, 2010
- Shigley, J.E., Mischke, C.R. & Budynas, R.G. (2004). *Mechanical Engineering Design* (7th edition), McGraw-Hill, ISBN 007-252036-1, New York
- Spotts, M.F., Shoup, T.E. & Hornberger, L.E. (2004). *Design of Machine Elements* (8th edition), Prentice Hall, ISBN 0-13-126955-0, Upper Saddle River, New Jersey
- Zamani, N.G. & Weaver, J.M. (2007). Catia V5: Tutorials Mechanism Design & Animation, Computer library, ISBN 978-86-7310-381-5, Cacak

# Gearbox Simulation Models with Gear and Bearing Faults

Endo Hiroaki<sup>1</sup> and Sawalhi Nader<sup>2</sup>

<sup>1</sup>Test devices Inc.,

<sup>2</sup>Prince Mohammad Bin Fahd University (PMU),

Mechanical Engineering Department, AlKhobar

<sup>1</sup>USA

<sup>2</sup>Saudi Arahi

#### 1. Introduction

Simulation is an effective tool for understanding the complex interaction of transmission components in dynamic environment. Vibro-dynamics simulation of faulty gears and rolling element bearings allows the analyst to study the effect of damaged components in controlled manners and gather the data without bearing the cost of actual failures or the expenses associated with an experiment that requires a large number of seeded fault specimens. The fault simulation can be used to provide the data required in training Neural network based diagnostic/prognostic processes.

# 2. Key elements in gearbox simulation

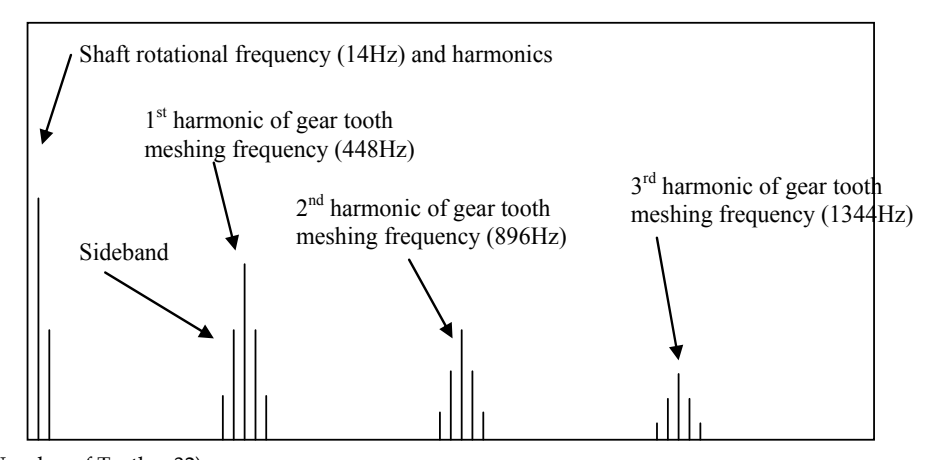
#### 2.1 Transmission error

Gears, by their inherent nature, cause vibrations due to the large pressure which occurs between the meshing teeth when gears transmit power. Meshing of gears involves changes in the magnitude, the position and the direction of large concentrated loads acting on the contacting gear teeth, which as a result causes vibrations. Extended period of exposure to noise and vibration are the common causes of operational fatigue, communication difficulties and health hazards. Reduction in noise and vibration of operating machines has been an important concern for safer and more efficient machine operations.

Design and development of quieter, more reliable and more efficient gears have been a popular research area for decades in the automotive and aerospace industries. Vibration of gears, which directly relates to noise and vibration of the geared machines, is typically dominated by the effects of the tooth meshing and shaft revolution frequencies, their harmonics and sidebands, caused by low (shaft) frequency modulation of the higher toothmesh frequency components. Typically, the contribution from the gear meshing components dominates the overall contents of the measured gearbox vibration spectrum (see Figure-2.1.1).

Transmission Error (TE) is one of the most important and fundamental concepts that forms the basis of understanding vibrations in gears. The name 'Transmission Error' was originally coined by Professor S. L. Harris from Lancaster University, UK and R.G. Munro,

his PhD student at the time. They came to the realization that the excitation forces causing the gears to vibrate were dependent on the tooth meshing errors caused by manufacturing and the bending of the teeth under load [1].



(Number of Teeth = 32)

Fig. 2.1.1. Typical spectrum composition of gear vibration signal.

TE is defined as the deviation of the angular position of the driven gear from its theoretical position calculated from the gearing ratio and the angular position of the pinion (Equation-2.1.1). The concept of TE is illustrated in Figure-2.1.2.

$$TE = \left(\theta_{gear} - \frac{R_{pinion}}{R_{gear}}\theta_{pinion}\right)$$
 (2.1.1)

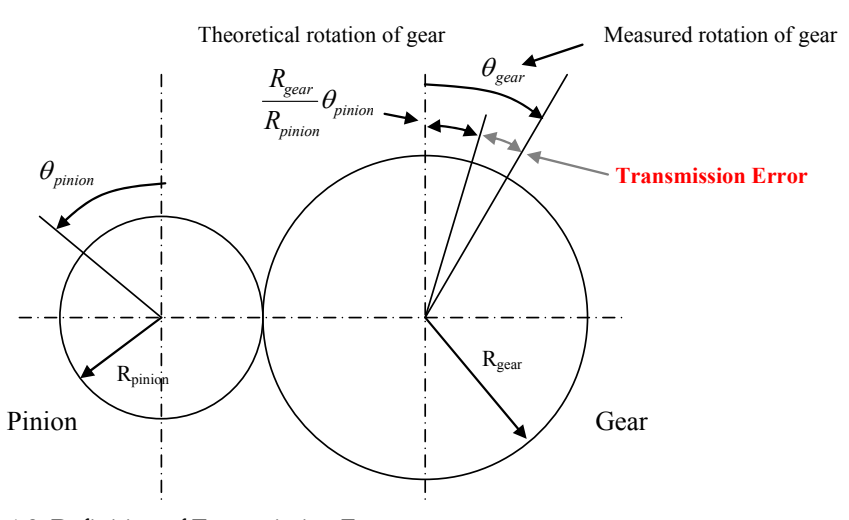


Fig. 2.1.2. Definition of Transmission Error.

What made the TE so interesting for gear engineers and researchers was its strong correlation to the gear noise and the vibrations. TE can be measured by different types of instruments. Some commonly used methods are: Magnetic signal methods, straingauge on the drive shaft, torsional vibration transducers, tachometers, tangential accelerometers and rotary encoders systems. According to Smith [2], TE results from three main sources: 1) Gear geometrical errors, 2) Elastic deformation of the gears and associated components and 3) Errors in mounting. Figure-2.1.3 illustrates the relationship between TE and its sources.

Transmission Error exists in three forms: 1) Geometric, 2) Static and 3) Dynamic. Geometric TE (GTE) is measured at low speeds and in the unloaded state. It is often used to examine the effect of manufacturing errors. Static TE (STE) is also measured under low speed conditions, but in a loaded state. STE includes the effect of elastic deflection of the gears as well as the geometrical errors. Dynamic TE (DTE) includes the effects of inertia on top of all the effects of the errors considered in GTE and in STE. The understanding of the TE and the behaviour of the machine elements in the geared transmission system leads to the development of realistic gear rotor dynamics models.

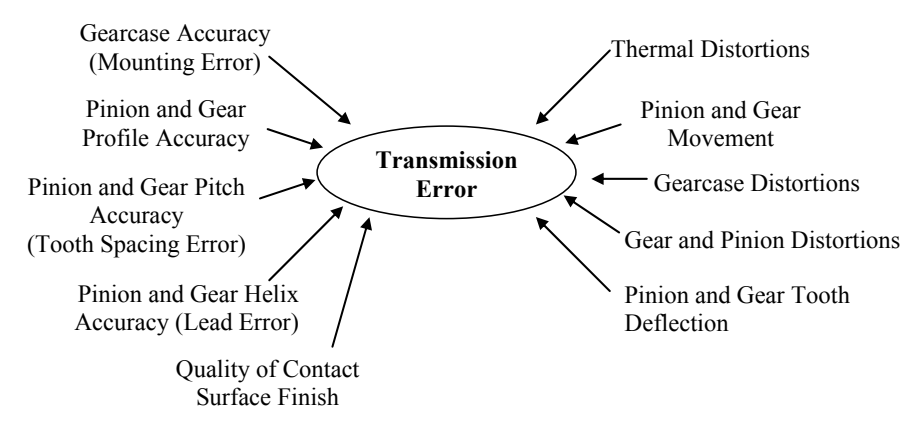


Fig. 2.1.3. Sources of Transmission Error.

## 2.2 Effect of gear geometric error on transmission error

A typical GTE of a spur gear is shown in Figure-2.2.1. It shows a long periodic wave (gear shaft rotation) and short regular waves occurring at tooth-mesh frequency. The long wave is often known as: Long Term Component: LTC, while the short waves are known as: Short Term Component: STC.

The LTC is typically caused by the eccentricity of the gear about its rotational centre. An example is given in Figure-2.2.2 to illustrate how these eccentricities can be introduced into the gears by manufacturing errors; it shows the error due to a result of the difference between the hobbing and the shaving centres.

The effect of errors associated with gear teeth appears in the STC as a localized event. The parabolic-curve-like effect of tooth tip relief is shown in Figure-2.2.3(a). The STC is caused mainly by gear tooth profile errors and base pitch spacing error between the teeth. The effect

of individual tooth profile errors on the GTE is illustrated in Figure-2.2.3(a). The GTE of a meshing tooth pair is obtained by adding their individual profile errors. The STC of gear GTE is synthesised by superposing the tooth pair GTEs separated by tooth base pitch angles (Figure-2.2.3 (b)).

Another common gear geometric error is tooth spacing or pitch errors, shown in Figure-2.2.4. The tooth spacing error appears in GTE as vertical raise or fall in the magnitude of a tooth profile error.

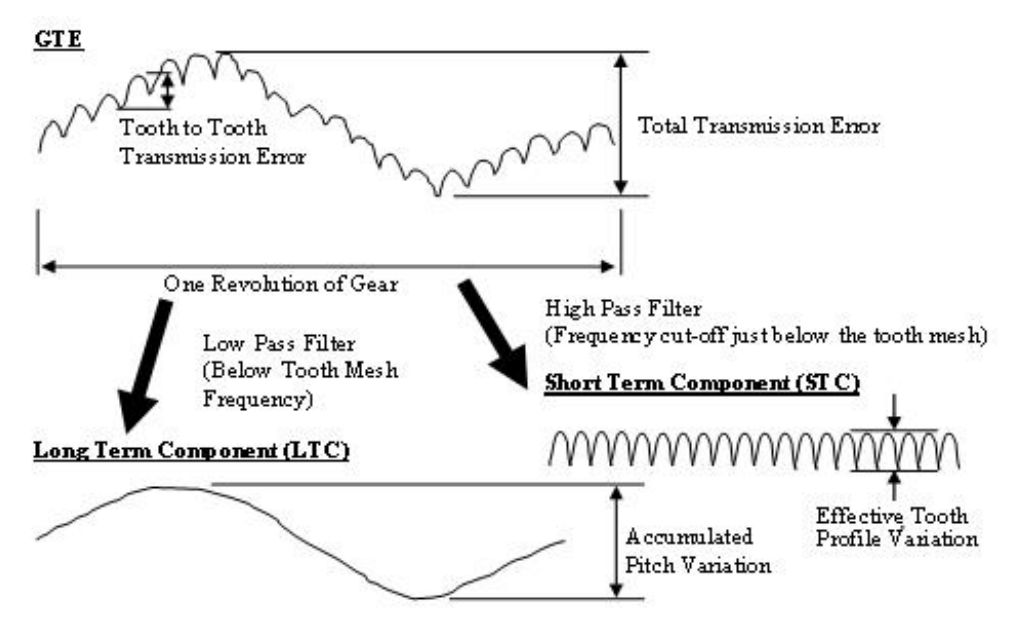


Fig. 2.2.1. A typical Geometrical Transmission Error.

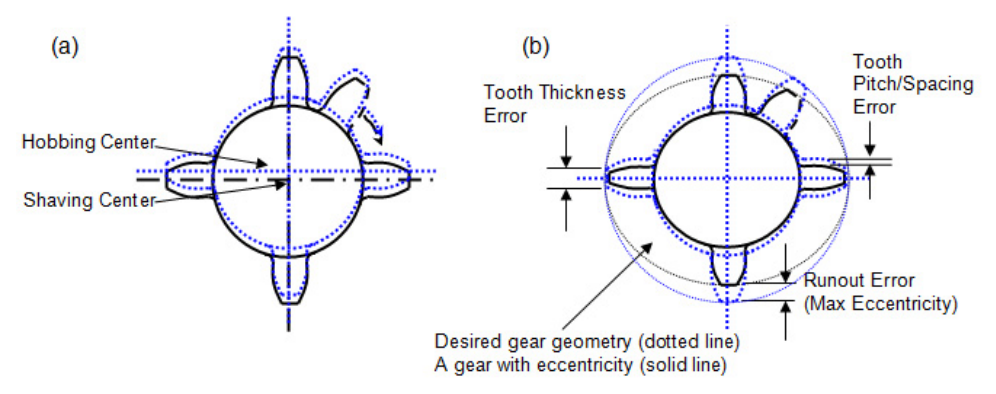


Fig. 2.2.2. (a) Eccentricity in a gear caused by manufacturing errors, (b) Resulting errors in gear geometry.

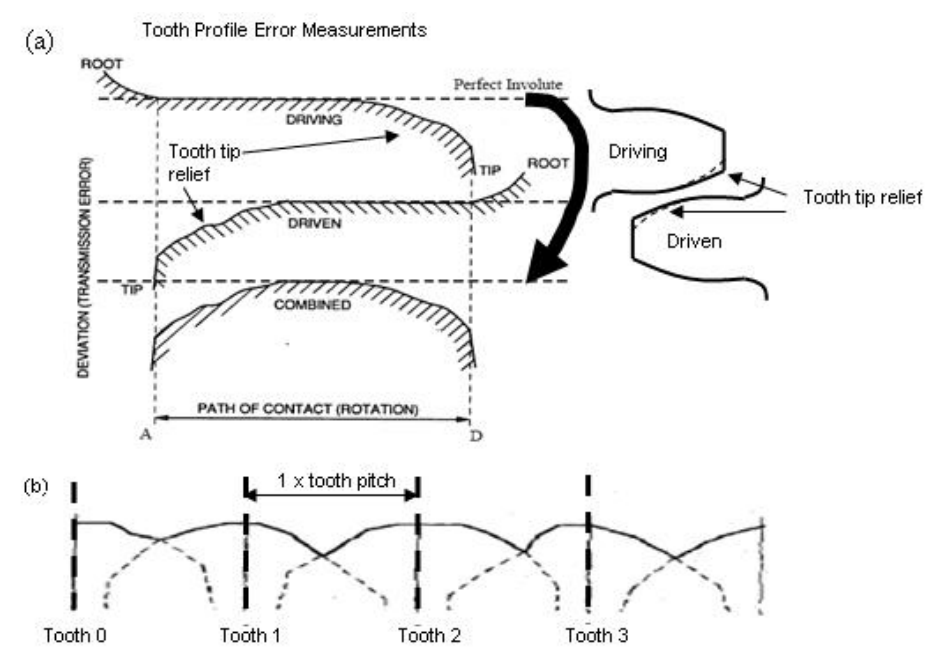


Fig. 2.2.3. (a) GTE of a meshing tooth pair (b) Resulting Short Term Component of GTE.

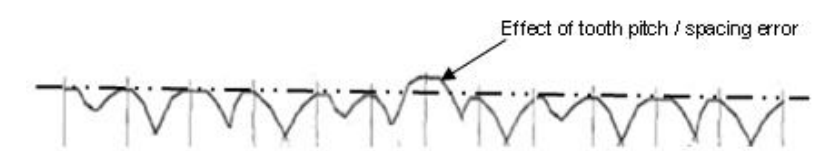


Fig. 2.2.4. Effect of spacing error appearing in short term component of GTE.

#### 2.3 Effect of load on transmission error

Elastic deflections occurring in gears are another cause of TE. Although gears are usually stiff and designed to carry very large loads, their deflection under load is not negligible. Typical deflection of gear teeth occurs in the order of microns ( $\mu m$ ). Although it depends on the amount of load gears carry, the effect of the deflection on TE may become more significant than the contribution from the gear geometry.

A useful load-deflection measure is that 14N of load per 1mm of tooth face width results in 1 $\mu$ m of deflection for a steel gear: i.e. stiffness = 14E10 $^{9}$  N/m/m for a tooth pair meshing at the pitch line. It is interesting to note here that the stiffness of a tooth pair is independent of its size (or tooth module) [3]. Deflection of gear teeth moves the gear teeth from their theoretical positions and in effect results in a continuous tooth pitch error: see Figure-2.3.1 (a). The effect of the gear deflection appears in the TE (STE) as a shifting of the GTE: Figure-2.3.1 (b).

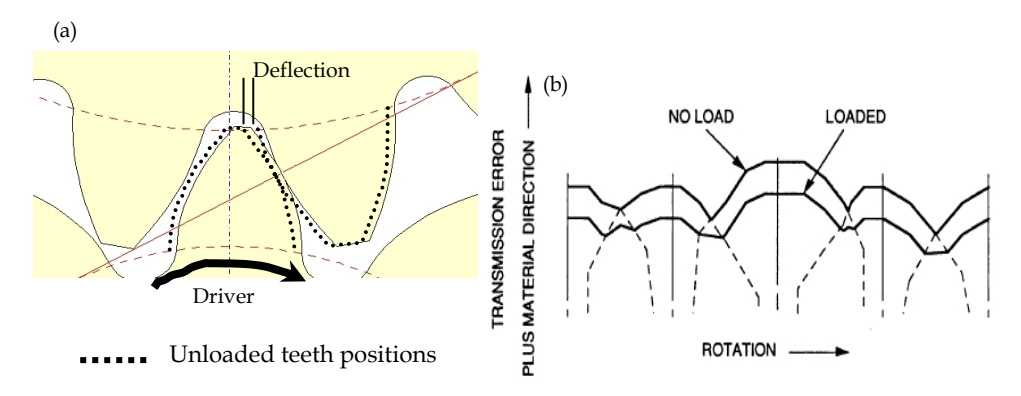


Fig. 2.3.1. (a) Deflection of gear tooth pair under load, (b) Effect of load on transmission error (TE).

Consider the more general situation where the deflection in loaded gears affects the TE significantly. Note that the following discussion uses typical spur gears (contact ratio = 1.5) with little profile modification to illustrate the effect of load on TE. Figure-2.3.2 illustrates the STE caused by the deflection of meshing gear teeth. The tooth profile chart shows a flat

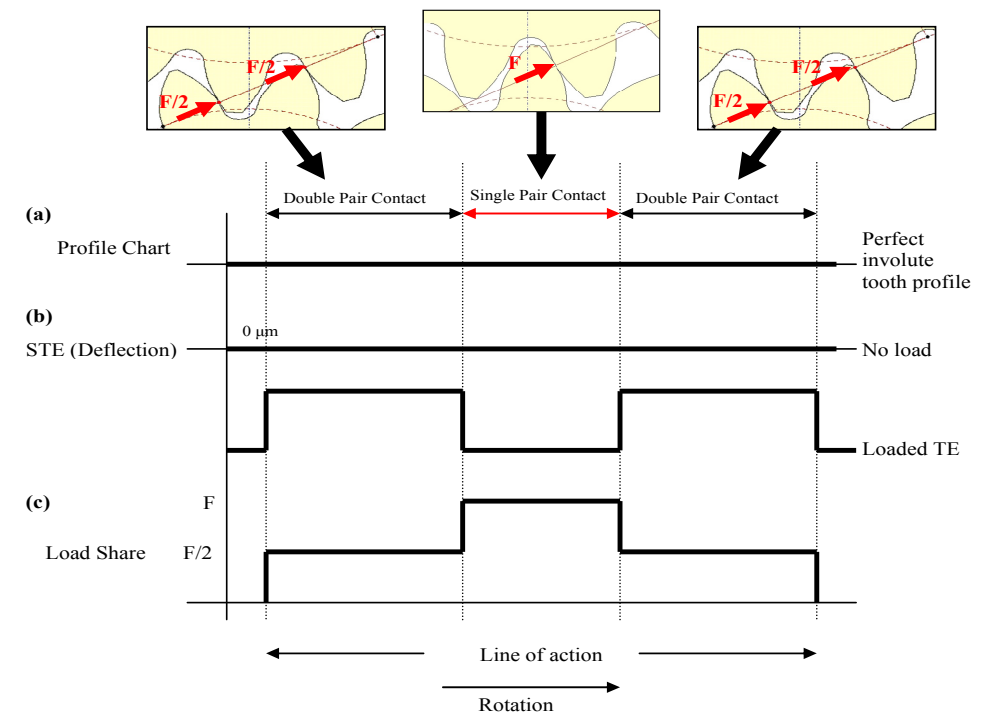


Fig. 2.3.2. Effect of Load on TE, (a) Tooth Profile Chart, (b) Static Transmission Error, (c) Loading acting on a tooth

line indicating the ideal involute profile of the tooth: Figure-2.3.2 (a). The effect of mesh stiffness variation due to the change in the number of meshing tooth pairs appears as steps in the STE plot: Figure-2.3.2 (b). The amount of deflection increases when a single pair of teeth is carrying load and decreases when the load is shared by another pair. The share of force carried by a tooth through the meshing cycle is shown in Figure-2.3.2 (c).

A paper published jointly by S.L. Harris, R. Wylie Gregory and R.G. Munro in 1963 showed how transmission error can be reduced by applying appropriate correction to the involute gear profile [4, 5]. The Harris map in Figure-2.3.3 shows that any gear can be designed to have STE with zero variation (i.e. a flat STE with constant offset value) for a particular load. The basic idea behind this technique is that the profile of gear teeth can be designed to cancel the effect of tooth deflection occurring at the given load.

Additionally, variation of TE can be reduced by increasing the contact ratio of the gear pair. In other words, design the gears so that the load is carried by a greater number of tooth pairs.

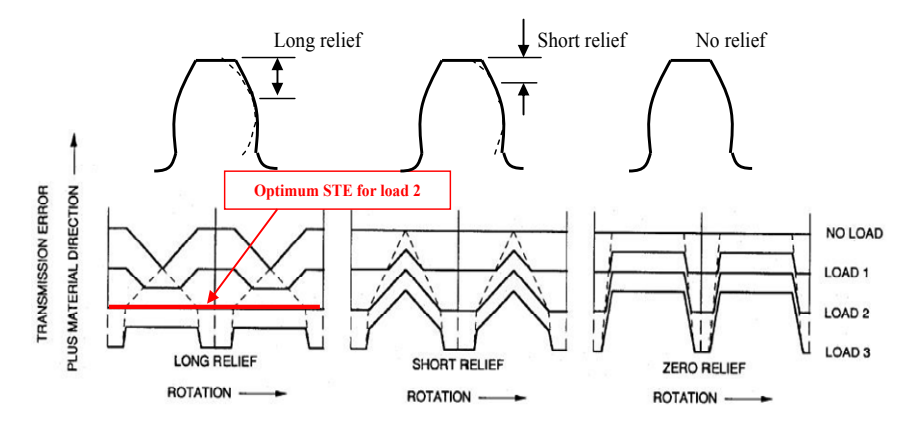


Fig. 2.3.3. Optimum tooth profile modification of a spur gear.

## 2.4 Modelling gear dynamics

It is a standardized design procedure to perform STE analysis to ensure smoothly meshing gears in the loaded condition. It was explained in this section how the strong correlation between the TE and the gear vibration makes the TE a useful parameter to predict the quietness of the gear drives. However, a more realistic picture of the gear's dynamic properties can not be captured without modelling the dynamics of the assembled gear drive system. Solution of engineering problems often requires mathematical modelling of a physical system. A well validated model facilitates a better understanding of the problem and provides useful information for engineers to make intelligent and well informed decisions.

A comprehensive summary of the history of gear dynamic model development is given by Ozguven and Houser [6]. They have reviewed 188 items of literature related to gear dynamic simulation existing up to 1988. In Table-2.4.1, different types of gear dynamics models were classified into five groups according to their objectives and

# **Group-1: Simple Dynamic Factor Models**

Most early models belong to this group. The model was used to study gear dynamic load and to determine the value of dynamic factor that can be used in gear root stress formulae. Empirical, semi-empirical models and dynamic models constructed specifically for determination of dynamic factor are included in this group.

#### Group-2: Models with Tooth Compliance

Models that consider tooth stiffness as the only potential energy storing element in the system. Flexibility of shafts, bearings etc is neglected. Typically, these models are single DOF spring-mass systems. Some of the models from this group are classified in group-1 if they are designed solely for determining the dynamic factor.

## Group-3: Models for Gear Dynamics

A model that considers tooth compliance and the flexibility of the relevant components. Typically these models include torsional flexibility of shafts and lateral flexibility of bearings and shafts along the line of action.

## **Group-4: Models for Geared Rotor Dynamics**

This group of models consider transverse vibrations of gear carrying shafts as well as the lateral component (NOTE: Transverse: along the Plane of Action, Lateral: Normal to the Plane of Action). Movement of the gears is considered in two mutually perpendicular directions to simulate, for example, whirling.

# **Group-5: Models for Torsional Vibrations**

The models in the third and fourth groups consider the flexibility of the gear teeth by including a constant or time varying mesh stiffness. The models belonging to this group differentiate themselves from the third and fourth groups by having rigid gears mounted on flexible shafts. The flexibility at the gearmesh is neglected. These models are used in studying pure (low frequency) torsional vibration problems.

#### Table 2.4.1. Classification of Gear Dynamic Models. (Ozguven & Houser [6])

functionality. Traditionally lumped parameter modelling (LPM) has been a common technique that has been used to study the dynamics of gears. Wang [7] introduced a simple LPM to rationalize the dynamic factor calculation by the laws of mechanics. He proposed a model that relates the GTE and the resulting dynamic loading. A large number of gear dynamic models that are being used widely today are based on this work. The result of an additional literature survey on more recently published materials by Bartelmus [8], Lin & Parker [9, 10], Gao & Randall [11, 12], Amabili & Rivola [13], Howard et al [14], Velex & Maatar [15], Blankenship & Singh [17], Kahraman & Blankenship [18] show that the fundamentals of the modelling technique in gear simulations have not changed and the LMP method still serves as an efficient technique to model the wide range of gear dynamics behaviour. More advanced LPM models incorporate extra functions to simulate specialized phenomena. For example, the model presented by P. Velex and M. Maatar [15] uses the individual gear tooth profiles as input and calculates the GTE directly from the gear tooth profile. Using this method they simulated how the change in contact behaviour of meshing gears due to misalignment affects the resulting TE.

FEA has become one of the most powerful simulation techniques applied to broad range of modern Engineering practices today. There have been several groups of researchers who attempted to develop detailed FEA based gear models, but they were troubled by the

challenges in efficiently modelling the rolling Hertzian contact on the meshing surfaces of gear teeth. Hertzian contact occurs between the meshing gear teeth which causes large concentrated forces to act in very small area. It requires very fine FE mesh to accurately model this load distribution over the contact area. In a conventional finite element method, a fully representative dynamic model of a gear requires this fine mesh over each gear tooth flank and this makes the size of the FE model prohibitively large.

Researchers from Ohio State University have developed an efficient method to overcome the Hertzian contact problem in the 1990s' [16]. They proposed an elegant solution by modelling the contact by an analytical technique and relating the resulting force distribution to a coarsely meshed FE model. This technique has proven so efficient that they were capable of simulating the dynamics of spur and planetary gears by [19, 20] (see Figure-2.4.1). For more details see the CALYX user's manuals [21, 22].

For the purpose of studies, which require a holistic understanding of gear dynamics, a lumped parameter type model appears to provide the most accessible and computationally economical means to conduct simulation studies.

A simple single stage gear model is used to explain the basic concept of gear dynamic simulation techniques used in this chapter. A symbolic representation of a single stage gear system is illustrated in Figure-2.4.2. A pair of meshing gears is modelled by rigid disks representing their mass/moment of inertia. The discs are linked by line elements that represent the stiffness and the damping (representing the combined effect of friction and fluid film damping) of the gear mesh. Each gear has three translational degrees of freedom (one in a direction parallel to the gear's line of action, defining all interaction between the gears) and three rotational degree of freedoms (DOFs). The stiffness elements attached to the centre of the disks represent the effect of gear shafts and supporting mounts. NOTE: Symbols for the torsional stiffnesses are not shown to avoid congestion.

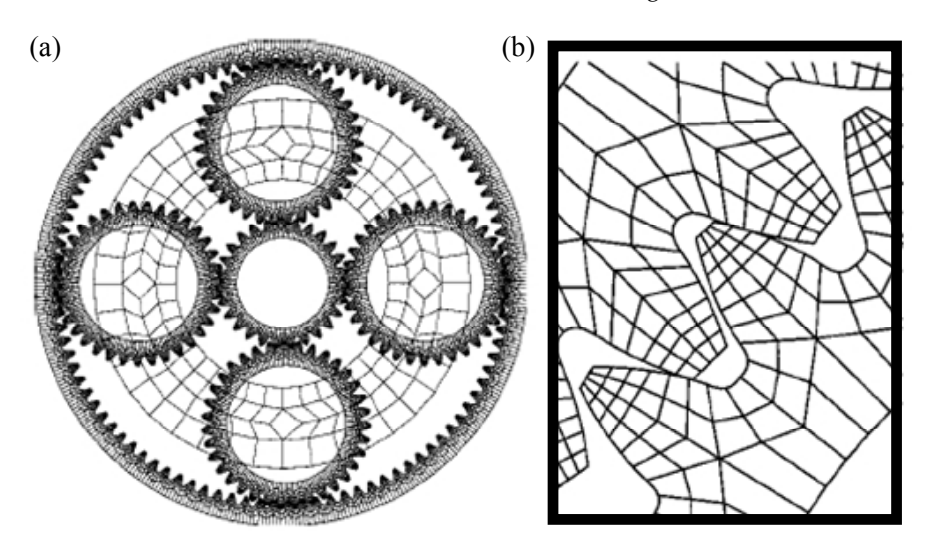
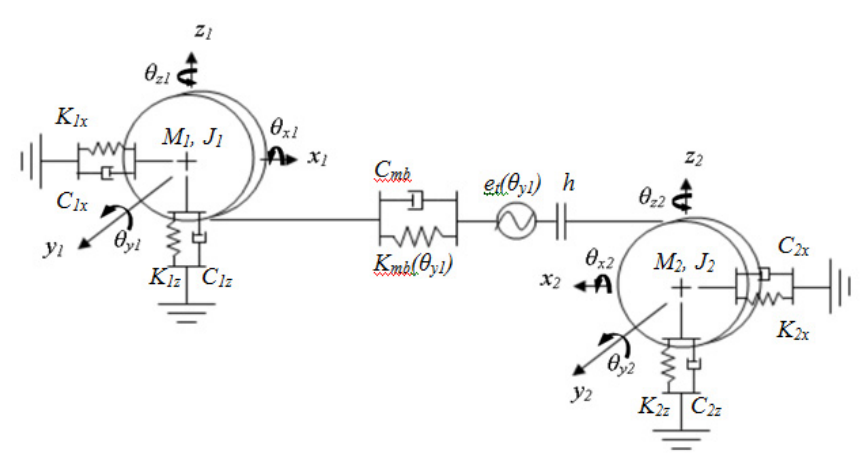


Fig. 2.4.1. (a) Parker's planetary gear model and (b) FE mesh of gear tooth. Contacts at the meshing teeth are treated analytically. It does not require dense FE mesh. (Courtesy of Parker et al. [20])



 $x_i$ ,  $y_i$ ,  $z_i$  Translation at  $i_{th}$  Degrees of Freedom.

 $\theta_{xi}$ ,  $\theta_{yi}$ ,  $\theta_{zi}$  Rotation about a translational axis at  $i_{th}$  Degrees of Freedom.

C,  $C_{mb}$  Damping matrices. The subscript 'mb' refers to damping at the gearmesh. Typically for  $C_{mb}$ ,  $\zeta = 3 \sim 7\%$ .

K,  $K_{mb}$  Linear stiffness elements. The subscript 'mb' refers to stiffness at the gearmesh.

*h* An 'on/off' switch governing the contact state of the meshing gear teeth.

 $\underline{e_t}$  A vector representing the combined effect of tooth topography deviations and misalignment of the gear pair.

*i* Index: *i*=1,2, 3 ...etc.

Fig. 2.4.2. A Typical Lumped Parameter Model of Meshing Gears.

The linear spring elements representing the Rolling Element Bearings (REB) are a reasonable simplification of the system that is well documented in many papers on gear simulation. For the purpose of explaining the core elements of the gear simulation model, the detail of REB as well as the casing was omitted from this section; more comprehensive model of a gearbox, with REB and casing, will be presented later in section 2.5.

Vibration of the gears is simulated in the model as a system responding to the excitation caused by a varying TE,  $'e_t'$  and mesh stiffness  $'K_{mb}'$ . The dominant force exciting the gears is assumed to act in a direction along the plane of action (PoA). The angular position dependent variables  $'e_t'$  and  $'K_{mb}'$  are expressed as functions of the pinion pitch angle  $(\theta_{y1})$  and their values are estimated by using static simulation. Examples of similar techniques are given by Gao & Randall [11, 12], Du [23] and Endo and Randall [61].

Equations of motion derived from the LPM are written in matrix format as shown in Equation-2.4.1. The equation is rearranged to the form shown in the Euqation-2.4.2; the effect of TE is expressed as a time varying excitation in the equation source. The dynamic response of the system is simulated by numerically solving the second order term (accelerations) for each step of incremented time. The effect of the mesh stiffness variation is implemented in the model by updating its value for each time increment.

$$M\ddot{x} + C(\dot{x} - \dot{e}_t) + K(x - e_t(\theta)) = F_s \tag{2.4.1}$$

$$M\ddot{\underline{x}} + C\dot{\underline{x}} + K\underline{x} = F_s + hC_{mh}(\theta)\dot{\underline{e}}_t + hK_{mh}(\theta)\underline{e}_t$$
 (2.4.2)

where,

 $\underline{x}$ ,  $\underline{\dot{x}}$ ,  $\underline{\ddot{x}}$  Vectors of translational and rotational displacement, velocity and acceleration.

 $\theta$  Angular position of pinion.

K,  $K_{mb}$  Stiffness matrices (where K includes the contribution from  $K_{mb}$ ). The subscript 'mb' refers to stiffness at the gearmesh.

C,  $C_{mb}$  Damping matrices (C including contribution from  $C_{mb}$ ). The subscript 'mb' refers to damping at the gearmesh.

h An 'on/off' switch governing the contact state of the meshing gear teeth.

*F* Static force vector.

 $e_t$  ,  $\dot{e}_t$  A vector representing the combined effect of tooth topography deviations.

#### 2.5 Modelling rolling element bearings and gearbox casing

For many practical purposes, simplified models of gear shaft supports (for example, the effect of rolling element bearings (REBs) and casing were modelled as simple springs with constant stiffnesses) can be effective tools. However, fuller representations of these components become essential in the pursuit of more complete and accurate simulation modelling.

For a complete and more realistic modelling of the gearbox system, detailed representations of the REBs and the gearbox casing are necessary to capture the interaction amongst the gears, the REBs and the effects of transfer path and dynamics response of the casing.

Understanding the interaction between the supporting structure and the rotating components of a transmission system has been one of the most challenging areas of designing more detailed gearbox simulation models. The property of the structure supporting REBs and a shaft has significant influence on the dynamic response of the system. Fuller representation of the REBs and gearbox casing also improves the accuracy of the effect transmission path that contorts the diagnostic information originated from the faults in gears and REBs. It is desired in many applications of machine health monitoring that the method is minimally intrusive on the machine operation. This requirement often drives the sensors and/or the transducers to be placed in an easily accessible location on the machine, such as exposed surface of gearbox casing or on the machine skid or on an exposed and readily accessible structural frame which the machine is mounted on.

The capability to accurately model and simulate the effect of transmission path allows more realistic and effective means to train the diagnostic algorithms based on the artificial intelligence.

#### 2.5.1 Modelling rolling element bearings

A number of models of REBs exist in literatures [24, 25, 26, 27] and are widely employed to study the dynamics and the effect of faults in REBs. The authors have adopted the 2 DoF model originally developed by Fukata [27] in to the LPM of the gearbox. Figure-2.5.1 (a)

illustrates the main components of the rolling element bearing model and shows the load zone associated with the distribution of radial loads in the REB as it supports the shaft. Figure-2.5.1 (b) explains the essentials of the bearing model as presented by [28]. The two degree-of-freedom REB model captures the load-deflection relationships, while ignoring the effect of mass and the inertia of the rolling elements. The two degrees of freedom ( $x_s$ ,  $y_s$ ) are related to the inner race (shaft). Contact forces are summed over each of the rolling elements to give the overall forces on the shaft.

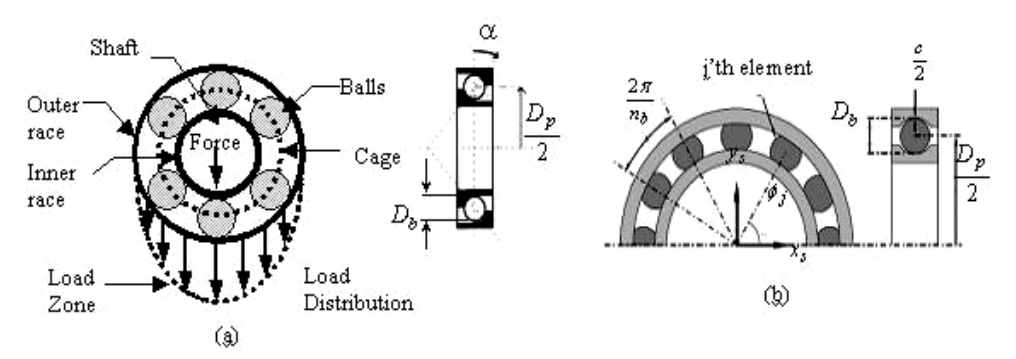


Fig. 2.5.1. (a) Rolling element bearing components and load distribution; (b) Two degree of freedom model. [28]

The overall contact deformation (under compression) for the j'th -rolling element  $\delta_j$  is a function of the inner race displacement relative to the outer race in the x and y directions  $((x_s - x_p), (y_s - y_p))$ , the element position  $\phi_j$  (time varying) and the clearance (c). This is given by:

$$\delta_i = (x_s - x_v)\cos\phi_i + (y_s - y_v)\sin\phi_i - c - \beta_i C_d \quad (j = 1, 2..)$$
(2.5.1)

Accounting for the fact that compression occurs only for positive values of  $\delta_j$ ,  $\gamma_j$  (contact state of  $\delta_i$  the rolling elements) is introduced as:

$$\gamma_{j} = \begin{cases} 1, & \text{if } \delta_{j} > 0 \\ 0, & \text{otherwise} \end{cases}$$
 (2.5.2)

The angular positions of the rolling elements  $\phi_j$  are functions of time increment dt, the previous cage position  $\phi_o$  and the cage speed  $\omega_c$  (can be calculated from the REB geometry and the shaft speed  $\omega_s$  assuming no slippage) are given as:

$$\phi_j = \frac{2\pi(j-1)}{n_b} + \omega_c dt + \phi_o \quad \text{with} \quad \omega_c = (1 - \frac{D_b}{D_p}) \frac{\omega_s}{2}$$
 (2.5.3)

The ball raceway contact force f is calculated by using traditional Hertzian theory (non-linear stiffness) from:

$$f = k_h \delta^n \tag{2.5.4}$$

The load deflection factor  $k_b$  depends on the geometry of contacting bodies, the elasticity of the material, and exponent n. The value of n=1.5 for ball bearings and n=1.1 for roller bearings. Using Equation-2.5.4 and summing the contact forces in the x and y directions for a ball bearing with  $n_b$  balls, the total force exerted by the bearings to the supporting structure can be calculated as follows:

$$f_x = k_b \sum_{j=1}^{n_b} \gamma_j \delta_j^{1.5} \cos \phi_j \text{ and } f_y = k_b \sum_{i=1}^{n_b} \gamma_i \delta_j^{1.5} \sin \phi_j$$
 (2.5.5)

The stiffness of the given REB model is non-linear, and is time varying as it depends on the positions of the rolling elements that determine the contact condition. The effect of slippage was introduced to the model by adding random jitters of 0.01-0.02 radians to the nominal position of the cage at each step.

#### 2.5.2 Gearbox casing model - Component mode synthesis method

Lumped parameter modelling (LPM) is an efficient means to express the internal dynamics of transmission systems; masses and inertias of key components such as gears, shafts and bearings can be lumped at appropriate locations to construct a model. The advantage of the LPM is that it provides a method to construct an effective dynamic model with relatively small number of degrees-of-freedoms (DOF), which facilitates computationally economical method to study the behaviour of gears and bearings in the presence of nonlinearities and geometrical faults [32, 33, 34, 35].

One of the limitations of the LPM method is that it does not account for the interaction between the shaft and the supporting structure; i.e. casing flexibility, which can be an important consideration in light weight gearboxes, that are common aircraft applications. Not having to include the appropriate effect of transmission path also results in poor comparison between the simulated and measured vibration signals.

Finite Element Analysis (FEA) is an efficient and well accepted technique to characterize a dynamic response of a structure such as gearbox casings. However, the use of FEA results in a large number of DOF, which could cause some challenges when attempt to solve a vibrodynamic model of a combined casing and the LMP of gearbox internal components. Solving a large number of DOFs is time consuming even with the powerful computers available today and it could cause a number of computational problems, especially when attempting to simulate a dynamic response of gear and bearing faults which involves nonlinearities.

To overcome this shortcoming, a number of reduction techniques [36, 37] have been proposed to reduce the size of mass and stiffness matrix of FEA models. The simplified gearbox casing model derived from the reduction technique is used to capture the key characteristics of dynamic response of the casing structure and can be combined with the LPM models of gears and REBs.

The Craig-Bampton method [37] is a dynamic reduction method for reducing the size of the finite element models. In this method, the motion of the whole structure is represented as a combination of boundary points (so called master degree of freedom) and the modes of the structure, assuming the master degrees of freedom are held fixed. Unlike the Guyan reduction [38], which only deals with the reduction of stiffness matrix, the Craig-Bumpton

method accounts for both the mass and the stiffness. Furthermore, it enables defining the frequency range of interest by identifying the modes of interest and including these as a part of the transformation matrix. The decomposition of the model into both physical DOFs (master DOFs) and modal coordinates allows the flexibility of connecting the finite elements to other substructures, while achieving a reasonably good result within a required frequency range. The Craig-Bumpton method is a very convenient method for modelling a geared transmission system as the input (excitation) to the system is not defined as forces, but as geometric mismatches at the connection points (i.e. gear transmission error and bearing geometric error). The following summary of the Craig-Bampton method is given based on the references [39-41].

In the Craig-Bampton reduction method, the equation of motion (dynamic equilibrium) of each superelement (substructure), without considering the effect of damping, can be expressed as in Equation-2.5.6:

$$[M]\{\ddot{u}\} + [k]\{u\} = \{F\} \tag{2.5.6}$$

Where [M] is the mass matrix, [k] is the stiffness matrix,  $\{F\}$  is the nodal forces,  $\{u\}$  and  $\{\ddot{u}\}$  are the nodal displacements and accelerations respectively. The key to reducing the substructure is to split the degrees of freedom into masters  $\{u_m\}$  (at the connecting nodes) and slaves  $\{u_s\}$  (at the internal nodes). The mass, the stiffness and the force matrices are rearranged accordingly as follows:

$$\begin{bmatrix}
M_{mm} & M_{ms} \\
M_{sm} & M_{ss}
\end{bmatrix}
\begin{Bmatrix}
\ddot{u}_{m} \\
\ddot{u}_{s}
\end{Bmatrix} + \begin{bmatrix}
k_{mm} & k_{ms} \\
k_{sm} & k_{ss}
\end{bmatrix}
\begin{Bmatrix}
u_{m} \\
u_{s}
\end{Bmatrix} = \begin{Bmatrix}
F_{m} \\
0
\end{Bmatrix}$$
(2.5.7)

The subscript m denotes master, s denotes slave. Furthermore, the slave degrees of freedom (internals) can be written by using generalized coordinates (modal coordinates by (q) using the fixed interface method, i.e. using the mode shapes of the superelement by fixing the master degrees of freedom nodes (connecting/ boundary nodes). The transformation matrix (T) is the one that achieves the following:

For the fixed interface method, the transformation matrix (T) can be expressed as shown in Equation-2.5.9:

$$T = \begin{bmatrix} I & 0 \\ G_{sm} & \phi_s \end{bmatrix} \tag{2.5.9}$$

where,

$$G_{sm} = -k_{ss}^{-1}k_{sm} (2.5.10)$$

and  $\phi_s$  is the modal matrix of the internal DOF with the interfaces fixed.

By applying this transformation, the number of DOFs of the component will be reduced. The new reduced mass and stiffness matrices can be extracted using Equations 2.5.11 & 2.5.12 respectively:

$$M_{reduced} = T^t MT (2.5.11)$$

and

$$k_{reduced} = T^t kT (2.5.12)$$

Thus Equation-2.5.7 can be re-written in the new reduced form using the reduced mass and stiffness matrices as well as the modal coordinates as follows:

$$\begin{bmatrix}
M_{bb} & M_{bq} \\
M_{qb} & M_{qq}
\end{bmatrix} \begin{Bmatrix} \ddot{u}_m \\
\ddot{q} \end{Bmatrix} + \begin{bmatrix} k_{bb} & 0 \\
0 & k_{qq} \end{bmatrix} \begin{Bmatrix} u_m \\
q \end{Bmatrix} = \begin{bmatrix} F_{reduced} \\
F_m \\
0 \end{Bmatrix}$$
(2.5.13)

Where  $M_{bb}$  is the boundary mass matrix i.e. total mass properties translated to the boundary points.  $k_{bb}$  is the interface stiffness matrix, i.e. stiffness associated with displacing one boundary DOF while the others are held fixed. The  $M_{bq}$  is the component matrix ( $M_{qb}$  is the transpose of  $M_{bq}$ ).

If the mode shapes have been mass normalized (typically they are) then:

$$k_{qq} = \begin{bmatrix} \backslash & 0 \\ \lambda_i & \\ 0 & \backslash \end{bmatrix}$$
 (2.5.14)

where  $\lambda_i$  is the eigenvalues;  $\lambda_i = k_i / m_i = \omega_i^2$ , and,

$$M_{qq} = \begin{bmatrix} \backslash & 0 \\ I & \\ 0 & \backslash \end{bmatrix}$$
 (2.5.15)

Finally the dynamic equation of motion (including damping) using the Craig-Bampton transform can be written as:

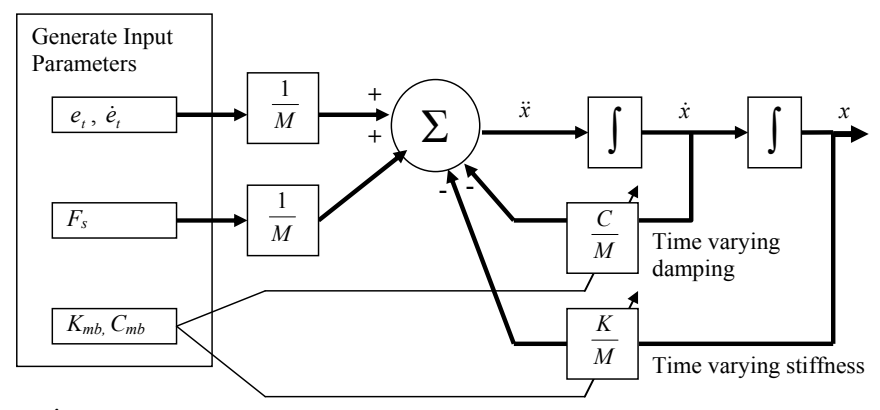
$$\begin{bmatrix} M_{bb} & M_{bq} \\ M_{ab} & I \end{bmatrix} \begin{bmatrix} \ddot{u}_m \\ \ddot{q} \end{bmatrix} + \begin{bmatrix} 0 & 0 \\ 0 & 2\zeta\omega \end{bmatrix} \begin{bmatrix} \dot{u}_m \\ \dot{q} \end{bmatrix} + \begin{bmatrix} k_{bb} & 0 \\ 0 & \omega^2 \end{bmatrix} \begin{bmatrix} u_m \\ q \end{bmatrix} = \begin{bmatrix} F_m \\ 0 \end{bmatrix}$$
(2.5.16)

where  $2\zeta\omega$  = modal damping ( $\zeta$  = fraction of critical damping)

For more detailed explanation of the techniques related to the modelling of rolling element bearings and the application of component mode synthesis (CMS) techniques, refer to the works by Sawalhi, Deshpande and Randall [41].

## 2.6 Solving the gear dynamic simulation models

A block diagram summarizing the time integral solution of a typical dynamic model with some time varying parameters is shown in Figure-2.6.1. There are a range of numerical algorithms available today to give solution of the dynamic models: direct time integration, harmonic balancing and shooting techniques, to name some commonly recognized methods.



(NOTE: 'J' stands for integration over a single step of incremented time)

Fig. 2.6.1. Dynamic Simulation Process

Sometimes the solution for gears requires simulation of highly non-linear events, for example, rattling and knocking in gears, which involve modelling of the contact loss. The works presented by R. Singh [42], Kahraman & Singh [43], Kahraman & Blankenship [18] and Parker & Lin [9, 10] show some examples of the "stiff" problems involving non-linearity due to contact loss and clearances.

The solution for these Vibro-Impact problems presents difficulties involving ill-conditioning and numerical "stiffness". In [42] Singh explains that ill-conditioning of a numerical solution occurs when there is a component with a large frequency ratio: ratio of gear mesh frequency to the natural frequency of the component.

The numerical stiffness in the gear dynamic simulation becomes a problem when gears lose contact. The relationship between the elastic force, relative deflection and gear mesh stiffness is illustrated in Figure-2.6.2. The gradient of the curve represent the gear mesh stiffness.

Contact loss between the gears occurs when the force between the gears becomes zero. The gears are then unconstrained and free to move within the backlash tolerance. The presence of a discontinuity becomes obvious when the derivative of the curve in Figure-2.6.2 (i.e. mesh stiffness) is plotted against the relative deflection. The discontinuity in the stiffness introduces instability in the numerical prediction.

In more formalized terms the "stiffness" of a problem is defined by local Eigen-values of the Jacobian matrix. Consider an equation of motion expressed in simple first order vector form 'f(x, t)', (Equation-2.6.1). Typically, the solution of an equation of motion is obtained by linearizing it about an operating point, say ' $x_0$ ', (Equation-2.6.2). Usually, most of the higher

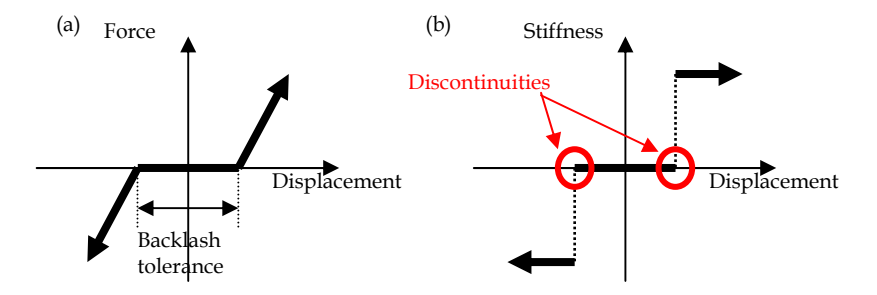


Fig. 2.6.2. Non-linearity due to contact loss in meshing gears; a) Force vs. Displacement, b) derivative of former, i.e. Stiffness vs. Displacement

order terms above the  $1^{st}$  derivative are ignored for linearization, which leaves the following expression (Equation-2.6.3). The differential term 'J' is called the Jacobian matrix (or Jacobian in short). The problems involving gear contact losses are "Stiff" problems because of the discontinuity in system derivatives (Jacobians). For a more detailed discussion on this topic refer to the work presented by Singh [42].

$$\underline{f}(x,t) = \frac{dx}{dt} \tag{2.6.1}$$

$$\underline{f}(x,t) \cong \underline{f}(x_0,t) + \left(\frac{df}{dx}\right)_{x_0} (x - x_0)$$
(2.6.2)

$$\underline{f}(x,t) \cong \underline{f}(x_0,t) + \underline{I}(x - x_0)$$
(2.6.3)

# 3. Modelling gearbox faults

The study of gear faults has long been an important topic of research for the development of gear diagnostic techniques based on vibration signal analysis. Understanding how different types of gear tooth faults affect the dynamics of gears is useful to characterise and predict the symptoms of the damage appearing in vibration signals [44, 45]. The strong link between the TE and the vibration of the gears was explained earlier. The effect of different types of gear tooth faults on TE can be studied by using the static simulation models. The result of static simulation can be then used to determine how different types of gear faults can be modelled into the dynamic simulation.

Gears can fail for a broad range of reasons. Finding a root cause of damage is an important part of developing a preventative measure to stop the fault from recurring. Analysis of gear failure involves a lot of detective works to link the failed gear and the cause of the damage. Comprehensive guidelines for gear failure analysis can be found in Alban [46], DeLange [47] and DANA [48]. AGMA (American Gear Manufacturers Association) recognizes four types of gear failure mode and a fifth category which includes everything else: Wear, Surface Fatigue, Plastic Flow, Breakage and associated gear failures [49].

The effect of gear tooth fillet cracks (TFC) and spalls on gear transmission error was studied in detail by using a static simulation models (FEA and LTCA (HyGears [50])). A pair of meshing gears were modelled and analysed in step incremented non-linear static environment. Note: the transmission error obtained from the static simulation models are referred to as Motion Errors (ME) here forth by following the HyGears convention.

It was explained earlier that the interaction between two meshing gears can be expressed in the dynamic model as time-varying stiffness, damping and gear tooth topological error elements linking the two lumped mass moments of inertia. The effect of gear tooth faults can be implemented into the dynamic simulation model as changes to these parameters. The understanding gained from the detailed simulation model studies of TFCs and spalls on gear motion has lead to the method of modelling the effect of the faults in dynamic model. The relevance between the types of gear faults to the selected parameters will be explained through subsequent sections.

Further to the simulation of gear tooth faults, this chapter also briefly touches on the modelling of spalls in rolling element bearings (REB), which is also a common type of faults in geared transmission systems.

#### 3.1 Modelling the effect of a fatigue crack in tooth fillet area of a gear

Classical tooth root fillet fatigue fracture is the most common cause of gear tooth breakages (Figure-3.1.1). Stress raisers, such as micro cracks from the heat treatment, hob tears, inclusions and grinding burns are common causes that initiate the cracks. The cracks occurring in the gear tooth fillet region progressively grow until the whole tooth or part of it breaks away. The breakage of a tooth is a serious failure. Not only the broken part fails, but serious damage may occur to the other gears as a result of a broken tooth passing though the transmission [48].

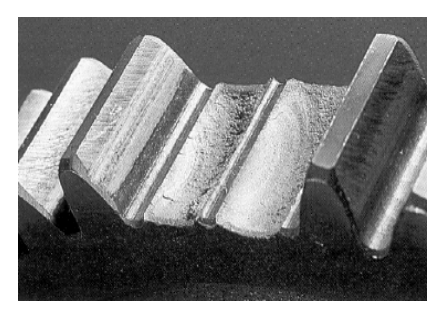


Fig. 3.1.1. A spur gear missing two teeth. They broke away due to the propagation of fatigue cracks. (Courtesy of DANA [48])

The research conducted for NASA by Lewicki [51] sets a clear guideline for predicting the trajectory of cracks occurring at the gear tooth fillet. Lewicki predicted crack propagation paths of spur gears with a variety of gear tooth and rim configurations, including the effect of: rim and web thickness, initial crack locations and gear tooth geometry factors (Diametral pitch, number of teeth, pitch radius and tooth pressure angle). A summary of the results is presented in Figure-3.1.2.

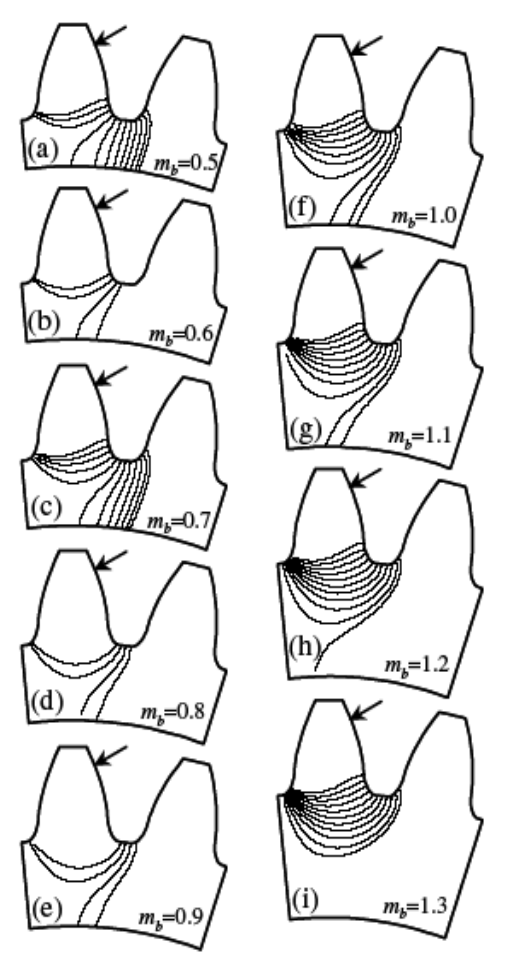


Fig. 3.1.2. Effect of backup ratio  $(m_b)$  and initial crack location on propagation path. (Lewicki [51])

A set of spur gears later used in the validation of the simulation result have a "backup ratio" (rim thickness divided by tooth height) greater than  $m_b$ =1.3. Therefore based on the Lewicki's prediction the cracks occurring in the tooth fillet region are most likely to propagate in the trajectory shown in Pattern Figure-3.1.2 (i); roughly 30~45° in to the tooth relative to the radial line path through the symmetric axis of the spur gear tooth profile.

Full 3D modelling of a propagating gear tooth crack is one of the actively researched areas. Some examples of simulation studies using the Boundary Element Method (BEM) are given in [52, 53, 54, 55]. The simulation studies using 3D models show complex behaviour crack growth from the small crack seeded at the middle of the gear tooth fillet. An example is shown in Figure-3.1.3 from "Modelling of 3D cracks in split spur gear", by Lewicki [52]. The crack front expands rapidly across the width of the gear tooth as it progresses into the thickness of the tooth. The tooth fillet crack (TFC) model used in this work assumes 2D

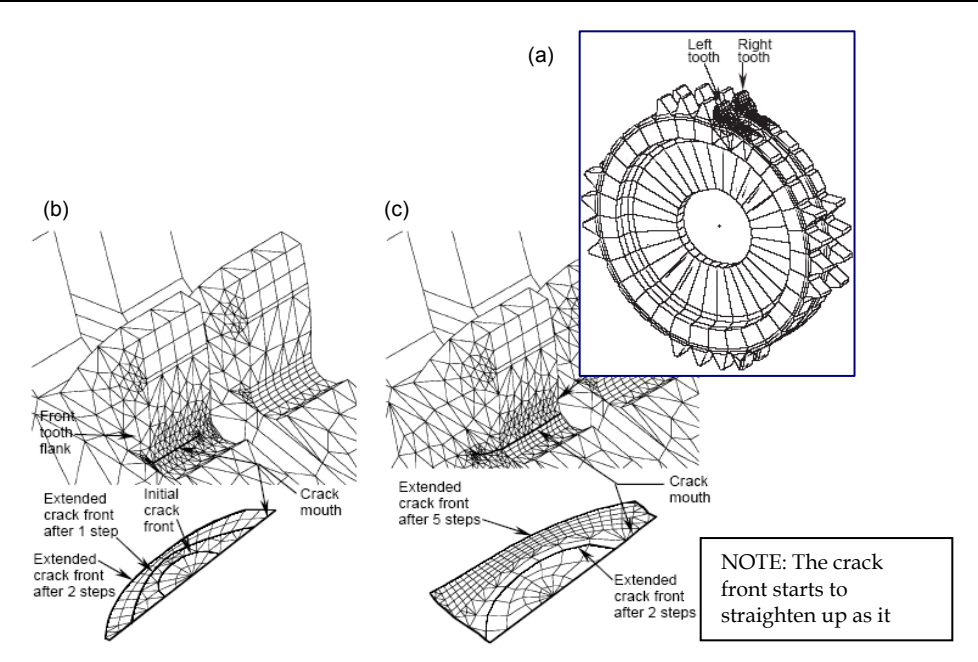


Fig. 3.1.3. 3D Crack propagation model. a) Boundary Element Model of Split Spur Gear, b) Close up of view of the gear teeth and crack section at earlier stage of development and c) more progressed crack. (Lewicki [53])

conditions which approximates the weakening of the cracked gear tooth when the crack is extended across the whole width of the tooth face.

The motion error (ME)<sub>2</sub> as obtained from the finite element (FE) model of a gear pair (32x32 teeth) presented in Figure-3.1.4<sub>2</sub> is shown in Figure-3.1.5. The MEs of the gears at different

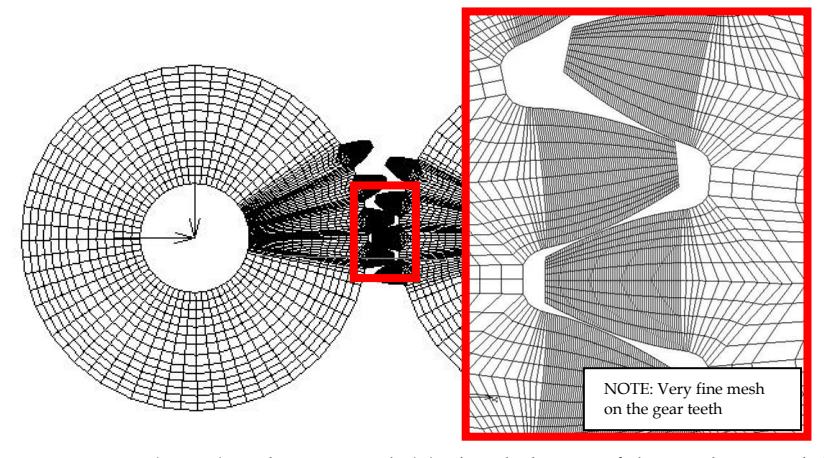


Fig. 3.1.4. Spur Gears (32x32) and its FE mesh (L), detailed view of the mesh around the gear teeth (R). [56]

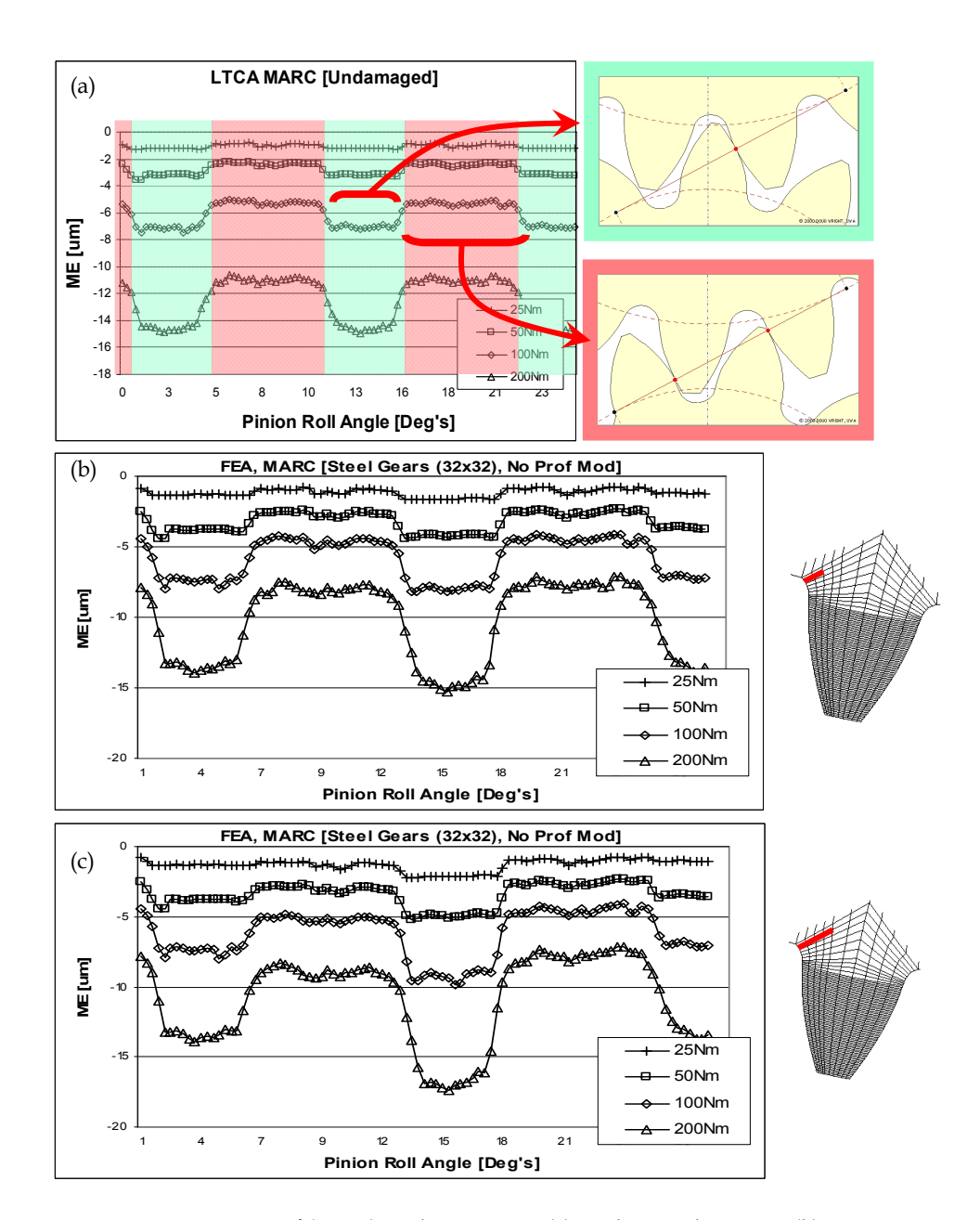


Fig. 3.1.5. Motion Errors of (32x32) teeth gear pairs; (a) Undamaged gear set; (b) TFC (L=1.18mm); (c) TFC (L=2.36mm)

amount of loadings (25, 50, 100 & 200Nm) are compared in the same plot. The magnitude of MEs increases with the larger loads as the deflection of the meshing teeth become greater with the larger loads. The change in the amount of ME is roughly in linear relationship with the load, which reflects the linear elastic behaviour of the gear tooth deflection. Note the square pattern of the ME, which resulted from the time (or angular position) dependent variation of gear mesh stiffness, due to the alternating single and double tooth engagement.

The plots presented in Figures 3.1.5 (b) & (c) show the MEs of the gears with tooth fillet cracks of three different sizes. The localized increase in the amount of ME over a period of ME pattern is a direct consequence of the reduced gear tooth stiffness caused by the TFC.

The plots shown in Figure-3.1.6 (a)  $\sim$  (c) are the residual ME (RME) obtained by taking the difference between the MEs of uncracked gears and the ones with TFCs. The RMEs show a "double stepped" pattern that reflects the tooth meshing pattern of the gears, where smaller step with less deflection occurs as the crack tooth enters the mesh and share the load with the adjacent tooth; the larger second step follows when the cracked tooth alone carries the load.

The RMEs of the TFCs show linearly proportional relationship between the amount of loading and the change in RME for a given crack size. The linear relationship between the loading and the amount of tooth deflection on a cracked gear tooth indicates that the effect of TFC can be modelled effectively as a localized change in the gear mesh stiffness.

The plots in Figure-3.1.7 show the transmission errors (TEs) measured from a pair of plastic gears with a root fillet cut (Figure-3.1.7 (a)), which the cut replicates a tooth fillet crack. The TEs of Figure 3.1.7 (c1-c3 and d1-d3) are compared to the simulated patterns of MEs (figure 3.1.7 (b)). Composite TEs (CTEs) and the zoomed view of the CTEs are shown in Figure-3.1.7 (c1 & d1) and (c2 & d2) respectively. The CTE combines the both long and short term components of the TE (LTC and STC) presented earlier in section 2.2 (figure 2.2.1). The resemblance between the simulated MEs and measured the TEs confirms the validity of the simulated effect of TFC. The STCs (c3 & d3) were obtained by high pass filtering the CTE. The pattern in the STCs shows clear resemblance to the simulated TFC effect (Figure3.1.7 (b)).

The simulation model used in this study does not consider the effect of plasticity. This assumption can be justified for a gear tooth with small cracks where localised effect of plasticity at the crack tip has small influence on the overall deflection of the gear tooth, which is most likely the case for the ideal fault detection scenario.

More recent work published by Mark [57, 60] explains that the plasticity can become a significant factor when work hardening effect can cause a permanent deformation of the cracked tooth. In this case, the meshing pattern of the gears changes more definitively by the geometrical error introduced in the gears by the bent tooth. In some cases the bent tooth result in rather complex meshing behaviour that involves tooth impacting. Further explanation on this topic is available from the works published by Mark [57, 60].

Within the limitation of the simulated TFC model discussed above, the approach to model the TFC as a localized variation in the gear mesh stiffness is acceptable for a small crack emerging in the gear tooth fillet area. For the purpose of developing a dynamic simulation model of a geared transmission system with an emerging TFC the model presented here offers a reasonable approach.

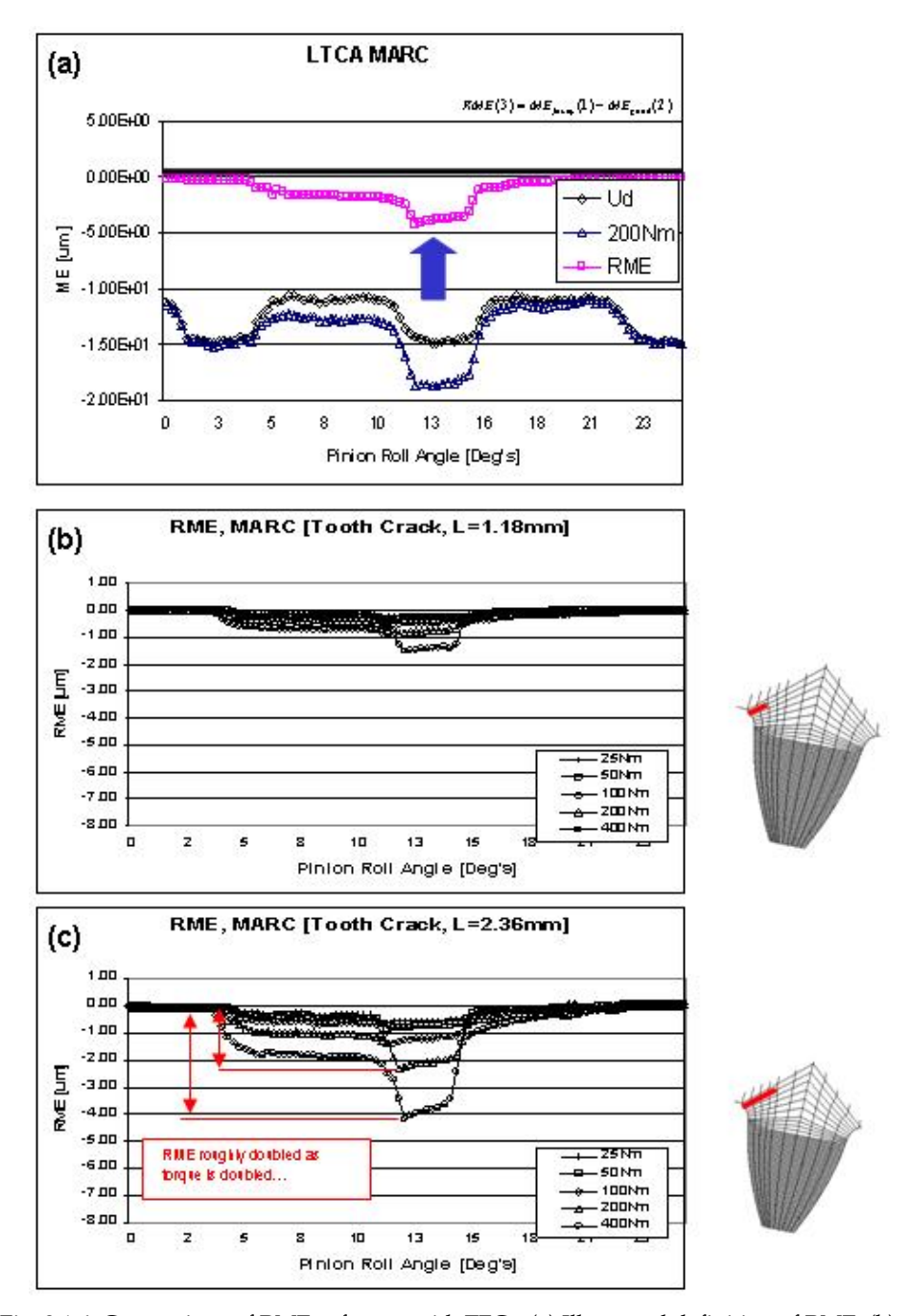


Fig. 3.1.6. Comparison of RMEs of gears with TFCs; (a) Illustrated definition of RME; (b) RMEs of TFC sizes L=1.18mm; (c) RMEs of TFC sizes L=2.36mm.

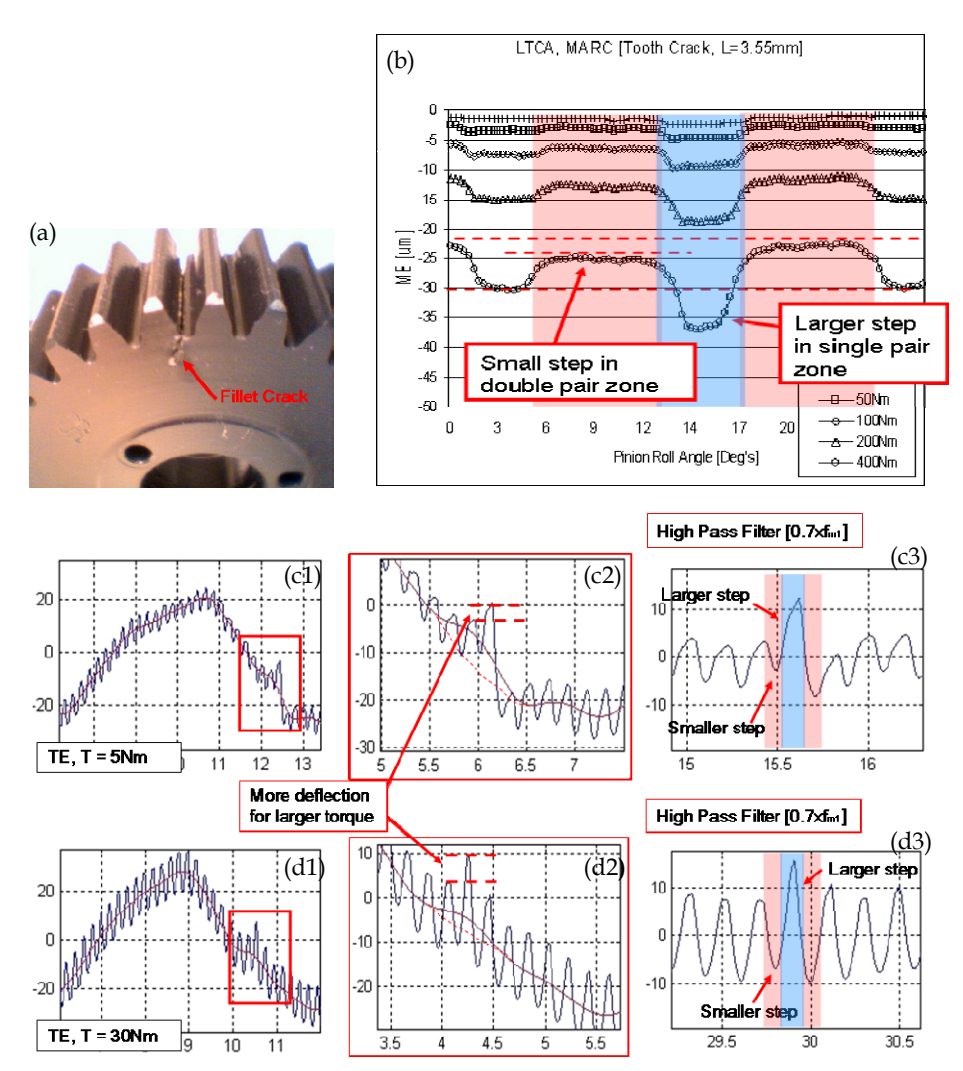


Fig. 3.1.7. Comparison of simulated vs. measured transmission errors; (a) Picture of a gear with a seeded TFC; (b) MEs from a FE model. (c1)  $\sim$  (c3) TEs of the gears with TFC loaded with 5Nm; (d1)  $\sim$  (d3) TEs of the gear with TFC loaded with 30Nm; CTE (c1, d1), Zoomed views (c2, d2) and STC (c3, d3).

# 3.2 Modelling the effect of a spall on a tooth face of a gear

Symptoms of surface fatigue vary, but they can generally be noticed by the appearance of cavities and craters formed by removal of surface material. The damage may start small or large and may grow or remain small. In some cases gears cure themselves as they wear off the damage: Initial pitting [47]. The terms "Spalling" and "Pitting" are often used indiscriminately to describe contact fatigue damages. Figure-3.2.1 shows some examples of

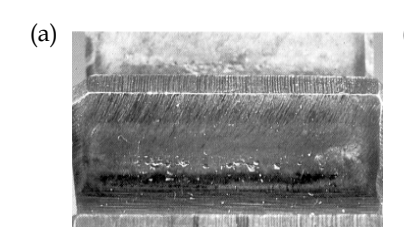




Fig. 3.2.1. Examples of (a) progressive pitting and (b) severe spalling damages on gear teeth. (DANA [48])

spalls and pitting occurring on a gear tooth. This work follows the definition of contact surface damage given by Tallian [58]: Spalling designated only as macro-scale contact fatigue, reserving the term pitting for the formation of pores and craters by processes other than fatigue cracking.

There are three distinctive phases in the development of surface fatigue damage:

- 1. Initial Phase: Bulk changes in the material structure take place around the highly stressed area under the contact path. Change in hardness, residual stress and some microscopic changes in the grain structure of the metal.
- 2. A Long Stable Phase: Microscopic flow occurs in the highly stressed area changing the material structure and residual stress conditions at the microscopic level. The change in the structure brought out by the microscopic flow can be observed by eyes in the illuminated etched areas.
- 3. Macroscopic Cracking: This is the last failure phase instituting the crack growth.

Spalls have a distinctive appearance that is characterised by how they were formed. A fully developed spall typically has its diameter much larger than its depth. The bottom of the spall has a series of serrations caused by propagating fatigue cracks running transverse to the direction of rolling contact. The bottom of the spall parallels the contact surface roughly at the depth of maximum unidirectional shear stress in Hertzian contact.

The sidewalls and the wall at the exiting side of the spall (as in the exiting of rolling contact) are often radially curved as they are formed by material breaking away from the fatigued area. The entrance wall of the spall is characterised by how it was initiated. Tallian [58] explains that shallow angled entry (less than 30° inclination to the contact surface) occurs when the spall is initiated by cracks on the surface. Spalls with steep entry (more than 45°) occur when the spall is initiated by subsurface cracks.

Surface originated spalls are caused by pre-existing surface damage (nicks and scratches). It is also known that lubrication fluid could accelerate the crack propagation when contact occurs in such a way that fluid is trapped in the cracks and squeezed at extremely high pressure as the contacting gear teeth rolls over it.

The subsurface originated spalls are caused by presence of inclusions (hard particles and impurities in the metal) and shearing occurs between the hard and the soft metal layers formed by case hardening. A spall caused by the initial breakage of the gear tooth surface continues to expand by forming subsequent cracks further down the rolling direction. Figure-3.2.2 illustrates the formation and expansion of spall damage by Ding & Rieger [59].

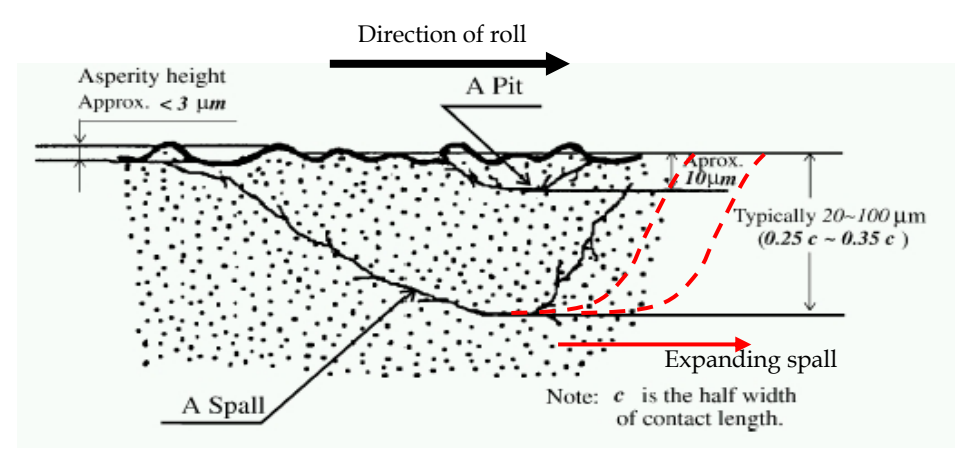


Fig. 3.2.2. Formation and expansion of spalls. (Ding & Rieger [59])

The result of contact stress analysis from HyGears [50] shows the occurrence of high stress concentration at the entrance and exit walls of the spall (Figure-3.2.3). The high stress concentration at these edges implies the likelihood of damage propagation in that direction. The result of the simulation corresponds to Tallian's [58] observation that spalls tend to expand in the direction of rolling contact. In the HyGears simulation the spall was modelled as a rectangular shaped recess on the tooth surface in the middle of the pitch line.

Typical spur gear tooth surfaces are formed by two curvatures: profile and lead curvatures. The 2D models are limited to simulating the effect of the spall crater on the gear tooth profile only. 3D simulation is required to comprehend the complete effect of spalls on the

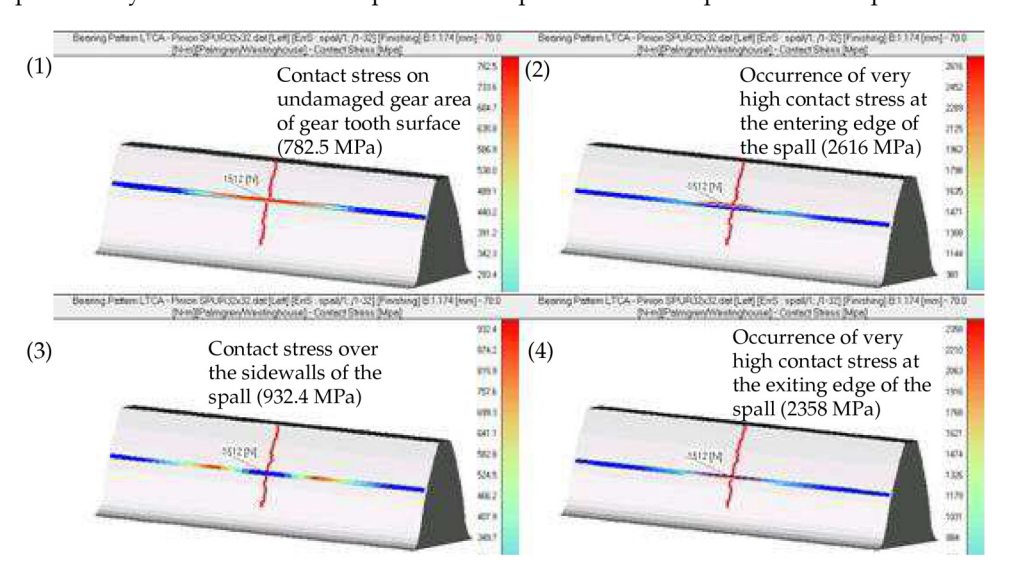


Fig. 3.2.3. HyGears analysis of contact stresses around the spall. [62]

contact surface of the gears. A study was carried out to investigate the effect of spalls on the ME using a 3D gear tooth model [62]. The result of the study showed that the effect of the spalls on the ME is completely dominated by the displacement caused by the topological error of the gear tooth surface caused by the fault.

Formation of spalls is a complicated process and it is one of the active research topics which have been studied for some time. Although there are several items in the literature that describe the properties and process of formation of spalls, no literature was sighted which defines the specific definition of shapes and sizes of spalls occurring on spur gear teeth.

Papers presented by Badaoui et al. [63, 64] and Mahfoudh et al. [65] show a successful example of simulating the effect of a spall on spur gear tooth by modelling the fault as prismatic slot cut into the gear tooth surface. Their results were validated by experiment. The model of the spall used in this work follows the same simplification of the general shape of the spalling fault. The simulation of the spall is bounded by these following assumptions:

- A spall is most likely to initiate at the centre of the pitchline on a gear tooth where maximum contact stress is expected to occur in the meshing spur gear teeth as the gears carry the load by only one pair of teeth.
- 2. The spall expand in size in the direction of rolling contact until it reaches the end of the single tooth pair contact zone as shown in Figure-3.2.4.
- 3. When the spall reaches the end of the single tooth pair contact zone, the spall will then expand across the tooth face following the position of the high contact stresses. The contact stress patterns shown in Figure-3.2.3 strongly support this tendency of spall growth.

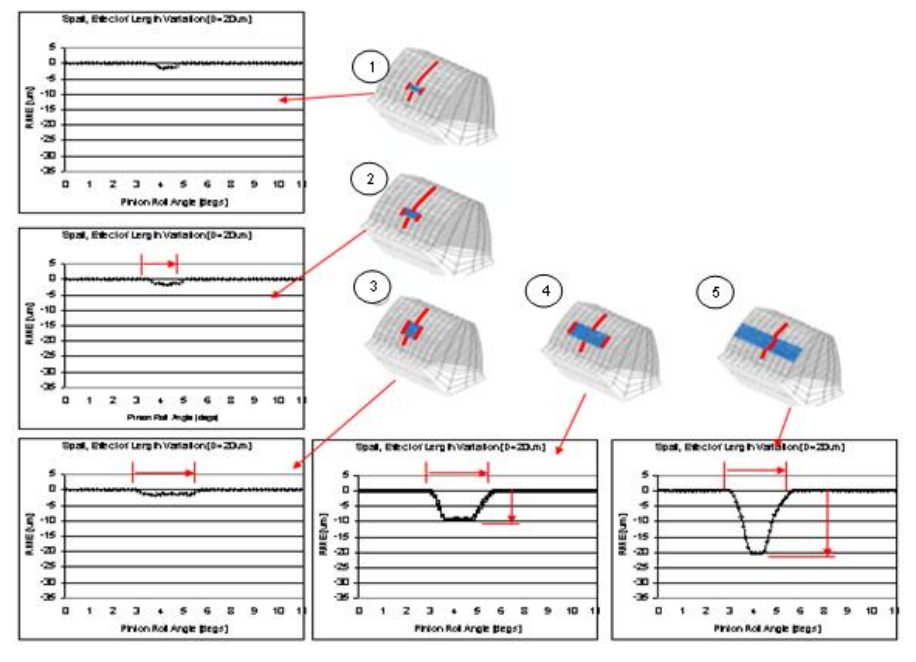


Fig. 3.2.4. A model of spall growth pattern and the resulting RME. [62]

The models of spalls were developed by following the set of assumptions described above. Resulting plots of the RMEs are presented in Figure-3.2.4 along with the shape illustration of spalls on a gear tooth. Note that the RMEs of the spalls form bucket shapes and their length and the depth are determined by the length and width of the spall; i.e. the shape of RME and the progression of the spall is directly related. This information can be used in diagnosis and prognosis of the fault.

The plots in Figure-3.2.5 show TEs measured from a pair of plastic gears with a spall (Figure-3.2.5 (a)). The change in the pattern of the TE due to the spall is comparable to the simulated pattern of the MEs (Figure-3.2.5 (b)). Composite TEs (CTEs) and the zoomed views of the CTEs are shown in Figure-3.2.5 (c1~c3). The resemblance between the simulated MEs and measured TEs confirms the validity of the simulated effect of TFC. The STCs (d1~d3) were obtained by high pass filtering the CTE. The pattern in the STCs shows clear correlation between the simulated and measured patterns of spall motion errors.

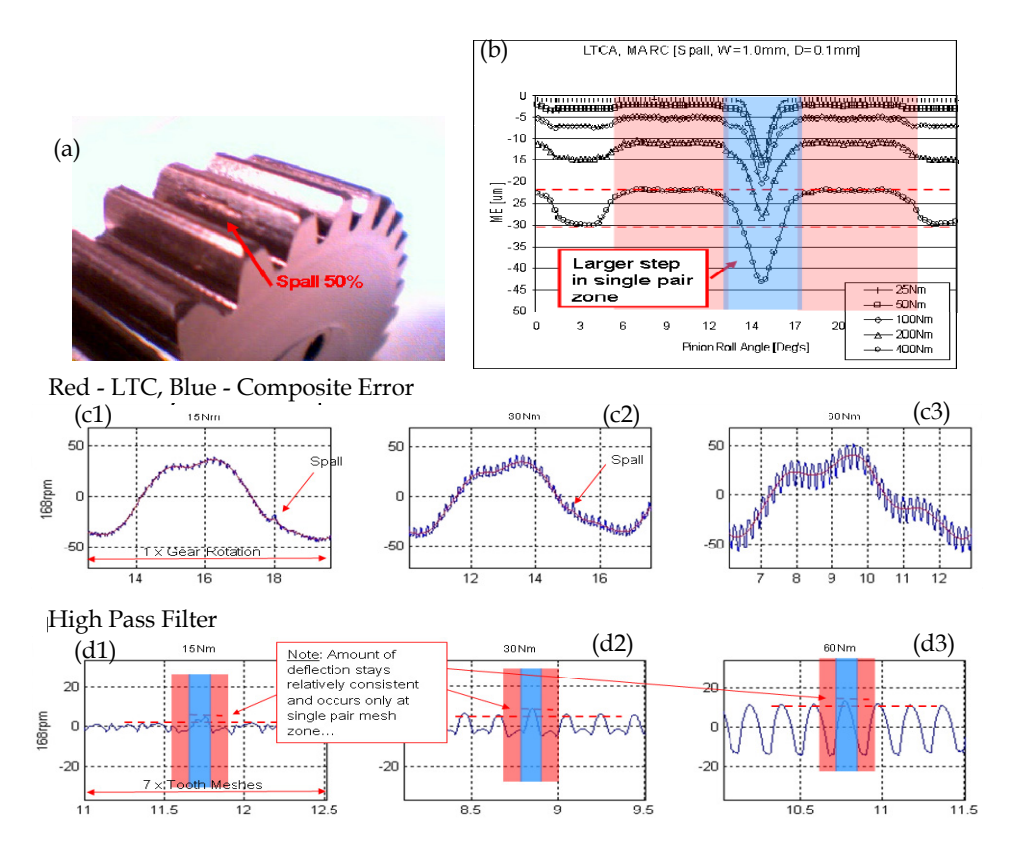


Fig. 3.2.5. Comparison of simulated vs. measured transmission errors; (a) Picture of a gear with a seeded Spall; (b) MEs from a FE model; (c1)  $\sim$  (c3) CTEs of the gear with the spall; (d1)  $\sim$  (d3) STCs of the gear with the spall; Applied torque: 15Nm (c1 & d1), 30Nm (c2, d2), 60Nm (c3, d3).

# 3.3 Simulating the effect of TFCs and spalls in a gear dynamics model

The FEA model based study of TFCs and spalls has lead to identifying some useful properties of the faults that can be used to model the effect of the faults in the lamped parameter type gear dynamics models.

The Residual Motion Errors (RME) of TFCs have shown double stepped patterns that were load dependent. The change in the amount of deflection in the gear mesh (i.e. ME) with a cracked tooth is influenced by the size of the crack and also by the amount of loading on the gears. The simulation result showed that the linearly proportional relationship between the torque applied to the gears and the resulting RME value. The bucket shaped RMEs of spalls were not affected by the loading condition but purely driven by the change in the contact path patterns of the meshing teeth, due to the geometrical deviation of the gear tooth surface caused by a spall. It was also understood from the simulation studies that the size and the shape of a spall affect the length and the depth of the bucket.

Based on the observation above, the effect of TFC was modelled as locally reduced tooth meshing stiffness and the spalls as direct displacement due to the topological alteration of the gear tooth surface. In the gear dynamic model is shown in Figure-3.3.1, the effect of a TFC was implemented as a reduction in stiffness " $K_m$ " over one gear mesh cycle. The change in the value of  $K_m$  was calculated from the FEA model mapped into an angular position dependent function in the gear dynamic model. A spall was implemented as a localized displacement mapped on the " $e_t$ ". An illustration of a TFC and a spall models in a gear rotor dynamic model is shown in Figure-3.3.1 [61].

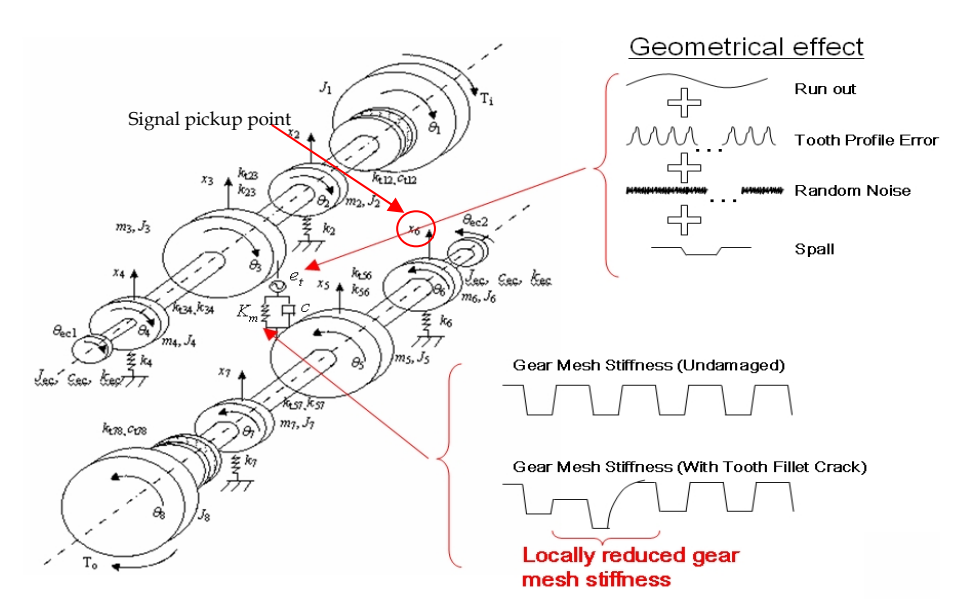


Fig. 3.3.1. Modelling of Gear Tooth Faults in Dynamic Model. [61]

Figures 3.3.2 (a1~a3) and 3.3.3 (a1~a3) show the simulated vibration signal (acceleration) from the LPM shown in the Figure-3.3.1. The signals were measured from the free end of the

driven shaft (see Figure-3.3.1). The residual signals shown in (b1~b3) of Figures 3.3.2 and 3.3.3 were obtained by subtracting the simulated vibration of undamaged gearbox from the damaged one. Two identical simulation models, one with a gear tooth fault (TFC or spall) and the other undamaged, were run in parallel and the difference between the two model out puts were taken to separate the effect of the gear faults. The impact like effect of the gear tooth faults is seen in both the gears with a TFC and a spall.

A comparison of the simulated signals shows that the magnitude of the TFC impulses is affected by the amount of torque applied to the gears, while the spall impulses are not. This response is consistent with the observation made in the static simulation of the gears in mesh.

Careful observation of the residual signal also reveals that the fault information is not only buried in the dominant effect of gearmesh, but also somewhat distorted by the effect of transmission path from the gearmesh to the point where the signal was measured. The effect of transmission path appears in the residual signal As the transient "tail" effect convolved over the impulse due to the gear fault (see Equation-3.3.1 and Figure-3.3.4 for illustration).

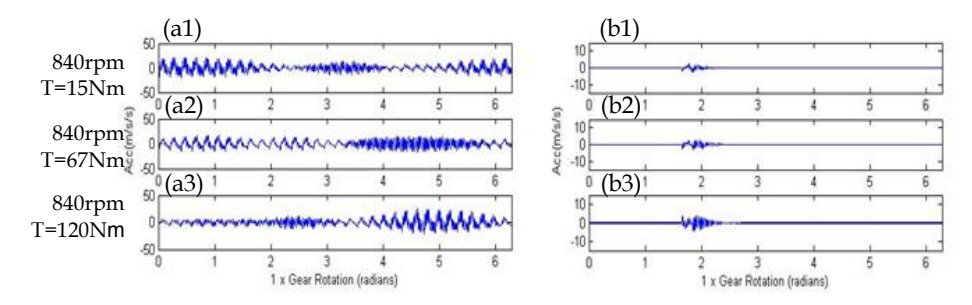


Fig. 3.3.2. Simulated gearbox vibration signal with the effect of a TFC.

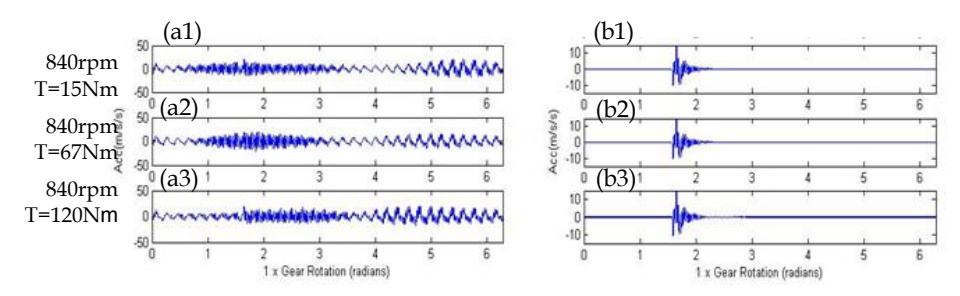


Fig. 3.3.3. Simulated gearbox vibration signal with the effect of a spall.

The residual signal of the TFC and the spall provide a useful means to understand the nature of diagnostic information of the faults. In machine condition monitoring signal processing techniques are often developed to detect and quantify the symptoms of a damage buried in a background noise. By being able to see the "clear" effect of a fault, the most effective signal processing technique can be applied to target and monitor the symptoms of the damage. The idea of using the simulated fault signals to design and improve the fault detection and machine condition monitoring techniques has been put to effective uses by Randall, Sawalhi and Endo [34, 35, 62, 66].

$$y = (e + w + n) * h$$
 (Note: \* represents convolution) (3.3.1)

# e: deterministic gear excitation (inherent in gear vibration)

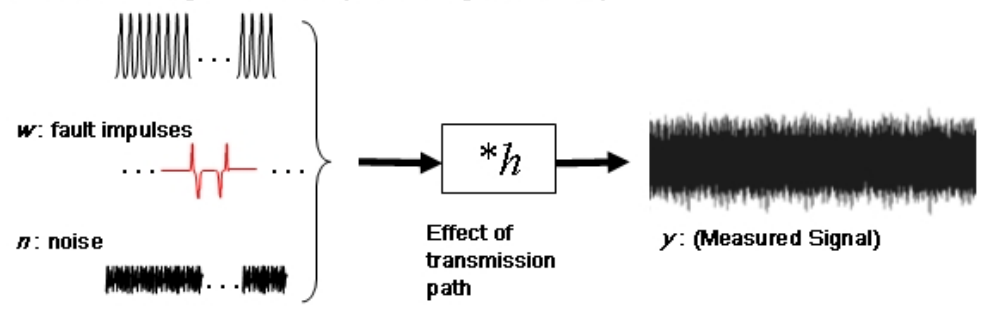


Fig. 3.3.4. Vibration of a Gearbox. [62]

# 3.4 Modelling a spall in a rolling element bearing

This section discusses a several simple but an effective methods of modelling a spall in the rolling element bearing model introduced previously in section 2.5.1. The ideas behind each modelling approach was discussed by using the example of modelling a spall in the outer race of a bearing. The same method can be easily expanded in to modelling an inner race spall and ball faults. More detailed explanation on this topic is available from the work published by Sawalhi and Randall [29, 30, 31, 34, 35, 66, 67].

The simplest form of a spall model can be implemented to the REB model by assuming instantaneous contact loss between the bearing races and rollig an element(s) as it pass over the spall. So, in reference to the rolling element model described above, the presence of a spall of a depth ( $C_d$ ) over an angular distance of ( $\Delta\phi_d$ ) can be modelled by using the fault switch  $\beta_j$  which defines the contact state of rolling elements over a defined angular position ( $\phi_d$ ). In effect, this mothod models the spall as a step function as shown in Figure-3.4.1 and further illustrated by Figure-3.4.2 (a), in which  $\beta_j$  is defined as follows:

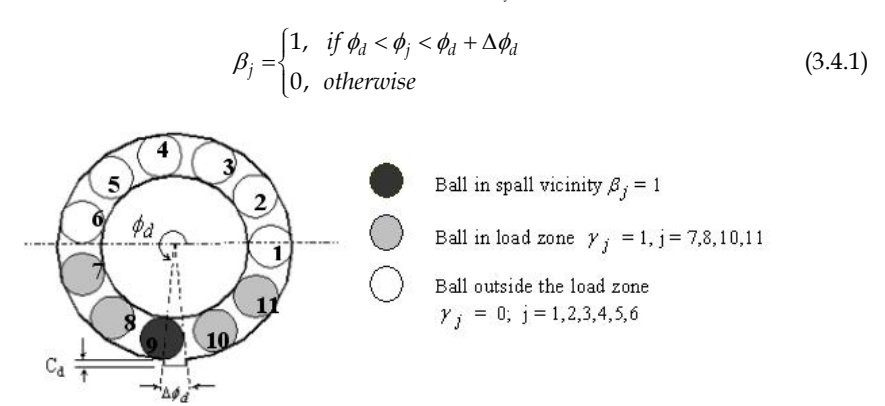


Fig. 3.4.1. Spall definition on the outer race [66]



Fig. 3.4.2. Modified model of a spall based on a more realistic ball trajectory. [66]

The outer race spall is fixed in location between  $\phi_d$  and  $\phi_d + \Delta \phi_d$ . This normally occurs in the load zone. An inner race spall rotates at the same speed as the rotor, i.e.  $\phi_d = \omega_c dt + \phi_{do}$  ( $\phi_{do}$ : initial starting location of the spall).

This model of the spall assumes that the rolling element will lose contact suddenly once it enters the spall region, and will regain contact instantly when exiting from that area (Figure-3.4.2 (a)). The abrupt change in the rolling element positions at the entry and exit of the spall results in very large impulsive forces in the system, which is not quite realistic. An modification on the previous model was introduced in [28] in which the depth of the fault ( $C_d$ ) was modelled as a function of ( $\phi_j$ ), Figure-3.4.2 (b). The improvement on the model is to represent more realistic trajectory of the rolling element movement based on the relative size of the rolling element and the depth of the spall. Although, the profile of the trajectory appears much less abrupt than the earlier version; and apears to have only one position that may result in impulse, it still resulted in two impulses which does not agree with the experimental observation.

Careful observation of the interaction between the rolling element and spall leads to the trajectory is shown in Figure-3.4.3. The entry path of the rolling element has been represented as having a fixed radius of curvature (equal to that of the rolling element); entry of the rolling element in to the spall is therefore somewhat smoother. The smoother change in curvature at the entry would then represent a step in acceleration. On exiting the spall, the centre of the rolling element would have to change the direction suddenly, this representing a step change in velocity or an impulse in acceleration. This has been modelled as a sudden change (i.e. similar to the original model [28]). The resulting acceleration signal

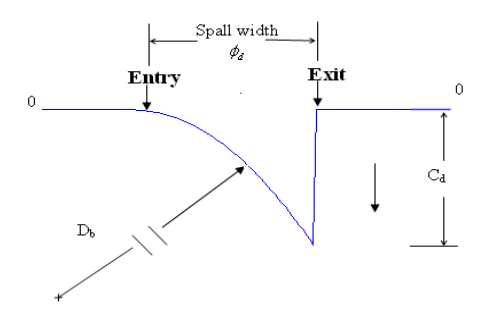


Fig. 3.4.3. A correlated model of a spall based on experimental data.

from this model appears to agree with the experimental observation, however author recommends further validation on this modelling approach and more updates are expected based on the findings.

For more detailed explanations on the modelling of REB fault refer to the works published by Sawalhi & Randall [29, 30, 31, 34, 35, 66, 67].

#### 4. Conclusion

The techniques for modelling the effect of gearbox faults: tooth fillet cracks, tooth face spalls and bearing spalls, were presented and discussed in this chapter. The main purpose of the damage modelling is to simulate the effect of the faults on the dynamics of a geared transmission system that can be used in improving the understanding of the diagnostic information that manifest in the vibration signal mix from a gearbox.

The fault detection and diagnostic techniques based on vibration signal analysis are the ideal non-destructive machine health monitoring method, that can be applied in a minimally intrusive manner; i.e. by attaching an accelerometer on a gearbox casing. However, the dynamic interaction amongst the machine elements of a gearbox is often complex and the vibration signals measured from the gearbox is not easy to interpret. The diagnostic information that directly related to an emerging fault in a gear or a bearing is typically buried in the dominating signal components that are driven by the mechanisms of the transmission system themselves: For example, gear meshing signals.

Traditionally, the researchers worked on development of a signal processing technique for the gearbox diagnosis have embarked on their endeavours by making educated assumptions on the properties of the diagnostic information of the faults. These assumptions are often based on their careful observation of a measured vibration signals. However, the relevance of this approach is often somewhat limited by the simple fact that it's not easy to observe the key details of the fault signals from the signal mix.

It was demonstrated in this chapter how simulation models can be put to effective uses for studying the properties of the fault signals in greater details. A method of isolating the fault signals from the simulated gearbox signal mix was described in the section 3.3. The residual signals obtained from this process showed how the faults manifested in the resulting vibration signals in the "cleaned" state. The observation of the simulated residual signals has led to an improved understanding of the characteristics of impulses caused by the faults and the distorting effect of the transmission path (from the origin of the fault signal to the measurement location). The improved understanding of the fault signal obtained from the simulation studies led to the development of more effective signal processing techniques [34, 35, 62, 66].

The models of the gearbox faults presented in this work require further refinement. Some of the areas of future improvement aforementioned in the main body of the chapter include; improving the understanding of; the effect of plastic deformation in gear TFC, the effect of spall shapes and the effect of non-linear dynamic interaction of the gears and bearings. Improving the correlation between the simulated and the measured signals is a good way to demonstrate the understanding of the effect of faults in a geared transmission system. This

knowledge compliments the design and development efforts in vibration signal analysis based machine condition monitoring technologies. In the near future, accurately simulated signals of a faulty gearbox can aid the machine learning process of fault diagnosis algorithms based on neural networks. Performing this task in experiments are time consuming and costly exercise; simulation model based approach appears much more desirable.

The authors hope that the work presented in this chapter will stir the thoughts and the new ideas in readers that will contribute to the advancement of the gear engineering and the technologies in detecting and diagnosing the incipient faults in geared transmission systems.

# 5. Nomenclature

Unless otherwise stated the following tables defines the symbols and the acronyms used in this chapter.

$\overline{A_1A}_2$	A vector connecting points $A_1$ and $A_2$
Ø	Pressure Angle
LoA	Line of Action
PoA	Plane of Action
LoC	Line of Centres
$R_{b}$ , $r_{b}$	Gear Base Radius and Pinion Base Radius
$R_{gear}$ , $r_{pinion}$	Gear Pitch Radius and Pinion Pitch Radius
R <sub>o</sub> and r <sub>o</sub>	Gear Outer Radius Pinion Outer Radius
$P_b$	Base pitch
CR	Contact Ratio
N	Number of teeth on a gear
TE	Transmission Error (Measured experimentally)
GTE	Geometrical Transmission Error
STE	Static Transmission Error
LTC	Long Term Composite of TE
STC	Short Term Composite of TE
ME	Motion Error (Numerically calculated TE)
$x_i, y_i, z_i$	Translation at $i_{th}$ Degrees of Freedom
$\theta$ xi, $\theta$ yi, $\theta$ zi	Rotation about a translational axis at $i_{th}$ Degrees of Freedom
$K$ , $K_{mb}$	Linear stiffness elements. The subscript $'mb'$ refers to stiffness at the gearmesh
$C$ , $C_{mb}$	Damping matrices. The subscript 'mb' refers to damping at the gearmesh.
Н	An 'on/off' switch governing the contact state of the meshing gear teeth.
$\underline{e_t}$	A vector representing the combined effect of tooth topography deviations and misalignment of the gear pair.
T	Torque

 $\underline{x}$ ,  $\dot{x}$ ,  $\ddot{x}$  Vectors of displacement, velocity and acceleration (translation)

 $\sigma$  Stress  $\varepsilon$  Strain

## 6. References

- [1] J. D. Smith, and D. B. Welbourn, 2000, "Gearing Research in Cambridge", Cambridge Gearing Publications
- [2] R. E. Smith, 1983, "Solving Gear Noise Problems with Single Flank Composite Inspection", The Gleason Works, Rochester, NY, USA
- [3] R. G. Munro, D. Houser, 2004, "Transmission Error Concepts", Notes from Gear Noise Intensive Workshop, 19th ~ 21st July 2004, Melbourne, Australia
- [4] R. W. Gregory, S. L. Harris and R. G. Munro, 1963a, "Dynamic Behaviour of Spur Gears", Proc IMechE, Vol. 178(1), pp 207-218
- [5] R. W. Gregory, S. L. Harris and R. G. Munro, 1963b, "Torsional Motions of a Pair of Spur Gears", Proc IMechE Applied Mechanics Convention, Vol. 178 (3J), pp 166-173
- [6] H. N. Ozguven and D. R. Houser, 1988a, "Mathematical Models Used in Gear Dynamics

   A Review", Journal of Sound and Vibration, 121(3), pp 383-411
- [7] C. C. Wang, 1985, "On Analytical Evaluation of Gear Dynamic Factors Based on Rigid Body Dynamics", Journal of Mechanism, Transmission and Automation in Design, Vol. 107, pp 301-311
- [8] W. Bartelmus, 2001, "Mathematical Modelling and Computer Simulations as an Aid to Gearbox Diagnostics", Mechanical Systems and Signal Processing, 15 (5), pp 855-871
- [9] J. Lin and R. G. Parker, 2002, "Mesh Stiffness Variation Instabilities in Two-Stage Gear Systems", Transaction of ASME, Jan 2002, Vol. 124, pp 68-76
- [10] R. G. Parker and J. Lin, 2001, "Modelling, Modal Properties, and Mesh Stiffness Variation Instabilities of Planetary Gears", NASA, NASA/CR-2001-210939
- [11] Y. Gao and R. B, Randall, 1999, "The Effect of Bearing and Gear Faults in Rolling Element Bearing Supported Gear Systems", DSTO Aeronautical and Maritime Research Laboratory, July 1999, CEVA-99-02
- [12] Y. Gao and R. B. Randall, 2000, "Simulation of Geometric, Static and Dynamic Gear Transmission Errors", DSTO Aeronautical and Maritime Research Laboratory, Jan 2000, CEVA-2000-01
- [13] M. Amabili, and A. Rivola, 1997, "Dynamic Analysis of Spur Gear Pairs: Steady-State Response and Stability of the SDOF Model with Time Varying Meshing Damping", Mechanical System and Signal Processing, 11 (3), pp 375-390
- [14] I. Howard, S. Jia and J. Wang, 2001, "The Dynamic Modelling of a Spur Gear in Mesh Including Friction and A Crack", Mechanical Systems and Signal Processing, 15 (5), pp 831-853
- [15] P. Velex and M. Maatar, 1996, "A Mathematical Model for Analysing the Influence of Shape Deviations and Mounting Error on Gear Dynamic Behaviour", Journal of Sound and Vibration, 191(5), pp 629-660
- [16] S. M. Vijayakar, 1991, "A Combined Surface Integral and Finite Element Solution for a Three-Dimensional Contact Problem", International Journal of Numerical Methods in Engineering, 31, pp 524-546

- [17] G. W. Blankenship and R. Singh, 1995, "A New Gear Mesh Interface Dynamic Model to Predict Multi-Dimensional Force Coupling and Excitation", Mechanical, Machine Theory, Vol. 30, No.1, pp43-57
- [18] A. Kahraman and G. W. Blankenship, 1996, "Interactions between Commensurate parametric and Forcing Excitations in A System with Clearance", Journal of Sound and Vibration, 194 (3), pp 317-336
- [19] R. G. Parker, 2000, "Non-Linear Dynamic Response of a Spur Gear Pair: Modelling and Experimental Comparisons", Journal of Sound and Vibration, 237(3), pp 435-455
- [20] R. G. Parker, V. Agashe and S. M. Vijayakar, 2000, "Dynamic Response of a Planetary Gear System Using a Finite Element/Contact Mechanics Model", Transaction of ASME, Sep 2000, Vol. 122, pp 304-310
- [21] CALYX, 2002, CALYX USER MANUAL, Advanced Numerical Solutions, Hilliard Ohio, U.S.A
- [22] HELICAL, 2002, HELICAL 3D USER's MANUAL, Advanced Numerical Solutions, Hilliard Ohio, U.S.A
- [23] S. Du, 1997, "Dynamic Modelling and Simulation of Gear Transmission Error for Gearbox Vibration Analysis", PhD dissertation, University of New South Wales
- [24] N. S. Feng, E. J. Hahn, and R. B. Randall, 2002, "Using transient analysis software to simulate vibration signals due to rolling element bearing defects", Proceedings of the 3rd Australian congress on applied Mechanics, 689-694, Sydney.
- [25] I. K. Epps and H. McCallion, 1994, "An investigation into the characteristics of vibration excited by discrete faults in rolling element bearings" (extract from PhD thesis of I.K. Epps), Annual Conference of the Vibration Association of New Zealand, Christchurch.
- [26] D. Ho, 1999, "Bearing Diagnostics and Self Adaptive Noise Cancellation", PhD dissertation, UNSW.
- [27] S. Fukata, E. H. Gad, T. Kondou, T. Ayabe and H. Tamura, 1985, "On the Vibration of Ball Bearings", Bulletin of JSME, 28 (239), pp. 899-904.
- [28] A. Liew, N.S. Feng and E. J. Hahn, 2002, "Transient rolling element bearing systems", Trans. ASME Turbines and Power, 124(4), pp. 984-991
- [29] N. Sawalhi and R.B. Randall, 2011, Vibration response of spalled rolling element bearings: observations, simulations and signal processing techniques to track the spall size. Mechanical Systems and Processing, 25 (3), (2011)
- [30] N. Sawalhi and R.B. Randall, 2010, "Improved simulations for fault size estimation in rolling element bearings", paper presented at the seventh International Conference on Condition Monitoring and Machinery Failure Prevention Technologies, Stratford-upon-Avon, England, 22-24 June (2010).
- [31] N. Sawalhi and R.B. Randall, 2008, "Localised fault diagnosis in rolling element bearings in gearboxes", paper presented at the Fifth International Conference on Condition Monitoring and Machinery Failure Prevention Technologies, Edinburgh, 15-18 July (2008).
- [32] J. Sopanen & A Mikkola, 2003, "Dynamic model of a deep-groove ball bearing including localized and distributed defects. Prt 1: Theory", Proc of IMechE, vol. 217, Prt K, J of Multi-body Dynamics, 2003, pp 201-211.
- [33] T. Tiwari, K. Gupta, O. Prakash, 2000, "Dynamic response of an unbalanced rotor supported on ball bearings", J of Sound & Vibration 238 (2000), pp757-779.

- [34] N. Sawalhi & R. B. Randall, 2008, "Simulating gear and bearing interaction in the presence of faults: Prt II Simulation of the vibrations produced by extended bearing faults", MSSP, Vol. 22, pp1952-1996 (2008).
- [35] N. Sawalhi & R. B. Randall, 2008, "Simulating gear and bearing interaction in the presence of faults: Prt I The combined gear bearing dynamic model and simulation of localized bearing faults", MSSP, Vol. 22, pp1924-1951 (2008).
- [36] Z.-Q. Qu, 2004, "Model order reduction technique: with applications in Finite Element Analysis", Springer, 2004.
- [37] R. Craig & M. Bumpton, 1968, "Coupling of substructures of dynamic analysis", AIAA Journal, 67 (1968), pp1313-1319.
- [38] B. M. Irons, 1967, "Structural eigenvalue problem-elimination of unwanted variables", AIAA Journal, 3(5), pp961-962.
- [39] L. Despnade, N.Sawalhi, R.B.Randall, "Improved Gearbox Simulations for Diagnostic and prognostics Purposes Using Finite Element Model Reduction Techniques", paper presented at the 6th Australasian Congress on Applied Mechanics, Perth, Australia, 12-15 December (2010
- [40] C. Carmignani, P. Forte & G. Melani, 2009, "Component modal synthesis modelling of a gearbox fro vibration monitoring simulation", The 6th Int'l conf on Condition Monitoring Manhinery Failure Prevention Technology, Dublin, Ireland.
- [41] N. Sawalhi, L. Deshpande and R. B. Randall, 2011, "Improved simulation of faults in gearboxes for diagnostic and prognostic purposes using a reduced finite element model of casing", AIAC 14 Fourteenth Australian International Aerospace Congress.
- [42] R. Singh, 1989, "Analysis of Automotive Neutral Gear Rattle", Journal of Sound and Vibration, Vol. 131 (2), pp177-196
- [43] A. Kahraman and R. Singh, 1991, "Interaction between Time-Varying Mesh Stiffness and Clearance Non-Linearity in Geared System", Journal of Sound and Vibration", 146, pp135-156
- [44] D. P. Townsend, 1997, "Gear and Transmission Research at NASA", NASA-TM-107428
- [45] A. K. Wong, 2001, "Vibration-Based Helicopter Health Monitoring An Overview of the Research Program in DSTO", DSTO-HUMS2001
- [46] L. E. Alban, 1985, "Systematic Analysis of Gear Failure", American Society of Metals, Metals Park OH, ISBN-0871702002
- [47] G. DeLange, 1999, "Analyzing Gear Failures", Hydrocarbon Processing, Features: 4/00, www.hydrocarbonprocessing.com
- [48] DANA, 2002, Raodranger, "Understanding Spur Gear Life", EATON and DANA Corporation, TRSM-0913, (www.roadranger.com)
- [49] ANSI/AGMA, 1995, "Appearance of Gear Teeth Terminology of Wear and Failure", American Gear Manufacturers Association, ANSI/AGMA 1010-E95
- [50] HyGears, HyGears © V2.0 Gear Design and Analysis Software, Involute Simulation Software Inc
- [51] D. G. Lewicki, 2001, "Gear Crack Propagation Path Studies Guidelines for Ultra-Safe Design", NASA-TM- 2001 211073
- [52] T. J. Curtin, R. A. Adey, J. M. W. Bayman and P. Marais, 1998, Computational Mechanics Inc, Billerica, Massachusetts, 01821, USA

- [53] D. G. Lewicki, 1998, "Three-Dimensional Gear Crack Propagation Studies", NASA-TM-1998-208827
- [54] S. Pehan, T. K. Hellen, J. Flasker and S. Glodes, 1997, "Numerical Methods for Determining Stress Intensity Factors VS Crack Depth in Gear Tooth Roots", Int J of Fatigue, Vol. 19, No. 10, pp677-685
- [55] M. Guagliano and L. Vergani, 2001, "Effect of Crack Closure on Gear Crack Propagation", Int J or Fatigue, Vol. 23, pp67-73
- [56] H. Endo, C. Gosselin, R. B. Randall, (Sept 2004), "The effects of localized gear tooth damage on the gear dynamics A comparison of the effect of a gear tooth root crack and a spall on the gear transmission error", IMechE, 8th International Conference on Vibrations in Rotating Machinery, University of Wales, Swansea
- [57] W. D. Mark, C. P. Reagor and D. R. McPherson, 2007, "Assessing the role of plastic deformation in gear-health monitoring by precision measurement of failed gears", MSSP, 21: pp177-192 (2007)
- [58] T. E. Tallian, 1992, "Failure Atlas fir Hertz Contact Machine Elements", ASME Press, ISBN 0-7918-0008-3
- [59] Y. Ding and N. F. Rieger, 2003, "Spalling formation Mechanism for Gears", Wear, 254 2003), pp1307-1317
- [60] W. D. Mark and C. P. Reagor, 2007, "Static transmission error vibratory excitation contribution from plastically deformed gear teeth caused by tooth bending fatigue damage", MSSP, 21: pp885-905 (2007)
- [61] H. Endo, R. B. Randall and C. Gosselin, 2004, "Differential Diagnosis of Spall vs. Cracks in the Gear Tooth Fillet Region", Journal of Failure Analysis and Prevention, Vol4, Issue 5, Oct 2004
- [62] H. Endo, R. B. Randall and C. Gosselin, 2008, "Differential Diagnosis of Spall vs. Cracks in the Gear Tooth Fillet region: Experimental Validation", Journal of Mechanical System and Signal Processing, due to be published on 19/Jan/2009, Vol23 Issue3.
- [63] M. EL Badaoui, J. Antoni, F. Guillet and J. Daniere, 2001a, "Use of the Moving Cepstrum Integral to Detect and Localise Tooth Spalls in Gears", Mechanical System and Signal Processing, 2001, 15 (5), 873-885
- [64] M. EL Badaoui, V. Cahouet, F. Guillet, J. Daniere and P. Velex, 2001b, "Modelling and Detection of Localized Tooth Defects in Geared Systems", Transaction of ASME, Sep, 2001, Vol. 123, pp422-430
- [65] J. Mahfoudh, C. Bard, M. Alattass and D. Play, 1995, "Simulation of Gearbox Dynamic Behaviour with Gear Faults", I Mech E, C492/045/95
- [66] N.Sawalhi, R.B.Randall and H.Endo, "Gear and bearing fault simulation applied to diagnostics and prognostics", paper presented at The 19th International Congress and Exhibition on Condition Monitoring and Diagnostic Engineering Management, Luleå, Sweden, June (2006).
- [67] N. Sawalhi, and R.B. Randall, Vibration response of spalled rolling element bearings: observations, simulations and signal processing techniques to track the spall size. Mechanical Systems and Processing, 25 (3), (2011).

# Split Torque Gearboxes: Requirements, Performance and Applications

Abraham Segade-Robleda, José-Antonio Vilán-Vilán, Marcos López-Lago and Enrique Casarejos-Ruiz *University of Vigo, Spain* 

## 1. Introduction

Although the simplest gear systems are those with just one gear engagement area between a pair of gears, alternatives are available for applications where it is necessary to transmit a very high torque in a very small space. One option to increase power density is to use the split torque systems that were mainly developed for the aviation industry. These gear systems are based on a very simple idea: division of the transmission of force between several contact areas, thereby increasing the contact ratio. This gives rise, however, to the problem of meshing four gears (Fig. 1).

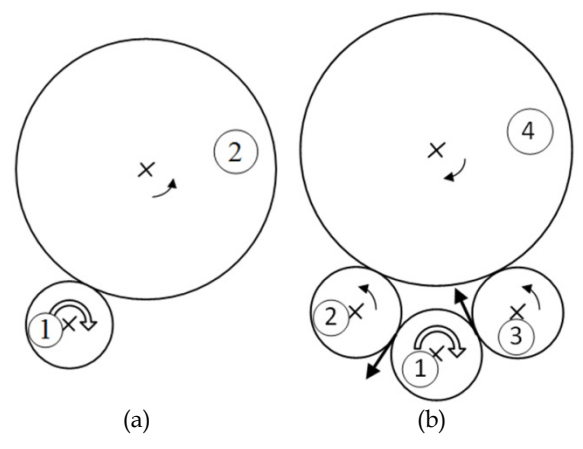


Fig. 1. (a) Standard gearbox assembly; (b) Split torque gearbox assembly

Split torque gearboxes are configurations where a driving pinion (1) meshes with two intermediate idler pinions (2, 3), which simultaneously act on another gear (4). From now on, this assembly will be called four-gear meshing. In this case, the torque split is from gear (1) to gears (2) and (3) which engage gear (4). This gear assembly results in the reduction in gear speed causing an increase in available torque; hence, the split torque transmission means we can use smaller gears.

The greater the number of gears that engage the same crown, the lower the torque exercised by each pinion. Gear assembles can have up to 14 gears engaging a single crown, as happens, for example, in tunnel boring machines.

This chapter explores four-gear meshing in a gear assembly that ensures a 50% torque split for each meshing area. Split torque gears are studied from two perspectives: first, the most common applications of split torque gearboxes in the aeronautical sector and second, the two most restrictive aspects of their application, namely:

- The geometric limitation of the four-gear assembly that requires simultaneous engagement for all four gears. Note that the four gears do not mesh correctly in just any position, although they may seem to do so initially. We will describe the conditions for simultaneous meshing of the four gears in general terms below.
- Torque split between the two gearbox paths must be as balanced as possible to ensure that neither of the paths is overloaded. The technology available to ensure proper torque split between two paths will be discussed below.

# 2. Applications

Gear transmission requirements for aircraft are very demanding, with a standard gear ratio between engine and rotor of 60:1 (Krantz, 1996). Moreover, the gear transmission system should be safe, reliable, lightweight and vibration-free. One of the most limiting factors is weight and there are three fundamental transmission parameters that greatly affect this factor:

- 1. The number of transmission stages. The greater the number of stages used to achieve the final gear ratio, the heavier the transmission, given that more common elements such as shafts and bearings are necessary.
- 2. The number of transmission paths, the basis for split torque gearboxes. Torque is divided between several transmission paths, resulting in a contact force in the smaller gear that means that smaller, and consequently lighter, gears can be used.
- 3. The final stage transmission ratio. Using a greater transmission ratio in the final stage enables weight to be reduced. This is because torque in previous steps is lower, making it possible to use smaller gears.

In helicopters, planetary gear systems are typically used for the final transmission stage, with planets consisting of between 3 and 18 gears and with planetary gearing transmission ratios between 5:1 and 7:1 (Krantz, 1996; White, 1989).

Using split-path arrangements with fixed shafts in the final transmission stage is a relatively recent development that offers a number of advantages over conventional systems, being several of them based on weight reduction for the overall transmission:

• It allows torque to be transmitted through various paths. This is a major advantage because when torque is split, the contact force between teeth is less and, hence, smaller, lighter gears can be used, therefore reducing the overall weight. Split torque however has the disadvantage that the torque must be shared equally between the paths. The problems associated with split torque are discussed in Section 4.

- It allows transmission path redundancy. Thus, if one transmission path fails during flight, operation can always be assured through another path. In many cases, consequently, gear transmissions are sized so that a single path can handle 100% of engine power.
- It achieves final-stage transmission ratios of around 10:1 to 14:1 (Krantz, 1996; White, 1989). This improvement over the 5:1 to 7:1 ratios for planetary gearboxes (Krantz, 1996; White, 1989) is reflected in a corresponding reduction in the weight of the transmission system.

Several patents for transmission systems that apply split torque have been filed by Sikorky Aircraft Corporation and McDonnell Douglas Helicopters (Gmirya & Kish, 2003; Gmirya, 2005; Craig et al., 1998) that refer either to complete or improved power transmission systems from the rotorcraft or aircraft engine to the rotor or propeller. Other studies that describe various aspects of split torque transmission systems, particularly their use in helicopter gearboxes (White, 1974, 1983, 1989, 1993, 1998), conclude that such gears have a number of advantages over traditional gear systems.

Below we describe two helicopter transmission systems that use multiple path gearboxes. The first is a helicopter gearbox used for laboratory tests of torque divided into two stages, and the second is a commercial helicopter three-stage gearbox that combines bevel, spur and helical gears.

# 2.1 Helicopter gearbox for laboratory testing

The gear transmission described below was used to perform numerous tests on the operation of split-torque transmissions (Krantz et al., 1992; Krantz, 1994, 1996; Krantz & Delgado, 1996), which can be considered a standard for aeronautical applications. The full assembly is depicted in Fig. 2.

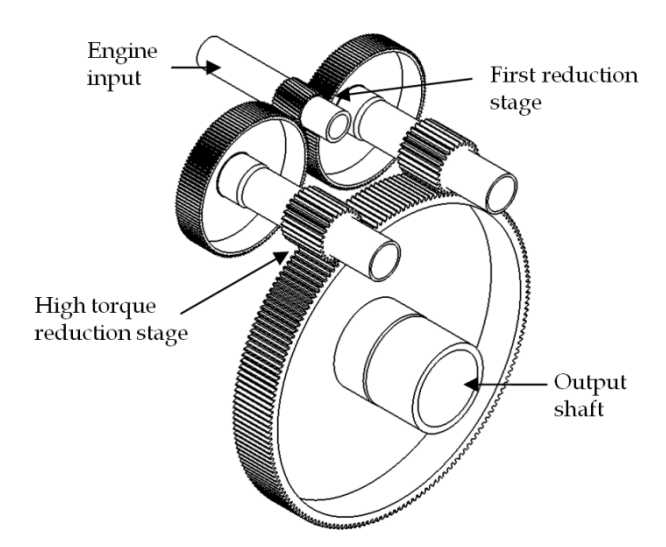


Fig. 2. Helicopter transmission for laboratory testing

The transmission is sized for input of 373 kW at a speed of 8780 rpm. As can be observed in Fig. 2, the transmission has two stages:

- First reduction stage. The first stage is a helical gear with a input pinion with 32 teeth and two output gears with 124 teeth each. The gear ratio is 3.875:1, resulting in an output speed of 2256.806 rpm. This is the stage where torque is split between the input pinion and the two output gears.
- High torque reduction stage. The output shaft is driven by a gear which is driven simultaneously by two spur pinions, each coaxial to the gear in the first reduction stage. The ratio between the gear teeth is 27/176, so the transmission ratio is 6.518:1, resulting in an output shaft speed of 347.6 rpm.

This configuration results in torque of 9017.56 Nm. being transmitted through two paths.

## 2.2 Commercial helicopter transmission

This gear transmission, studied in depth by White (1998), is sized for two engines, each with a continuous rating of 1200 kW turbine at a nominal speed of 22976 rpm. The main rotor speed is 350 rpm for an overall speed reduction ratio of nearly 66:1. Fig. 3 depicts a plan view of the gear transmission and Fig. 4 is a three-dimensional view showing the gears.

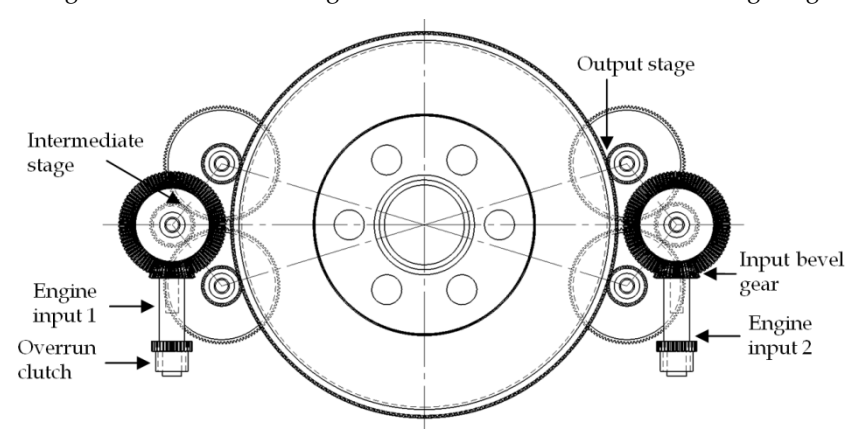


Fig. 3. Arrangement of gear trains between engines.

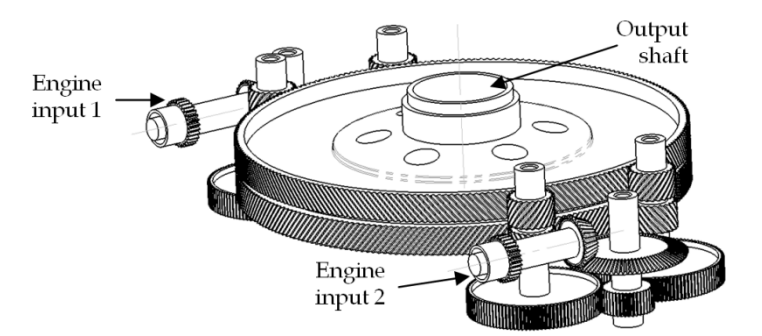


Fig. 4. Three-dimensional view of the gear train arrangement

Total transmission reduction is achieved by three gearing stages, clearly depicted in Fig. 3 and Fig. 4:

- Engine input. Engine torque is accepted by an overrun clutch, mounted with a bevel pinion. This bevel gear, with a between-teeth ratio of 34/84, produces a transmission ratio of 2.470:1. In this stage, the output velocity is 9299 rpm.
- Intermediate stage. Dual offset spur gears are driven by a single pinion. The betweenteeth ratio of 41/108 produces a transmission ratio of 2.634:1, resulting in an output shaft speed of 3530 rpm. This meshing results in the first split in torque between the two intermediate gears.
- High-torque output stage. A double-helical gear is driven by a pinion coaxial with each
  intermediate stage gear. In this stage, the torque is split again between the two helical
  pinions, with the result that the output shaft simultaneously receives torque from four
  pinions for each bevel gear. In this transmission it is very convenient to combine torque
  split with reduction, as greater torque is transmitted in each stage.

The between-teeth gear ratio is 23/232, so the transmission ratio is 10.087:1, resulting in an output shaft speed of 350 rpm.

This configuration uses double-helical gearing at the output stage to drive the output shaft. The helical pinions have opposing angles, which ensures equilibrium between the axial forces. When a double gear operates on the output shaft, the area of support is twice that of a simple gear. This causes a reduction in contact force, which in turn results in a reduction ratio that is twice that of the simple case, with the corresponding reduction in weight and mechanical load.

Overall, this constitutes a transmission ratio of 65.64:1, with the total torque in the output shaft exercised by each engine of 28818Nm, split between the four pinions that engage the output shaft crown. This calculation is based on estimating overall losses, with each input engine operating independently, of 12%.

One of the main problems in split torque transmission is ensuring equal torque split between the paths. To ensure correct torque split, a long, torsionally flexible shaft is used between the intermediate-stage spur gear and the output-stage helical pinions. Section 4 describes the methods most frequently used to ensure correct torque split between paths.

# 3. Feasible geometric configurations

To ensure simultaneous meshing of four gears (Fig. 1), configuration must comply with certain geometric constraints. A number of studies describe the complexity of simultaneous gearing in split torque gearboxes (Kish, 1993a) and in planetary gear systems (Henriot, 1979, Parker & Lin, 2004); other studies approach the problem generically (Vilán-Vilán et al., 2010), describing possible solutions that ensure the simultaneous meshing of four gears.

For four gears to mesh perfectly, the teeth need to mesh simultaneously at the contact points. The curvilinear quadrilateral and the pitch difference are defined below in order to express the meshing condition. From now on we will use this nomenclature of our own devising -that is, curvilinear quadrilateral - to indicate the zone defined by portions of pitch circles in the meshing area (Fig. 5). The pitch difference is the sum of pitches in the input and output gears minus the sum of pitches in the idler gears at the curvilinear quadrilateral. For perfect engagement between the four gears, the pitch difference must coincide with a whole number of pitches.

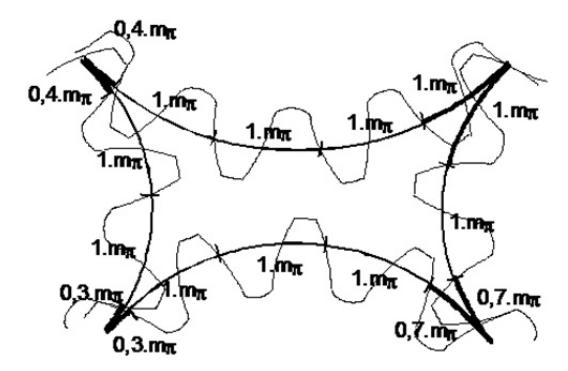


Fig. 5. General conditions for simultaneous meshing of four gears

A relationship is thus established between the position of the gears, as defined by the relative distance between centres, and the number of teeth in each of the gears. Below we explore two possible cases of over-constrained gears:

- CASE 1. Four outside gears.
- CASE 2. Three outside gears and one ring gear.

## 3.1 Case 1. Four outside gears

For a gearbox with the geometry illustrated in Fig. 6, it is possible to locate the different positions that will produce suitable meshing between gears, in function of the number of teeth in each gear, by defining the value of the angles  $\alpha$ ,  $\beta$ ,  $\delta$  and  $\gamma$ .

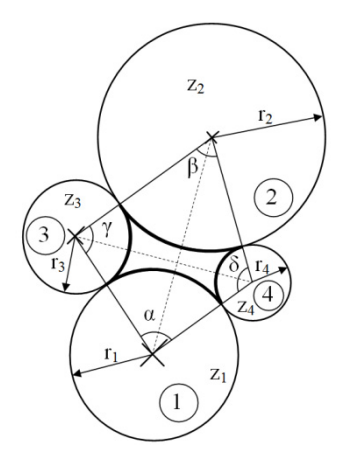


Fig. 6. Nomenclature for the four-gear case

The condition described in the previous section can be mathematically expressed as follows (see Nomenclature):

$$r_1 \cdot \alpha + r_2 \cdot \beta - r_3 \cdot \gamma - r_4 \cdot \delta = n \cdot (m\pi) \quad n \in \mathbb{Z}$$
 (1)

where n is the pitch difference in the curvilinear quadrilateral. As previously mentioned, n must be a whole number to ensure suitable meshing between gears.

We thus obtain an equation with four unknowns  $(\alpha, \beta, \gamma, \delta)$ . The three remaining relationships can be obtained from the quadrilateral that joins the centres of the pitch circles (this quadrilateral will be denoted the rectilinear quadrilateral). Finally, we come to a transcendental equation (2) from which  $\alpha$  can be obtained according to the number of teeth in the gears.

$$e_{1} - f \cdot \cos \left[ A_{1} \cdot \mathbf{\alpha} + B_{1} \cdot \arccos\left(\frac{c_{1} - a_{1} + b_{1} \cdot \cos \mathbf{\alpha}}{d_{1}}\right) + C_{1} \right] = g_{1} - h_{1} \cdot \cos \left[ A'_{1} \cdot \mathbf{\alpha} + B'_{1} \cdot \arccos\left(\frac{c_{1} - a_{1} + b_{1} \cdot \cos \mathbf{\alpha}}{d_{1}}\right) + C'_{1} \right]$$

$$(2)$$

Once the angle  $\alpha$  has been determined, we can calculate:

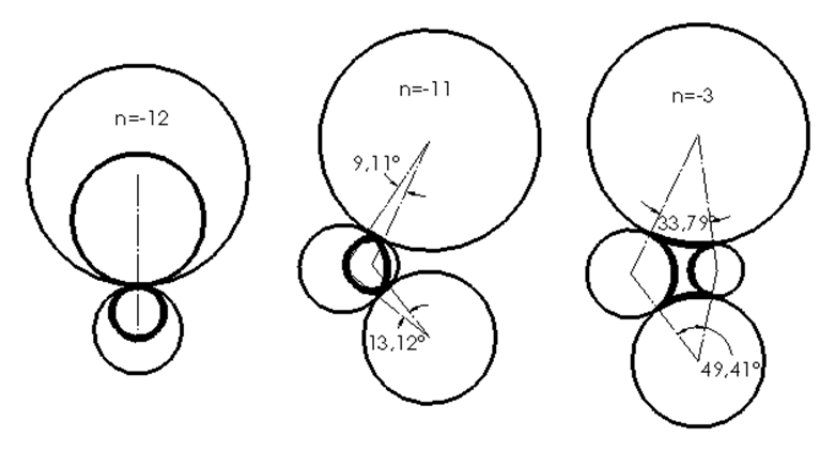
$$\beta = \arccos\left(\frac{c_1 - a_1 + b_1 \cdot \cos \alpha}{d_1}\right) \tag{3}$$

$$\gamma = A_1 \cdot \alpha + B_1 \cdot \beta + C_1 \tag{4}$$

$$\delta = A'_{1} \cdot \alpha + B'_{1} \cdot \beta + C'_{1} \tag{5}$$

 $a_1$ ,  $b_1$ ,  $c_1$ ,  $d_1$ ,  $e_1$ ,  $f_1$ ,  $g_1$ ,  $h_1$ ,  $A_1$ ,  $B_1$ ,  $C_1$ ,  $A_1'$ ,  $B_1'$  and  $C_1'$  are numerical relationships among the teeth number from each wheel that must mesh simultaneously. The value of each coefficient is listed in the Appendix.

The transcendental equation for obtaining  $\alpha$  has several solutions, all representing possible assemblies for the starting gears. For example, for four-gear meshing with the next teeth numbers:  $z_1$ =30,  $z_2$ =50,  $z_3$ =20 and  $z_4$ =12 (see Nomenclature), all the possible solutions for the gear can be encountered. In this case solutions are n = -12, -11, -3, -2, -1, 0, 1, 2, 3, 4, 7, 29 and 30, where n is the pitch difference between the two sides of the curvilinear quadrilateral (a whole number that ensures suitable meshing). Fig. 7 shows some of the possible meshing solutions.



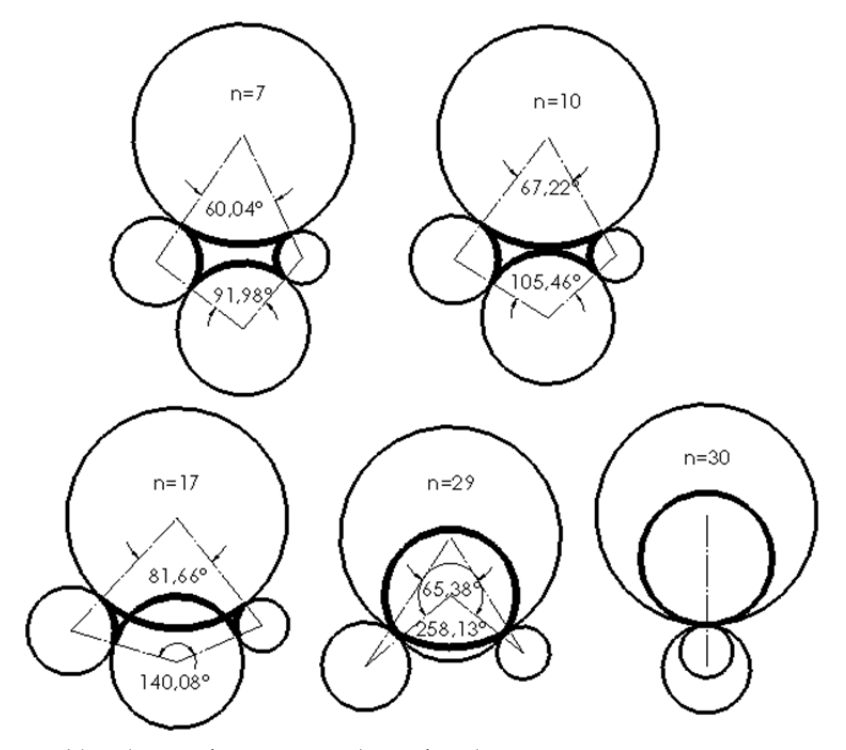


Fig. 7. Feasible solutions for given numbers of teeth

# 3.2 Case 2. Three outside gears and one ring gear

In this case torque is transmitted from a driving pinion (1) to a ring gear (2) through two idler pinions (3) and (4). Two solutions are available depending on the geometry of the rectilinear quadrilateral that joins the centres of the pitch circles, either crossed (Fig. 8 (a)) or non-crossed (Fig. 8 (b)). The starting equation is different for each of these cases.

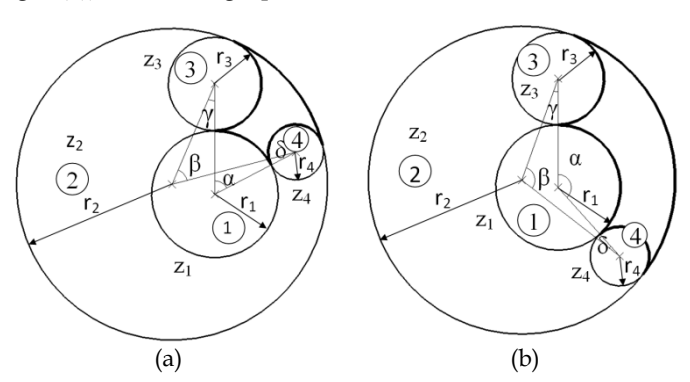


Fig. 8. Solutions for three outside gears and one ring gear: (a) crossed quadrilateral (b) non-crossed quadrilateral

For the crossed quadrilateral configuration, the starting equation is (see Nomenclature):

$$z_1 \cdot \alpha + z_2 \cdot \beta + z_3 \cdot \gamma - z_4 \cdot \delta = \pi \cdot (2 \cdot n + z_3 + z_4) \tag{6}$$

Finally, we come to the same transcendental equation (2), where the coefficients are  $a_2$ ,  $b_2$ ,  $c_2$ ,  $d_2$ ,  $e_2$ ,  $f_2$ ,  $g_2$ ,  $h_2$ ,  $A_2$ ,  $B_2$ ,  $C_2$ ,  $A_2'$ ,  $B_2'$  and  $C_2'$ , whose values are listed in the Appendix.

For the non-crossed quadrilateral configuration, the starting equation is:

$$z_1 \cdot \alpha - z_2 \cdot \beta - z_3 \cdot \gamma - z_4 \cdot \delta = \pi \cdot (2 \cdot n - 2 \cdot z_2 + z_3 + z_4) \tag{7}$$

Finally, we come to the same transcendental equation (2), where the coefficients become  $a_2$ ,  $b_2$ ,  $c_2$ ,  $d_2$ ,  $e_2$ ,  $f_2$ ,  $g_2$ ,  $h_2$ ,  $h_3$ 

# 3.3 A particular case: Outside meshing with equal intermediate pinions

A common split torque gear assembly is one with two equally sized idler pinions (Fig. 9).

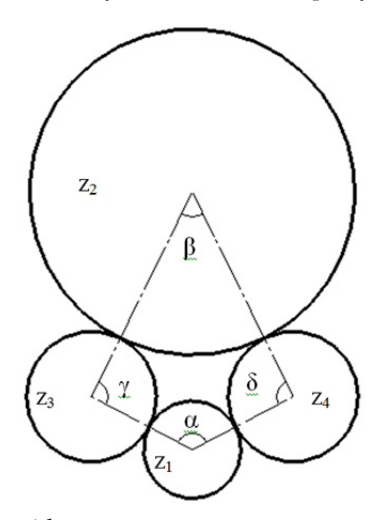


Fig. 9. Idler pinions in an outside gear

The solution is obtained by particularizing the general solution for four outside wheels and imposing the condition  $z_3$ =  $z_4$ , or  $\gamma$ =  $\delta$ . The following equations are defined for the curvilinear quadrilateral:

$$z_1 \cdot \alpha + z_2 \cdot \beta - 2 \cdot z_3 \cdot \gamma = n \cdot 2\pi \tag{8}$$

$$\alpha + \beta + 2 \cdot \gamma = 2\pi \tag{9}$$

$$(z_1 + z_3) \cdot \sin\left(\frac{\alpha}{2}\right) = (z_2 + z_3) \cdot \sin\left(\frac{\beta}{2}\right)$$
 (10)

Resolving the system, the following transcendental function in  $\alpha$  is obtained:

$$\frac{z_1 + z_3}{z_2 + z_3} \cdot \sin\left(\frac{\alpha}{2}\right) = \sin\left[\frac{z_3 + n}{z_2 + z_3} \cdot \pi - \frac{z_1 + z_3}{z_2 + z_3} \cdot \left(\frac{\alpha}{2}\right)\right]$$
(11)

The solutions for the other angles can now be obtained:

$$\beta = 2 \cdot \arcsin \left[ \frac{z_1 + z_3}{z_2 + z_3} \cdot \sin \left( \frac{\alpha}{2} \right) \right]$$
 (12)

$$\gamma = \pi - \frac{\alpha}{2} - \frac{\beta}{2} \tag{13}$$

# 4. Load sharing

The main problem in the design of split torque gearboxes is to ensure that torque is equally split between different paths. Small deviations in machining can result in one of the paths with 100% of torque and the other path operating entirely freely (Kish & Webb, 1992). This situation causes excessive wear in one of the paths and renders the torque split system ineffective.

Below we describe approaches to ensuring equal torque split between different paths in split torque gear arrangements. The main types are:

- 1. Geared differential. This differential mechanism, frequently used in the automotive sector, delivers equal torques to the drive gears of a vehicle.
- 2. Pivoted systems. These use a semi-floating pinion constrained both to pivot normal to the line of action and to seek a position where tooth loads are equal.
- 3. Quill shafts. A torsion divider with a separate gear and pinion, each supported on its own bearings, are connected through the quill shaft, which allows torsional flexibility.

The use of any of these systems to ensure correct torque split makes the gearbox heavier and assembly and maintenance more complex, which is why a number of authors do not support the use of systems that ensure torque split. Described below are the main systems that ensure correct torque split and discussed also are the proposals of authors who advocate for not using special systems.

#### 4.1 Geared differential

One way to ensure correct torque split between two branches is to use a differential system. The great disadvantage of this system, however, is that resistive torque lost in one branch leads to loss of the full engine torque. Different differential mechanisms can be used, with assemblies very similar to those in vehicles or to the system depicted in Fig. 10. Assembled at the entry point to the gearbox is an input planetary system that acts as a differential that ensures load sharing. This transmission accepts power from three input engines, each of which has a differential system that ensures balanced torque splitting. Power is input from each engine to the sun gear of the differential planetary system. The carrier is the output to a bevel pinion that drives one torque splitting branch while the ring gear drives the other torque splitting branch. As the carrier and the ring gear rotate in opposite directions, the bevel pinions are arranged on opposite sides to ensure correct rotation direction. Each output bevel gear drives one pinion which then combines power into the output gear.

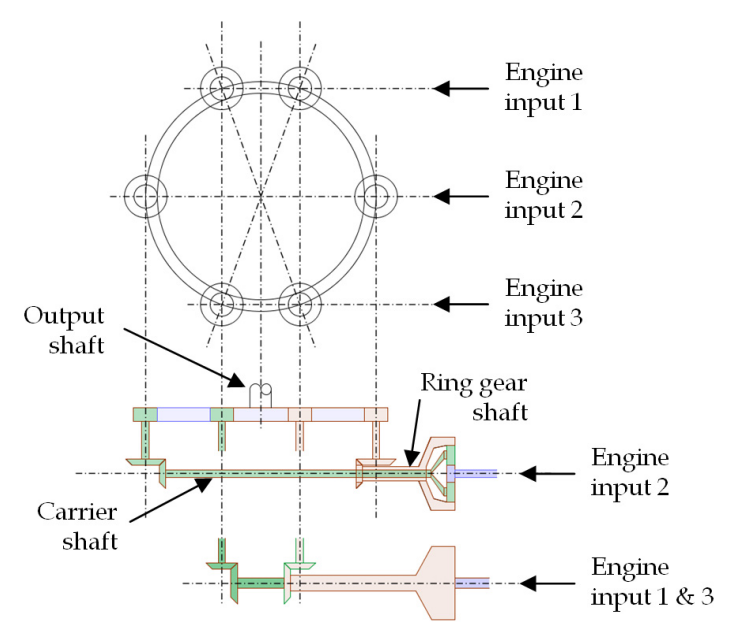


Fig. 10. Schematic view of split torque main transmission

# 4.2 Pivoted systems

One type of pivoted systems is described in detail in a patent (Gmirya, 2005) for split torque reduction applied to an aerial vehicle propulsion system (Fig. 11). "The input pinion (64) engages with gears (66) and (68). The input pinion is defined along the gear shaft  $A_G$ , the first gear

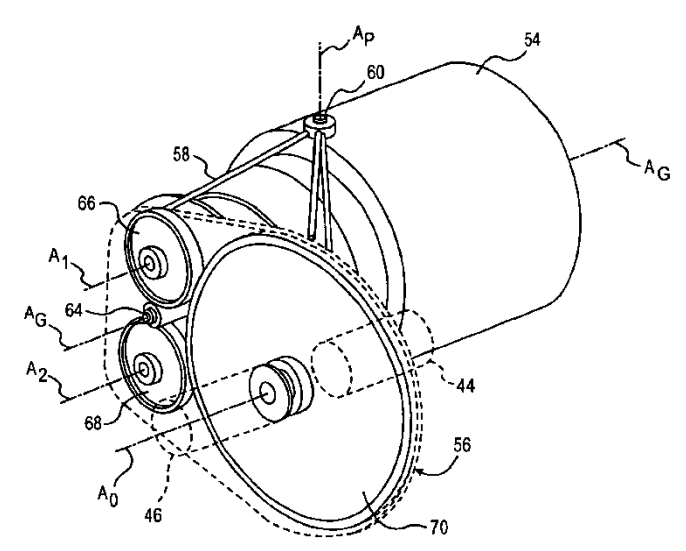


Fig. 11. Perspective view of the split torque gearbox with pivoted engine support (Gmirya, 2005)

(66) defines a first gear rotation shaft  $A_1$  and the second gear (68) defines a second gear rotation shaft  $A_2$ . The axes  $A_G$ ,  $A_1$  and  $A_2$  are preferably located transversally to the pivot axis  $A_p$ . The first gear (66) and the second gear (68) engage an output gear (70). The output gear (70) defines an output rotation shaft  $A_0$  and is rotationally connected to the translational driveshaft (44) and the rotor driveshaft (46) to power, respectively, the translational propulsion system and the rotor system".

The assembly transmits torque from the pinion (64), which operates at very high revolutions, to the output shaft (44 -46) via two paths. The pivot system works as follows: since the input pinion (64) meshes with two gears (66) and (68), the pivoted engine arrangement permits the input pinion (64) to float until gear loads between the input gear (64), the first gear (66) and the second gear (68) are balanced. Irrespective of gear teeth errors or gearbox shaft misalignments, the input pinion will float and split torque between the two gears.

#### 4.3 Quill shafts

Below we describe assemblies used in systems that allow some torsion in the split torque shafts (Smirnov, 1990; Cocking, 1986) in order to minimize the difference in torque split between paths. These systems achieve their goal in several ways:

- Conventional systems (Kish, 1993a) assemble intermediate shafts with some torsional
  flexibility so that angular deviation produced between the input and output pinions
  adjusts the torque transmitted via the two paths.
- Other systems are based on elastomeric elements in the shaft (Isabelle et al., 1992, Kish & Webb, 1992) or materials with a lower elastic modulus (Southcott, 1999), such as an idler pinion constructed of nylon or a similar material (Southcott, 1999). This solution is not explored here because the torque transmitted is reduced.
- Yet other systems operate on the basis of spring elements (Gmirya & Vinayak, 2004).

The use of such elements in the design adds weight and makes both initial assembly and maintenance more complex, thereby losing to some degree the advantages of split torque gearboxes. Described below are the most representative types of quill shaft.

## 4.3.1 Conventional quill shafts

Conventional quill shaft design involves assembly on three different shafts (Fig. 12). The

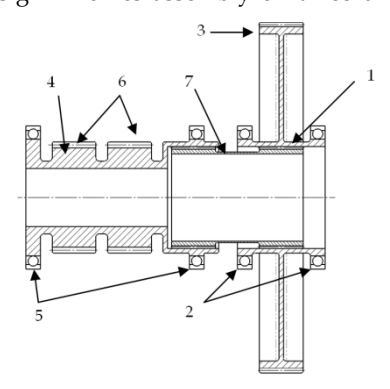


Fig. 12. Conventional assembly of a quill shaft

input shaft (1) is assembled with two separate bearings (2) and the input gear (3). The output shaft (4) is assembled with two separate bearings (5) and, in this case, two output pinions (6). The quill shaft is a third shaft (7) that connects the other two shafts. Due to a lower polar moment of inertia, it admits torsional flexibility, resulting in a small angular deviation between the input and output shafts. The value of the angular deviation is proportional to the transmitted torque; thus, if one path transmits more torque than the other, the angular deviation is greater, allowing the shaft that transmits less torque to increase its load.

#### 4.3.2 Quill shafts based on elastomeric elements

Elastomeric elements are frequently used in quill shafts given their low elastic modulus. For example, one system (Isabelle et al., 1992), based on using elastomers (Fig. 13), consists of "an annular cylindrical elastomeric bearing (14) and several rectangular elastomeric bearing pads (16). The elastomeric bearing (14) and bearing pads (16) have one or more layers (60); each layer (60) has an elastomer (62) with a metal backing strip (64) secured by conventional means such as vulcanization, bonding or lamination".

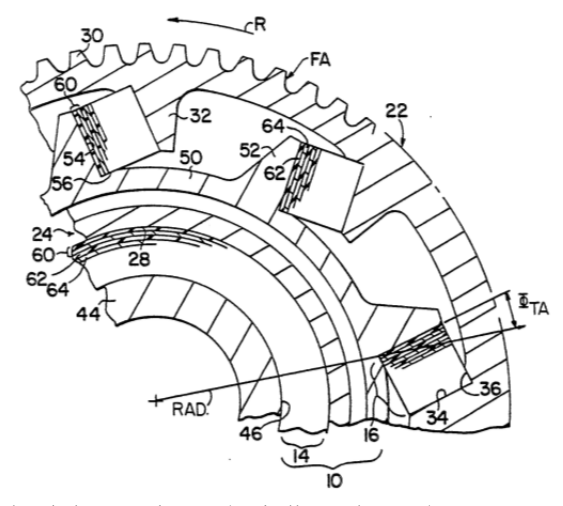


Fig. 13. Elastomeric load sharing device (Isabelle et al., 1991)

The annular cylindrical elastomeric bearing (14) absorbs possible misalignments between shafts resulting from defects in assembly. The rectangular elastomeric bearing pads (16) are responsible for providing torsional flexibility to the shafts of the possible gear paths in order to ensure equal torque transmission.

Another elastomer-based system (Kish & Webb, 1992) (Fig. 14) consists of an assembly with "a central shaft (21) and a pair of bull pinions (22) and (23). The shaft (21) is supported by the bearings (24) and (25); a gear flange (26) at the end of the shaft has bolt holes (27) and teeth (28) on the outer circumference. A spur gear (29) is held to the flange (26) using upper and lower rims (30) and (31), consisting of flat circular disks (32) with bolt holes (33) and an angled outer wall (34). Gussets (35) between the wall and the disk increase rim stiffness to minimize deflection. One or more elastomer layers (36), bonded to the outer surface (37) of the wall (34), act as an elastomeric torsional isolator".

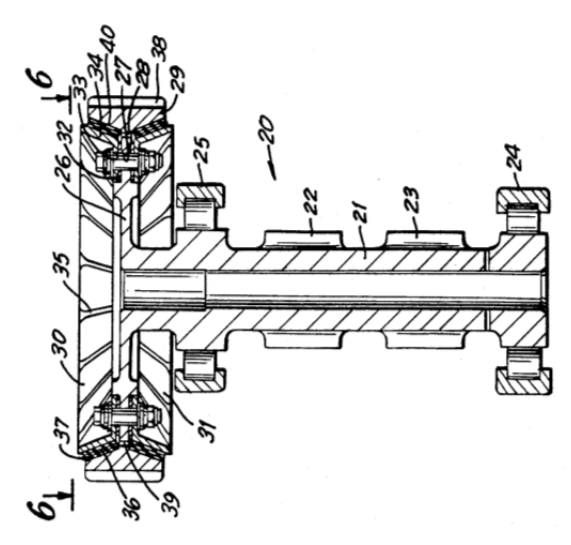


Fig. 14. Gear assembly using an elastomeric torsional isolator (Kish & Webb, 1992)

This assembly was tested in the Advanced Rotorcraft Transmission project (Kish, 1993a), by comparing it with conventional quill shafts. It was concluded that the torque split was excellent and also had other advantages such as lower transmission of force to supports, less vibration and less noise during operation.

The main problem with using elastomers to achieve proper torque split is their degradation over time, especially when used in high-torque gear transmissions where temperatures are high and there is contact with oil. Some authors therefore propose the use of metallic elements to achieve the same effect as the quill shaft.

## 4.3.3 Quill shafts based on spring elements

Some authors propose the use of metallic elements to achieve the same effect as the quill shaft. One such system (Gmirya & Vinayak, 2004) (Fig. 15) is based on achieving this effect by using "at least one spring element (30) placed between and structurally connecting the gear shaft (32) and the outer ring of gear teeth (34). The gear shaft (32) has flange elements (36) that project radially outboard of the shaft. The ring of gear teeth (34), similarly, has a flange element (38) that projects radially inward towards the gear shaft". In this case, a pair of spring elements (30) is arranged on each side of the gear teeth flange element (38)".

This assembly is designed in such a way that the spring elements absorb torsional deflection between the gears, thereby ensuring proportional torque split between paths.

## 4.4 No use of special systems

Split torque gearboxes are used in order to reduce the weight of the gear system, so the simplest option is assembly without special systems for regulating torque split. Several authors support this option, for example, Kish (1993a, 1993b), who concluded from tests that acceptable values can be achieved without using any special torque split system, simply by

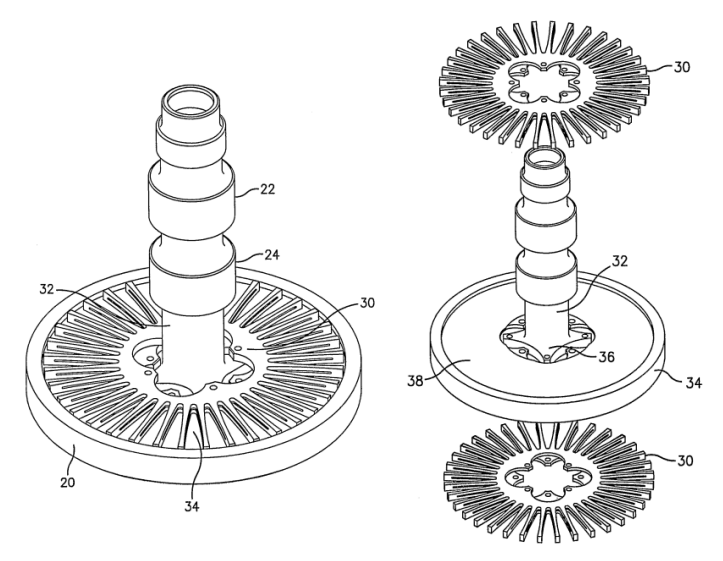


Fig. 15. Load sharing gear in combination with a double helical pinion (Gmirya & Vinayak, 2004)

ensuring manufacturing according to strict tolerances and correct assembly. Krantz (1996) proposed the use of the clocking angle as a design parameter to achieve adequate torque split between paths. This author has studied the effects of gearshaft twisting and bending, and also tooth bending, Hertzian deformations within bearings and the impact of bearing support movement on load sharing.

Krantz (1996) defined the clocking angle as  $\beta$  and described the assembly prepared for measurement (Fig. 16): "The output gear is fixed from rotating and a nominal counter-clockwise

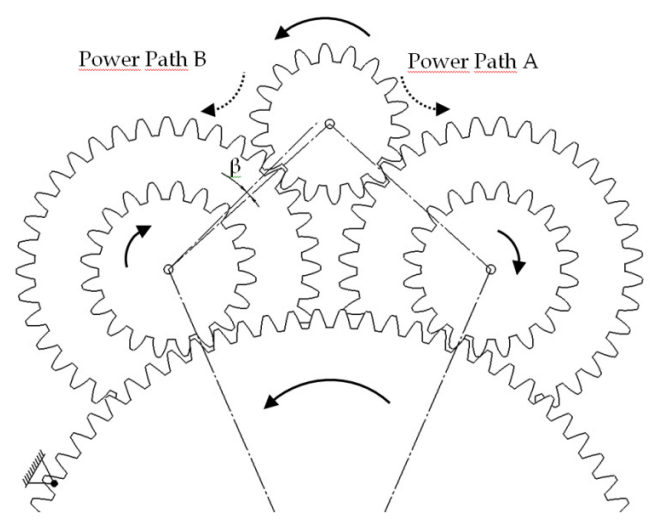


Fig. 16. Assembly for measurement of the clocking angle

torque is applied to the input pinion so that the gear teeth come into contact. When all the gear teeth for both power paths come into contact, then the clocking angle  $\beta$  is, by definition, equal to zero. If the teeth of one power path are not in contact, then the clocking angle  $\beta$  is equal to the angle that the first-stage gear would have to be rotated relative to the second-stage pinion to bring all the teeth into contact".

The tests show that suitable (47 per cent/53 per cent) load sharing can be achieved merely by taking into account the clocking angle and ensuring proper machining and assembly.

This research into the clocking angle has been followed up by subsequent authors (Parker & Lin, 2004) who have studied how contact between different planetary gears is sequenced.

#### 5. Conclusion

Choosing the correct assembly for aircraft power transmission is a key factor in the quest for weight reduction. Although technological advances in mechanical components can help achieve weight reduction in gear systems, their influence is much less than that of choosing the correct gear assembly.

Planetary gear or split torque systems are typically used in helicopter gear transmissions. The fundamental advantage of the split torque systems is that less weight is achieved by equal torque transmission and gear transmission ratios. This advantage is based primarily on arguments as follows:

- In the final transmission stage where the greatest torque is achieved, the use of several
  paths for the transmission ratio means that, given equal torque and stress levels in the
  teeth, the ratio between output torque/weight will be better in torque split gear systems
  than in planetary gear systems.
- In the final transmission stage, transmission ratios of around 5:1 or 7:1 are achieved by planetary gearboxes used with a single stage, compared to 10:1 or 14:1 for split torque gears used in the final stage.
- The possibility of achieving higher transmission ratios in split torque gearboxes makes it possible to use a smaller number of gear stages, resulting in lighter gear systems.
- Split torque gearboxes need fewer gears and bearings that planetary gearboxes, which means lower transmission losses.
- A key factor for aircraft use is that split torque gearboxes improve reliability by using multiple power paths; thus, if one path fails, operation is always assured through another path.
- The main disadvantage of the split torque gearboxes is when torque split between the
  possible paths is uneven; however, several solutions are available to ensure correct
  torque split.

These arguments would indicate the advisability of using this type of transmission in aircraft gear systems.

#### 6. Nomenclature

- m gear module
- r<sub>i</sub> radius of the pitch circle of wheel i

number of teeth in wheel i  $\mathbf{z}_{i}$ angle formed by the lines between centres, between wheels 341 α angle formed by the lines between centres, between wheels 324 β angle formed by the lines between centres, between wheels 231 γ δ angle formed by the lines between centres, between wheels 142 pitch difference between the two sides of the curvilinear quadrilateral n

# 7. Appendix

The numerical relationships among the teeth number used in the text are listed below.  $C_1$ ,  $C_1$ ,  $C_2$ ,  $C_2$ ,  $C_3$  and  $C_3$  are functionS of n, a whole number which represents the pitch difference in the curvilinear quadrilateral.

$$a_1 = (z_1 + z_3)^2 + (z_1 + z_4)^2 \tag{14}$$

$$b_1 = 2 \cdot (z_1 + z_3) \cdot (z_1 + z_4) \tag{15}$$

$$c_1 = (z_2 + z_3)^2 + (z_2 + z_4)^2 \tag{16}$$

$$d_1 = 2 \cdot (z_2 + z_3) \cdot (z_2 + z_4) \tag{17}$$

$$e_1 = (z_1 + z_3)^2 + (z_2 + z_3)^2$$
 (18)

$$f_1 = 2 \cdot (z_1 + z_3) \cdot (z_2 + z_3) \tag{19}$$

$$g_1 = (z_1 + z_4)^2 + (z_2 + z_4)^2$$
 (20)

$$h_1 = 2 \cdot (z_1 + z_4) \cdot (z_2 + z_4) \tag{21}$$

$$A_1 = \frac{z_1 + z_4}{z_3 - z_4} \tag{22}$$

$$B_1 = \frac{z_2 + z_4}{z_3 - z_4} \tag{23}$$

$$C_1 = 2\pi \cdot \frac{z_4 + n}{z_4 - z_3} \tag{24}$$

$$A_1' = \frac{z_1 + z_3}{z_4 - z_3} \tag{25}$$

$$B_1' = \frac{z_2 + z_3}{z_4 - z_3} \tag{26}$$

$$C_1' = 2\pi \cdot \frac{z_3 + n}{z_3 - z_4} \tag{27}$$

$$a_2 = (z_1 + z_3)^2 + (z_1 + z_4)^2$$
 (28)

$$b_2 = 2 \cdot (z_1 + z_3) \cdot (z_1 + z_4) \tag{29}$$

$$c_2 = (z_2 - z_3)^2 + (z_2 - z_4)^2 \tag{30}$$

$$d_2 = 2 \cdot (z_2 - z_3) \cdot (z_2 - z_4) \tag{31}$$

$$e_2 = (z_1 + z_3)^2 + (z_2 - z_3)^2$$
 (32)

$$f_2 = 2 \cdot (z_1 + z_3) \cdot (z_2 - z_3) \tag{33}$$

$$g_2 = (z_1 + z_4)^2 + (z_2 - z_4)^2$$
 (34)

$$h_2 = 2 \cdot (z_1 + z_4) \cdot (z_2 - z_4) \tag{35}$$

$$A_2 = \frac{z_1 + z_4}{z_4 - z_3} \tag{36}$$

$$B_2 = \frac{z_2 - z_4}{z_4 - z_3} \tag{37}$$

$$C_2 = \pi \cdot \frac{2 \cdot n + z_3 + z_4}{z_3 - z_4} \tag{38}$$

$$A_2' = \frac{z_1 + z_3}{z_4 - z_2} \tag{39}$$

$$B_2' = \frac{z_2 - z_3}{z_4 - z_3} \tag{40}$$

$$C_2' = \pi \cdot \frac{2 \cdot n + z_3 + z_4}{z_3 - z_4} \tag{41}$$

$$A_3 = \frac{z_1 + z_4}{z_3 - z_4} \tag{42}$$

$$B_3 = \frac{z_4 - z_2}{z_3 - z_4} \tag{43}$$

$$C_3 = \pi \cdot \frac{2 \cdot n - 2 \cdot z_2 + z_3 + 3 \cdot z_4}{z_4 - z_3} \tag{44}$$

$$A_3' = \frac{z_1 + z_3}{z_4 - z_3} \tag{45}$$

$$B_3' = \frac{z_3 - z_2}{z_4 - z_3} \tag{46}$$

$$C_{3}' = \pi \cdot \frac{2 \cdot n - 2 \cdot z_2 + 3 \cdot z_3 + z_4}{z_3 - z_4} \tag{47}$$

# 8. References

- Cocking, H. (1986). The Design of an Advanced Engineering Gearbox. *Vertica*. Vol 10, No. 2, Westland Helicopters and Hovercraft PLC, Yeovil, England, pp. 213-215
- Craig, G. A.; Heath, G. F. & Sheth, V. J. (1998). Split Torque Proprotor Transmission, McDonnell Douglas Helicopter Co., *U.S. Patent* Number 5,823,470
- Gmirya, Y.; Kish, J.G. (2003). Split-Torque Face Gear Transmission, Sikorsky Aircraft Corporation, U.S. Patent Number 6,612,195
- Gmirya, Y. & Vinayak, H. (2004). Load Sharing Gear for High Torque, Split-Path Transmissions. Sikorsky Aircraft Corporation. *International Patent PCT*. WO 2004/094093
- Gmirya, Y. (2005). Split Torque Gearbox With Pivoted Engine Support, Sikorsky Aircraft Corp., U.S. Patent Number 6,883,750
- Henriot G. (1979). Traité théorique et pratique des engrenages (I), Ed. Dunod, 6th Edition, ISBN 2-04-015607-0, Paris, France, pp. 587-662
- Isabelle, C.J; Kish & J.G, Stone, R.A. (1992). Elastomeric Load Sharing Device. United Technologies Corporation. *U.S. Patent* Number 5,113,713
- Kish, J.G. & Webb, L.G. (1992). Elastomeric Torsional Isolator. United Technologies Corporation. U.S. Patent Number 5,117,704
- Kish, J.G. (1993a). Sikorsky Aircraft Advanced Rotorcraft Transmission (ART) Program Final Report. NASA CR-191079, NASA Lewis Research Center, Cleveland, OH
- Kish, J.G. (1993b). Comanche Drive System. *Proceedings of the Rotary Wing Propulsion Specialists Meeting*, American Helicopter Society, Williamsburg, VA, pp. 7
- Krantz, T.L.; Rashidi, M. & Kish, J.G. (1992). *Split Torque Transmission Load Sharing*, in: Technical Memorandum 105,884, NASA Lewis Research Center, Cleveland, Ohio. Army Research Laboratory Technical Report 92-C-030
- Krantz, T.L. (1994). Dynamics of a Split Torque Helicopter Transmission, in: Technical Memorandum 106,410, NASA Lewis Research Center, Cleveland, Ohio. Army Research Laboratory Technical Report ARL-TR-291
- Krantz, T.L. (1996). A Method to Analyze and Optimize the Load Sharing of Split Path Transmissions, in: Technical Memorandum 107,201, NASA Lewis Research Center, Cleveland, Ohio. Army Research Laboratory Technical Report ARL-TR-1066
- Krantz, T.L. & Delgado, I.R. (1996). Experimental Study of Split-Path Transmission Load Sharing, in: Technical Memorandum 107,202, NASA Lewis Research Center, Cleveland, Ohio. Army Research Laboratory Technical Report ARL-TR-1067

- Parker, R.G., Lin, J. (2004). Mesh phasing relationships in planetary and epicyclic gears, Journal of Mechanical Design. Vol. 126, Issue 2, pp. 365-370, ISSN 1050-0472, eISSN 1528-9001
- Smirnov, G. (1990). Multiple-Power-Path Nonplanetary Main Gearbox of the Mi-26 Heavy-Lift Transport Helicopter, in: Vertiflite, Mil Design Bureau, Moscow, Vol. 36, pp. 20-23, ISSN 0042-4455
- Southcott, B. (1999). Gear Arrangement. Adelaide Gear Pty. Ltd. U.S. Patent Number 5,896,775
- Vilán-Vilán, J.A.; Segade-Robleda, A.; López-Lago, M & Casarejos-Ruiz, E. (2010), Feasible Geometrical Configurations for Split Torque Gearboxes With Idler Pinions, *Journal* of Mechanical Design, Vol. 132, Issue 12, pp. 121,011, 8 pages, ISSN 1050-0472, eISSN 1528-9001
- White, G. (1974). New Family of High-Ratio Reduction Gear With Multiple Drive Paths, Proceedings of the Institution of Mechanical Engineers., Vol. 188, pp. 281-288, ISSN 020-3483
- White, G. (1983). A 2400 kW Lightweight Helicopter Transmission Whit Split Torque Gear Trains, ASME Paper 84 Det-91
- White, G. (1989). Split-Torque Helicopter Transmission With Widely Separated Engines. Proceedings of the Institution of Mechanical Engineers. Vol 203, Number G1, pp. 53-65, ISSN 0954-4100
- White, G. (1993). 3600 HP Split-Torque Helicopter Transmission, in: Mechanical Systems Technology Branch Research Summary, 1985-1992, NASA Technical Memorandum 106,329
- White, G. (1998). Design study of a split-torque helicopter transmission, in: *Proceedings of the Institution of Mechanical Engineers, Part G: Journal of Aerospace Engineering*. Vol. 212, No. 2, pp. 117-123, ISSN 0954-4100, eISSN 2041-3025.

# On the Modelling of Spur and **Helical Gear Dynamic Behaviour**

Velex Philippe University of Lyon, INSA Lyon, LaMCoS UMR CNRS, France

#### 1. Introduction

This chapter is aimed at introducing the fundamentals of spur and helical gear dynamics. Using three-dimensional lumped models and a thin-slice approach for mesh elasticity, the general equations of motion for single-stage spur or helical gears are presented. Some particular cases including the classic one degree-of-freedom model are examined in order to introduce and illustrate the basic phenomena. The interest of the concept of transmission errors is analysed and a number of practical considerations are deduced. Emphasis is deliberately placed on analytical results which, although approximate, allow a clearer understanding of gear dynamics than that provided by extensive numerical simulations. Some extensions towards continuous models are presented.

#### 2. Nomenclature

b: face width

 $C_m$ ,  $C_r$ : pinion, gear torque

e(M),  $E_{MAX}(t)$ : composite normal deviation at M, maximum of e(M) at time t.

E,E\*: actual and normalized depth of modification at tooth tips

 $\mathbf{F}_{\mathbf{e}}(t) = \int_{-\infty}^{\infty} k(M) \delta e(M) \mathbf{V}(\mathbf{M}) dM$ : time-varying, possibly non-linear forcing term associated

with tooth shape modifications and errors

 $\mathbf{G} = \mathbf{V}_0 \mathbf{V}_0^T$ 

H(x): unit Heaviside step function (H(x) = 1 if x > 1; H(x) = 0 otherwise)

 $k_m$ ,  $k(t,\mathbf{q})$ : average and time-varying, non-linear mesh stiffness

 $k(t) = k_m (1 + \alpha \varphi(t))$ , linear time-varying mesh stiffness

 $k_0$ : mesh stiffness per unit of contact length

k(M), mesh stiffness per unit of contact length at M

 $k_{\Phi p}$  : modal stiffness associated with (  $\omega_p$  ,  $\Phi_{\mathbf{p}}$  )

 $\left[\mathbf{K}_{\mathbf{G}}(t)\right] = \int_{L(t,\mathbf{q})} k(M) \mathbf{V}(\mathbf{M}) \mathbf{V}(\mathbf{M}) \mathbf{V}(\mathbf{M})^{\mathrm{T}} dM : \text{ time-varying, possibly non-linear gear mesh}$ 

stiffness matrix

 $L(t,\mathbf{q})$ : time-varying, possibly non-linear, contact length

 $L_m = \varepsilon_\alpha \frac{b}{\cos \beta_b}$ : average contact length

 $\widehat{m} = \frac{I_{02}I_{01}}{Rb_1^2I_{02} + Rb_2^2I_{01}}$ : equivalent mass

 $m_{\Phi_p}$  : modal mass associated with (  $\omega_p$  ,  $\mathbf{\Phi}_{\mathbf{p}}$  )

 $\mathbf{n}_1$ : outward unit normal vector with respect to pinion flanks

NLTE: no-load transmission error

 $O_1, O_2$ : pinion, gear centre

 $Pb_a$ : apparent base pitch

 $Rb_1$ ,  $Rb_2$ : base radius of pinion, of gear

(s,t,z): coordinate system attached to the pinion-gear centre line, see Figs. 1&2

 $T_m$ : mesh period.

TE, TE<sub>s</sub>: transmission error, quasi-static transmission error under load

V(M),  $V_0$ , structural vector, averaged structural vector

W: projection vector for the expression of transmission error, see (44-1)

(X,Y,z): coordinate system associated with the base plane, see Fig. 2

 $\mathbf{X}_0 = \overline{\mathbf{K}}^{-1} \mathbf{F}_0$ : static solution with averaged mesh stiffness (constant)

 $\mathbf{X}_{s}$  ,  $\mathbf{X}_{\text{D}}$   $\mathbf{X}$  : quasi-static, dynamic and total (elastic) displacement vector (time-dependent)

 $Z_1, Z_2$ : tooth number on pinion, on gear

 $\alpha$ : small parameter representative of mesh stiffness variations, see (30)

 $\alpha_n$ : apparent pressure angle

 $\beta_h$ : base helix angle

$$\delta_m = \frac{F_S}{k_m} = \mathbf{V}^T \mathbf{X}_0$$
: static mesh deflection with average mesh stiffness

 $\delta e(M) = E_{MAX}(t) - e(M)$ : instantaneous initial equivalent normal gap at M

 $\Delta(M)$ : mesh deflection at point M

 $\varepsilon_{\alpha}$ : theoretical profile contact ratio

 $\varepsilon_{\scriptscriptstyle B}$ : overlap contact ratio

$$\Lambda = \frac{Cm}{Rb_1b\,k_0}$$
, deflection of reference

 $\Phi_{p}$ :  $p^{th}$  eigenvector of the system with constant averaged stiffness matrix

 $\zeta_P$ : damping factor associated with the  $p^{th}$  eigenfrequency

 $\Gamma$  : dimensionless extent of profile modification (measured on base plane)

$$\tau = \frac{t}{T_{--}}$$
, dimensionless time

 $\omega_{p}: p^{th}$  eigenfrequency of the system with constant averaged stiffness matrix

 $\overline{\omega}_{pn} = \frac{\omega_p}{n\Omega_1}$ , dimensionless eigenfrequency

 $\Omega_1, \Omega_2$ : pinion, gear angular velocity

 $\bar{\mathbf{A}}$ : vector  $\mathbf{A}$  completed by zeros to the total system dimension

- $\left(\bullet\right)^* = \frac{\left(\bullet\right)}{\delta_m}$ , normalized displacement with respect to the average static mesh deflection
- $(\hat{\bullet}) = \frac{(\bullet)}{k_m}$ , normalized stiffness with respect to the average mesh stiffness

# 3. Three-dimensional lumped parameter models of spur and helical gears

# 3.1 Rigid-body rotations - State of reference

It is well-known that the speed ratio for a pinion-gear pair with perfect involute spur or helical teeth is constant as long as deflections can be neglected. However, shape errors are present to some extent in all gears as a result of machining inaccuracy, thermal distortions after heat treatment, etc. Having said this, some shape modifications from ideal tooth flanks are often necessary (profile and/or lead modifications, topping) in order to compensate for elastic or thermal distortions, deflections, misalignments, positioning errors, etc. From a simulation point of view, rigid-body rotations will be considered as the references in the vicinity of which, small elastic displacements can be superimposed. It is therefore crucial to characterise rigid-boy motion transfer between a pinion and a gear with tooth errors and/or shape modifications. In what follows, e(M) represents the equivalent normal deviation at the potential point of contact M (sum of the deviations on the pinion and on the gear) and is conventionally positive for an excess of material and negative when, on the contrary, some material is removed from the ideal geometry. For rigid-body conditions (or alternatively under no-load), contacts will consequently occur at the locations on the contact lines where e(M) is maximum and the velocity transfer from the pinion to the gear is modified compared with ideal gears such that:

$$\left(Rb_1\Omega_1 + Rb_2\Omega_2\right)\cos\beta_b + \frac{dE_{MAX}(t)}{dt} = 0$$
(1)

where  $E_{\text{MAX}}(t) = \max_{M}(e(M))$  with  $\max_{M}()$ , maximum over all the potential point of contact at time t

The difference with respect to ideal motion transfer is often related to the notion of no-load transmission error *NLTE* via:

$$\frac{d}{dt}(NLTE) = Rb_1 \Omega_1 + Rb_2 \Omega_2 = -\frac{1}{\cos \beta_b} \frac{dE_{MAX}(t)}{dt}$$
 (2)

Using the Kinetic Energy Theorem, the rigid-body dynamic behaviour for frictionless gears is controlled by:

$$J_1 \Omega_1 \dot{\Omega}_1 + J_2 \Omega_2 \dot{\Omega}_2 = C_m \Omega_1 + C_r \Omega_2 \tag{3}$$

with  $J_1, J_2$ : the polar moments of inertia of the pinion shaft line and the gear shaft line respectively.  $C_m, C_r$ : pinion and gear torques.

The system with 4 unknowns ( $\Omega_1$ ,  $\Omega_2$ ,  $C_m$ ,  $C_r$ ) is characterised by equations (2) - (3) only, and 2 parameters have to be imposed.

# 3.2 Deformed state - Principles

Modular models based on the definition of gear elements (pinion-gear pairs), shaft elements and lumped parameter elements (mass, inertia, stiffness) have proved to be effective in the simulation of complex gear units (Küçükay, 1987), (Baud & Velex, 2002). In this section, the theoretical foundations upon which classic gear elements are based are presented and the corresponding elemental stiffness and mass matrices along with the possible elemental forcing term vectors are derived and explicitly given. The simplest and most frequently used 3D representation corresponds to the pinion-gear model shown in Figure 1. Assuming that the geometry is not affected by deflections (small displacements hypothesis) and provided that mesh elasticity (and to a certain extent, gear body elasticity) can be transferred onto the base plane, a rigid-body approach can be employed. The pinion and the gear can therefore be assimilated to two rigid cylinders with 6 degrees of freedom each, which are connected by a stiffness element or a distribution of stiffness elements (the discussion of the issues associated with damping and energy dissipation will be dealt with in section 4.3). From a physical point of view, the 12 degrees of freedom of a pair represent the generalised displacements of i) traction:  $u_1, u_2$  (axial displacements), ii) bending:  $v_1, v_2, v_3$ (translations in two perpendicular directions of the pinion/gear centre),  $\varphi_1, \psi_1, \varphi_2, \psi_2$ (bending rotations which can be assimilated to misalignment angles) and finally, iii) torsion:

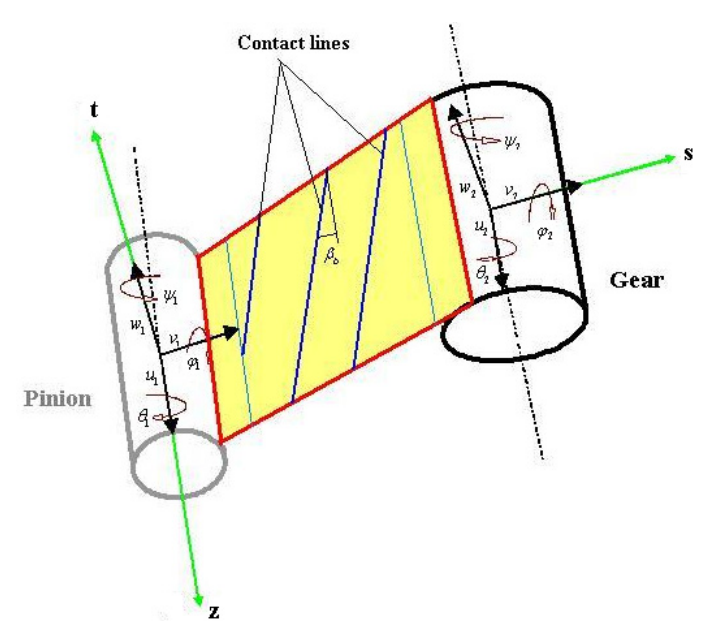


Fig. 1. A 3D lumped parameter model of pinion-gear pair.

 $\theta_1, \theta_2$  which are small angles associated with deflections superimposed on rigid-body rotations  $\Theta_1 = \int\limits_0^t \Omega_1(\sigma) d\sigma$  (pinion) and  $\Theta_2 = \int\limits_0^t \Omega_2(\sigma) d\sigma$  (gear). Following Velex and Maatar (1996), screws of infinitesimal displacements are introduced whose co-ordinates for solid k (conventionally k=1 for the pinion, k=2 for the gear) can be expressed in two privileged coordinate systems: i) ( $\mathbf{s}, \mathbf{t}, \mathbf{z}$ ) such that  $\mathbf{z}$  is in the shaft axis direction (from the motor to the load machine),  $\mathbf{s}$  is in the centre-line direction from the pinion centre to the gear centre and  $\mathbf{t} = \mathbf{z} \times \mathbf{s}$  (Fig. 1) or, ii) ( $\mathbf{X}, \mathbf{Y}, \mathbf{z}$ ) attached to the base plane (Fig. 1):

$$\begin{cases}
S_k \\
W_k (\mathbf{O}_k) = v_k \mathbf{s} + w_k \mathbf{t} + u_k \mathbf{z} \\
\mathbf{\omega}_k = \varphi_k \mathbf{s} + \psi_k \mathbf{t} + \theta_k \mathbf{z}
\end{cases} \text{ or } \begin{cases}
\mathbf{u}_k (\mathbf{O}_k) = V_k \mathbf{X} + W_k \mathbf{Y} + u_k \mathbf{z} \\
\mathbf{\omega}_k = \Phi_k \mathbf{X} + \Psi_k \mathbf{Y} + \theta_k \mathbf{z}
\end{cases}$$

$$k=1,2$$
(4)

where  $O_1, O_2$  are the pinion and gear centres respectively

#### 3.3 Deflection at a point of contact - Structural vectors for external gears

Depending on the direction of rotation, the direction of the base plane changes as illustrated in Figure 2 where the thicker line corresponds to a positive rotation of the pinion and the finer line to a negative pinion rotation about  $axis(O_1, \mathbf{z})$ .

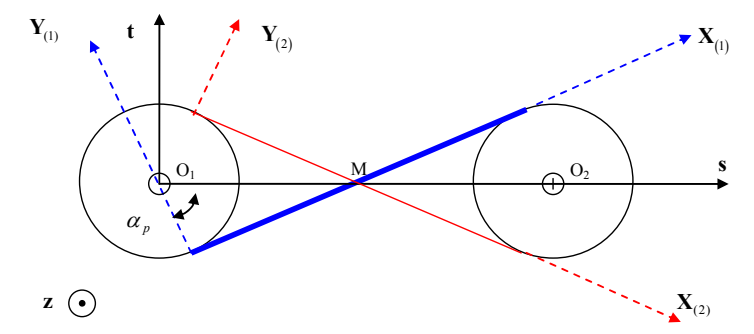


Fig. 2. Directions of rotation and planes (lines) of action. (the thicker line corresponds to a positive rotation of pinion)

For a given helical gear, the sign of the helix angle on the base plane depends also on the direction of rotation and, here again; two configurations are possible as shown in Figure 3.

Since a rigid-body mechanics approach is considered, contact deflections correspond to the interpenetrations of the parts which are deduced from the contributions of the degrees-of-freedom and the initial separations both measured in the normal direction with respect to the tooth flanks. Assuming that all the contacts occur in the theoretical base plane (or plane of action), the normal deflection  $\Delta(M)$  at any point M, potential point of contact, is therefore expressed as:

$$\Delta(M) = \mathbf{u}_1(\mathbf{M}) \cdot \mathbf{n}_1 - \mathbf{u}_2(\mathbf{M}) \cdot \mathbf{n}_1 - \delta e(M)$$
 (5)

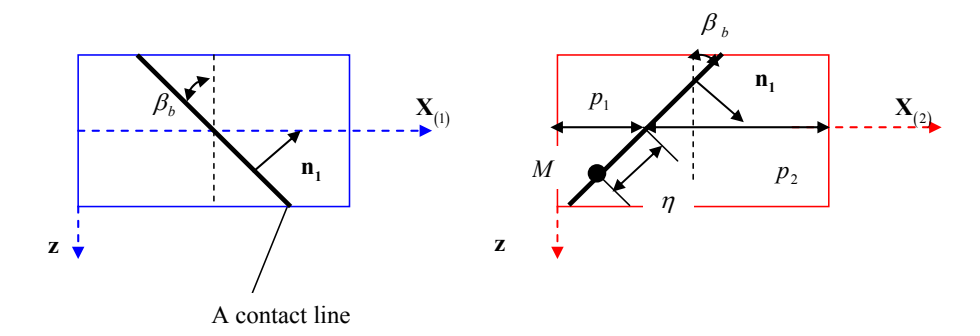


Fig. 3. Helix angles on the base plane.

where  $\delta e(M) = \max_{M} (e(M)) - e(M)$  is the equivalent initial normal gap at M caused by tooth modifications and/or errors for example,  $\mathbf{n}_1$  is the outward unit normal vector to pinion tooth flanks (Fig.3)

Using the shifting property of screws, one obtains the expression of  $\Delta(M)$  in terms of the screw co-ordinates as:

$$\Delta(M) = \mathbf{u}_1(\mathbf{O}_1) \cdot \mathbf{n}_1 + (\mathbf{\omega}_1 \times \mathbf{O}_1 \mathbf{M}) \cdot \mathbf{n}_1 - \mathbf{u}_2(\mathbf{O}_2) \cdot \mathbf{n}_1 - (\mathbf{\omega}_2 \times \mathbf{O}_2 \mathbf{M}) \cdot \mathbf{n}_1 - \delta \varepsilon(M)$$
(6)

which is finally expressed as:

$$\Delta(M) = \begin{bmatrix} \mathbf{n}_1 \\ \mathbf{O}_1 \mathbf{M} \times \mathbf{n}_1 \\ -\mathbf{n}_1 \\ -\mathbf{O}_2 \mathbf{M} \times \mathbf{n}_1 \end{bmatrix}^{\mathrm{T}} \begin{bmatrix} \mathbf{u}_1(\mathbf{O}_1) \\ \mathbf{\omega}_1 \\ \mathbf{u}_2(\mathbf{O}_2) \\ \mathbf{\omega}_2 \end{bmatrix} - \delta e(M)$$
 (7)

or, in a matrix form:

$$\Delta(M) = \mathbf{V}(\mathbf{M})^{\mathsf{T}} \mathbf{q} - \delta e(M) \tag{8}$$

where V(M) is a structural vector which accounts for gear geometry (Küçükay, 1987) and  $\mathbf{q}$  is the vector of the pinion-gear pair degrees of freedom (superscript T refers to the transpose of vectors and matrices)

The simplest expression is that derived in the (X,Y,z) coordinate system associated with the base plane leading to:

$$\mathbf{V}(\mathbf{M})^{T} = \langle \cos \beta_{b}, 0, \varepsilon \sin \beta_{b}, -\zeta \varepsilon R b_{1} \sin \beta_{b}, \eta - \varepsilon p_{1} \sin \beta_{b}, \zeta R b_{1} \cos \beta_{b}, \\ -\cos \beta_{b}, 0, -\varepsilon \sin \beta_{b}, -\zeta \varepsilon R b_{2} \sin \beta_{b}, -[\eta + \varepsilon p_{2} \sin \beta_{b}], \zeta R b_{2} \cos \beta_{b} \rangle$$

$$\mathbf{q}^{T} = \langle V_{1} \quad W_{1} \quad u_{1} \quad \Phi_{1} \quad \Psi_{1} \quad \theta_{1} \quad V_{2} \quad W_{2} \quad u_{2} \quad \Phi_{2} \quad \Psi_{2} \quad \theta_{2} \rangle$$

$$(9)$$

where  $Rb_1$ ,  $Rb_2$  are the pinion, gear base radii;  $\beta_b$  is the base helix angle (always considered as positive in this context);  $p_1$ ,  $p_2$ ,  $\eta$  are defined in Figure 3;  $\varepsilon = \pm 1$  depending on the sign of the helix angle;  $\zeta = +1$  for a positive rotation of the pinion and  $\zeta = -1$  for a negative rotation of the pinion.

An alternative form of interest is obtained when projecting in the (s,t,z) frame attached to the pinion-gear centre line:

$$\mathbf{V}(\mathbf{M})^{T} = \left\langle \cos \beta_{b} \sin \alpha_{p}, \quad \zeta \cos \beta_{b} \cos \alpha_{p}, \quad \varepsilon \sin \beta_{b}, \quad -\zeta \varepsilon R b_{1} \sin \beta_{b} \sin \alpha_{p} - \zeta \left( \eta - \varepsilon p_{1} \sin \beta_{b} \right) \cos \alpha_{p} \right.$$

$$\left[ -\varepsilon R b_{1} \sin \beta_{b} \cos \alpha_{p} + \left( \eta - \varepsilon p_{1} \sin \beta_{b} \right) \sin \alpha_{p} \right], \quad \zeta R b_{1} \cos \beta_{b}, \quad -\cos \beta_{b} \sin \alpha_{p}, \quad -\zeta \cos \beta_{b} \cos \alpha_{p},$$

$$\left. -\varepsilon \sin \beta_{b}, \quad -\zeta \varepsilon R b_{2} \sin \beta_{b} \sin \alpha_{p} + \zeta \left( \eta + \varepsilon p_{2} \sin \beta_{b} \right) \cos \alpha_{p} \right.$$

$$\left. - \left[ \varepsilon R b_{2} \sin \beta_{b} \cos \alpha_{p} + \left( \eta + \varepsilon p_{2} \sin \beta_{b} \right) \sin \alpha_{p} \right], \quad \zeta R b_{2} \cos \beta_{b} \right. \right\rangle$$

$$\mathbf{q}^{T} = \left\langle v_{1} \quad w_{1} \quad u_{1} \quad \varphi_{1} \quad \psi_{1} \quad \theta_{1} \quad v_{2} \quad w_{2} \quad u_{2} \quad \varphi_{2} \quad \psi_{2} \quad \theta_{2} \right. \right\rangle$$

$$(10)$$

#### 3.4 Mesh stiffness matrix and forcing terms for external gears

For a given direction of rotation, the usual contact conditions in gears correspond to single-sided contacts between the mating flanks which do not account for momentary tooth separations which may appear if dynamic displacements are large (of the same order of magnitude as static displacements). A review of the mesh stiffness models is beyond the scope of this chapter but one usually separates the simulations accounting for elastic convection (i.e., the deflection at one point *M* depends on the entire load distribution on the tooth or all the mating teeth (Seager, 1967)) from the simpler (and classic) thin-slice approach (the deflection at point *M* depends on the load at the same point only). A discussion of the limits of this theory can be found in Haddad (1991), Ajmi & Velex (2005) but it seems that, for solid gears, it is sufficiently accurate as far as dynamic phenomena such as critical speeds are considered as opposed to exact load or stress distributions in the teeth which are more dependent on local conditions. Neglecting contact damping and friction forces compared with the normal elastic components on tooth flanks, the elemental force transmitted from the pinion onto the gear at one point of contact *M* reads:

$$\mathbf{dF}_{1/2}(\mathbf{M}) = k(M)\Delta(M)dM\,\mathbf{n}_1\tag{11}$$

with k(M): mesh stiffness at point M per unit of contact length

The resulting total mesh force and moment at the gear centre  $O_2$  are deduced by integrating over the time-varying and possibly deflection-dependent contact length  $L(t, \mathbf{q})$  as:

$$\left\{F_{1/2}\right\} \begin{cases}
\mathbf{F}_{1/2} = \int\limits_{L(t,\mathbf{q})} k(M)\Delta(M)dM \,\mathbf{n}_{1} \\
\mathbf{M}_{1/2}(\mathbf{O}_{2}) = \int\limits_{L(t,\mathbf{q})} k(M)\Delta(M)\mathbf{O}_{2}\mathbf{M} \times \mathbf{n}_{1} dM
\end{cases} \tag{12-1}$$

Conversely the mesh force wrench at the pinion centre  $O_1$  is:

$$\left\{F_{2/1}\right\} \begin{cases}
\mathbf{F}_{2/1} = -\int\limits_{L(t,\mathbf{q})} k(M)\Delta(M)dM \,\mathbf{n}_{1} \\
\mathbf{M}_{2/1}(\mathbf{O}_{1}) = -\int\limits_{L(t,\mathbf{q})} k(M)\Delta(M)\mathbf{O}_{1}\mathbf{M} \times \mathbf{n}_{1} \,dM
\end{cases} \tag{12-2}$$

The mesh inter-force wrench can be deduced in a compact form as:

$$\begin{aligned}
\{F_{M}\} & \begin{cases} \{F_{2/1}\} \\ \{F_{1/2}\} \end{cases} = -\int_{L(t,\mathbf{q})} k(M)\Delta(M)\mathbf{V}(\mathbf{M})dM
\end{aligned} \tag{13}$$

and introducing the contact normal deflection  $\Delta(M) = \mathbf{V}(\mathbf{M})^{\mathrm{T}} \mathbf{q} - \delta e(M)$  finally leads to:

$$\{F_{M}\} = -\lceil \mathbf{K}_{G}(t) \rceil \mathbf{q} + \mathbf{F}_{e}(t)$$
(14)

where  $[\mathbf{K}_{G}(t)] = \int_{L(t,\mathbf{q})} k(M) \mathbf{V}(\mathbf{M}) \mathbf{V}(\mathbf{M})^{T} dM$  is the time-varying gear mesh stiffness matrix

 $\mathbf{F}_{\mathbf{e}}(t) = \int_{L(t,\mathbf{q})} k(M) \delta e(M) \mathbf{V}(\mathbf{M}) dM$  is the excitation vector associated with tooth shape modifications and errors

# 3.5 Mass matrix of external gear elements-Additional forcing (inertial) terms

For solid *k* (pinion or gear), the dynamic sum with respect to the inertial frame can be expressed as:

$$\mathbf{\Sigma}_{\mathbf{k}}^{0} = m_{k} \left[ \left( \ddot{v}_{k} - e_{k} \dot{\Omega}_{k} \sin \Theta_{k} - e_{k} \Omega_{k}^{2} \cos \Theta_{k} \right) \mathbf{s} + \left( \ddot{w}_{k} + e_{k} \dot{\Omega}_{k} \cos \Theta_{k} - e_{k} \Omega_{k}^{2} \sin \Theta_{k} \right) \mathbf{t} + \ddot{u}_{k} \mathbf{z} \right]$$
(15)

where  $m_k$  and  $e_k$  are respectively the mass and the eccentricity of solid k

A simple expression of the dynamic moment at point  $O_k$  can be obtained by assuming that  $O_k$  is the centre of inertia of solid k and neglecting gyroscopic components (complementary information can be found in specialised textbooks on rotor dynamics (see for instance (Lalanne & Ferraris, 1998)):

$$\delta_{\mathbf{k}}^{0}(O_{k}) \cong I_{k} \ddot{\varphi}_{k} \mathbf{s} + I_{k} \ddot{\psi}_{k} \mathbf{t} + I_{0k} (\dot{\Omega}_{k} + \ddot{\theta}_{k}) \mathbf{z}$$

$$\tag{16}$$

where  $I_k$  is the cross section moment of inertia and  $I_{0k}$  is the polar moment of solid k

Using the same DOF arrangement as for the stiffness matrices, a mass matrix for the piniongear system can be deduced as (note that the same mass matrix is obtained in the (X,Y,z) coordinate system):

$$[\mathbf{M}_{G}] = \mathbf{diag}(m_{1}, m_{1}, m_{1}, I_{1}, I_{1}, I_{01}, m_{2}, m_{2}, m_{2}, I_{2}, I_{02})$$
(17-1)

along with a forcing term associated with inertial forces (whose expression in (X,Y,z) has the same form on the condition that angles  $\Theta_{1,2}$  are measured from X and Y):

$$\mathbf{F}_{G}(t) = \left\langle m_{1}e_{1}(\dot{\Omega}_{1}\sin\Theta_{1} + \Omega_{1}^{2}\cos\Theta_{1}) - m_{1}e_{1}(\dot{\Omega}_{1}\cos\Theta_{1} - \Omega_{1}^{2}\sin\Theta_{1}) \quad 0 \quad 0 \quad 0 \quad -I_{01}\dot{\Omega}_{1} \right.$$

$$\left. m_{2}e_{2}(\dot{\Omega}_{2}\sin\Theta_{2} + \Omega_{2}^{2}\cos\Theta_{2}) - m_{2}e_{2}(\dot{\Omega}_{2}\cos\Theta_{2} - \Omega_{2}^{2}\sin\Theta_{2}) \quad 0 \quad 0 \quad 0 \quad -I_{02}\dot{\Omega}_{2} \right\rangle$$

$$(17-2)$$

#### 3.6 Usual simplifications

Examining the components of the structural vectors in (9) and (10), it can be noticed that most of them are independent of the position of the point of contact M with the exception of those related to bending slopes  $\Psi_{1,2}$  or  $\varphi_{1,2}$ ,  $\psi_{1,2}$ . Their influence is usually discarded especially for narrow-faced gears so that the mesh stiffness matrix can be simplified as:

$$\left[\mathbf{K}_{\mathbf{G}}(t)\right] \cong \int_{L(t,\mathbf{q})} k(M) dM \, \mathbf{V}_{0} \, \mathbf{V}_{0}^{\mathrm{T}} = k(t,\mathbf{q}) \mathbf{G}$$
(18)

where  $V_0$  represents an average structural vector and  $k(t, \mathbf{q})$  is the time-varying, possibly non-linear, mesh stiffness function (scalar) which plays a fundamental role in gear dynamics.

#### 3.6.1 Classic one-DOF torsional model

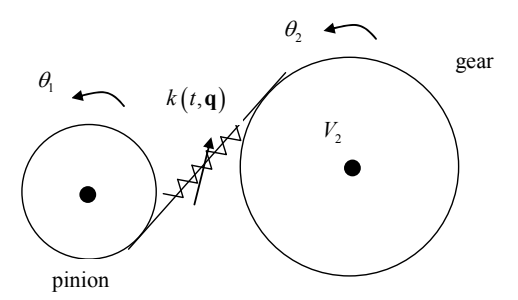


Fig. 4. Basic torsional model.

Considering the torsional degrees-of-freedom only (Figure 4), the structural vector reads (keeping solely the non-zero components):

$$\mathbf{V}(\mathbf{M}) = \mathbf{V}_0 = \begin{bmatrix} \zeta Rb_1 \\ \zeta Rb_2 \end{bmatrix} \cos \beta_b \tag{19}$$

and the following differential system is derived  $(\zeta^2 = 1)$ :

$$\begin{bmatrix} I_{01} & 0 \\ 0 & I_{02} \end{bmatrix} \begin{bmatrix} \ddot{\theta}_1 \\ \ddot{\theta}_2 \end{bmatrix} + k(t, \theta_1, \theta_2) \cos^2 \beta_b \begin{bmatrix} Rb_1^2 & Rb_1Rb_2 \\ Rb_1Rb_2 & Rb_2^2 \end{bmatrix} \begin{bmatrix} \theta_1 \\ \theta_2 \end{bmatrix} =$$

$$= \begin{bmatrix} Cm \\ Cr \end{bmatrix} + \int_{L(t, \mathbf{q})} k(M) \delta e(M) dM \begin{bmatrix} \zeta Rb_1 \\ \zeta Rb_2 \end{bmatrix} \cos \beta_b - \begin{bmatrix} I_{01}\dot{\Omega}_1 \\ I_{02}\dot{\Omega}_2 \end{bmatrix}$$
(20)

Note that the determinant of the stiffness matrix is zero which indicates a rigid-body mode (the mass matrix being diagonal). After multiplying the first line in (20) by  $Rb_1I_{02}$ , the second line by  $Rb_2I_{01}$ , adding the two equations and dividing all the terms by  $\left(I_{10}Rb_2^2+I_{20}Rb_1^2\right)$ , the semi-definite system (20) is transformed into the differential equation:

$$\widehat{m}\ddot{x} + k(t,x)x = F_t + \zeta \cos \beta_b \int_{L(t,x)} k(M) \delta e(M) dM - \kappa \frac{d^2}{dt^2} (NLTE)$$
(21)

With  $x = Rb_1\theta_1 + Rb_2\theta_2$ , relative apparent displacement

$$\widehat{m} = \frac{I_{02}I_{01}}{Rb_1^2I_{02} + Rb_2^2I_{01}}$$
, equivalent mass

 $\kappa = \Omega_1^2 \frac{I_{02}}{Rb_2^2}$  when the pinion speed  $\Omega_1$  and the output torque  $C_r$  are supposed to be constant.

#### 3.6.2 A simple torsional-flexural model for spur gears

The simplest model which accounts for torsion and bending in spur gears is shown in Figure 5. It comprises 4 degrees of freedom, namely: 2 translations in the direction of the line of action  $V_1, V_2$  (at pinion and gear centres respectively) and 2 rotations about the pinion and gear axes of rotation  $\theta_1, \theta_2$ . Because of the introduction of bending DOFs, some supports (bearing/shaft equivalent stiffness elements for instance) must be added.

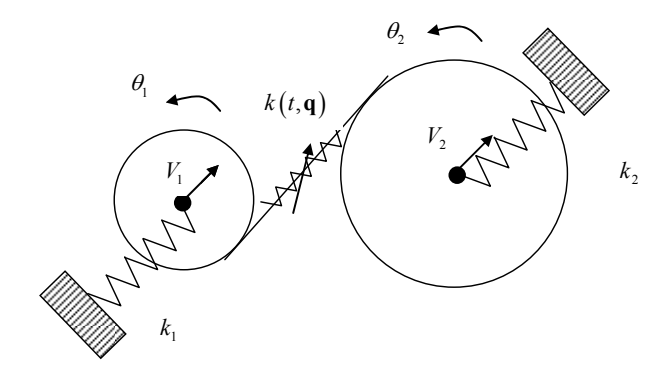


Fig. 5. Simplified torsional-flexural spur gear model.

The general expression of the structural vector V(M) (9) reduces to:

$$\mathbf{V_0}^T = \langle 1 \quad \zeta Rb_1 \quad -1 \quad \zeta Rb_2 \rangle \tag{22}$$

Re-writing the degree of freedom vector as  $\mathbf{q}^{*T} = \langle v_1 \ Rb_1\theta_1 \ v_2 \ Rb_2\theta_2 \rangle$ , the following parametrically excited differential system is obtained for linear free vibrations:

$$M\ddot{q}^* + K(t)q^* = 0$$
 (23-1)

$$\mathbf{M} = \begin{bmatrix} m_1 & & & & \\ & I_{01}/Rb_1^2 & & & \\ & & m_2 & & \\ & & & I_{02}/Rb_2^2 \end{bmatrix}; \quad \mathbf{K}(t) = \begin{bmatrix} k(t)+k_1 & \zeta k(t) & -k(t) & \zeta k(t) \\ & k(t) & -\zeta k(t) & k(t) \\ & & k(t)+k_2 & -\zeta k(t) \\ & & k(t) \end{bmatrix}$$
(23-2)

*Remark:* The system is ill-conditioned since rigid-body rotations are still possible (no unique static solution). In the context of 3D models with many degrees of freedom, it is not interesting to solve for the normal approach  $Rb_1\theta_1 + Rb_2\theta_1$  as is done for single DOF models. The problem can be resolved by introducing additional torsional stiffness element(s) which can represent shafts; couplings etc. thus eliminating rigid-body rotations.

#### 4. Mesh stiffness models - Parametric excitations

#### 4.1 Classic thin-slice approaches

From the results in section 2-5, it can be observed that, in the context of gear dynamic simulations, the mesh stiffness function defined as  $k(t,\mathbf{q}) = \int\limits_{L(t,\mathbf{q})} k(M)dM$  plays a key role.

This function stems from a 'thin-slice' approach whereby the contact lines between the mating teeth are divided in a number of independent stiffness elements (with the limiting case presented here of an infinite set of non-linear time-varying elemental stiffness elements) as schematically represented in Figure 6.

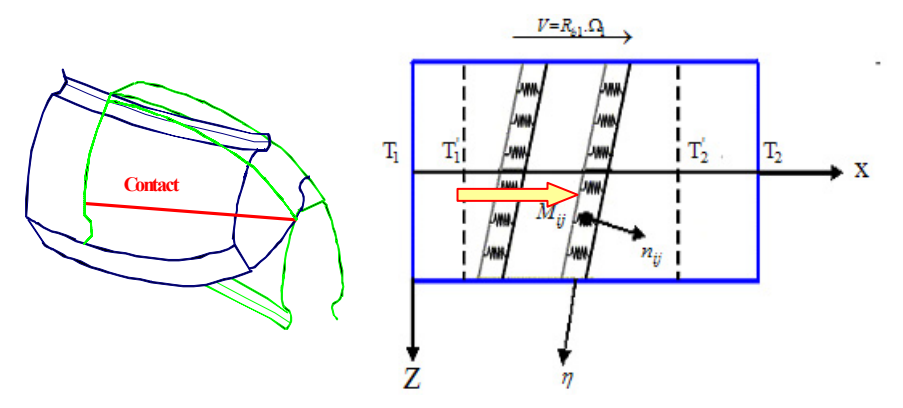


Fig. 6. 'Thin-slice' model for time-varying mesh stiffness.

Since the positions of the teeth (and consequently the contact lines) evolve with time (or angular positions), the profiles slide with respect to each other and the stiffness varies because of the contact length and the individual tooth stiffness evolutions. The definition of mesh stiffness has generated considerable interest but mostly with the objective of calculating accurate static tooth load distributions and stress distributions. It has been shown by Ajmi and Velex (2005) that a classic 'thin-slice' model is sufficient for dynamic calculations as long as local disturbances (especially near the tooth edges) can be ignored. In this context, Weber and Banascheck (1953) proposed a analytical method of calculating tooth deflections of spur gears by superimposing displacements which arise from i) the contact

between the teeth, ii) the tooth itself considered as a beam and, iii) the gear body (or foundation) influence. An analytical expression of the contact compliance was obtained using the 2D Hertzian theory for cylinders in contact which is singular as far as the normal approach between the parts (contact deflection) is concerned. The other widely-used formulae for tooth contact deflection comprise the analytical formula of Lundberg (1939), the approximate Hertzian approach originally used at Hamilton Standard (Cornell, 1981) and the semi-empirical formula developed by Palmgren (1959) for rollers. The tooth bending radial and tangential displacements were derived by equating the work produced by one individual force acting on the tooth profile and the strain energy of the tooth assimilated to a cantilever of variable thickness. Extensions and variants of the methodology were introduced by Attia (1964), Cornell (1981) and O'Donnell (1960, 1963) with regard to the foundation effects. Gear body contributions were initially evaluated by approximating them as part of an elastic semi-infinite plane loaded by the reactions at the junction with the tooth. A more accurate expression for this base deflection has been proposed by Sainsot et al. (2004) where the gear body is simulated by an elastic annulus instead of a half-plane. Figure 7 shows two examples of mesh stiffness functions (no contact loss) calculated by combining Weber's and Lundberg's results for a spur and a helical gear example. It can be observed that the stiffness fluctuations are stronger in the case of conventional spur gears compared with helical gears for which the contact variations between the teeth are smoother.

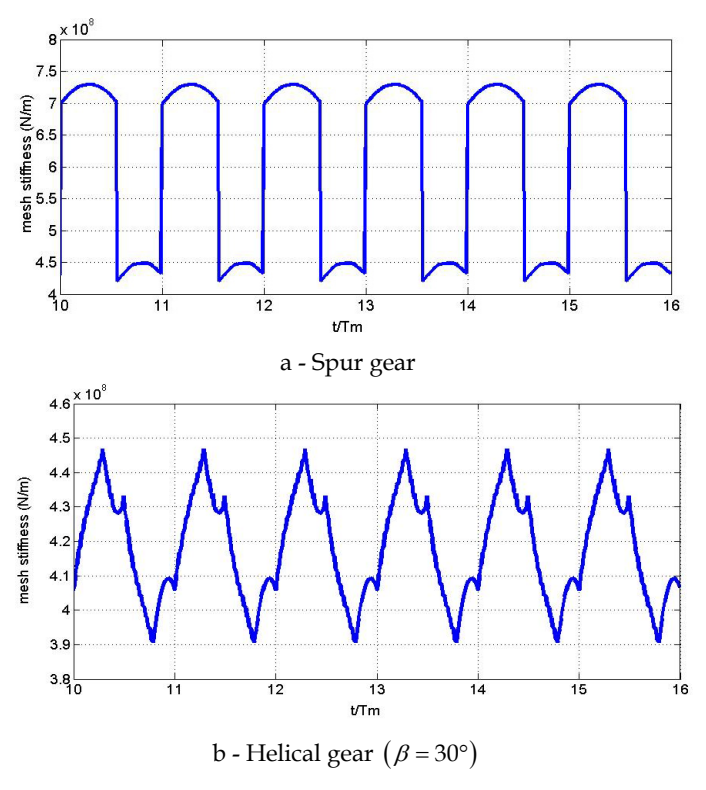


Fig. 7. Examples of mesh stiffness functions for errorless gears.

Although the results above are based on simplified bi-dimensional approaches, they are still widely used in gear design. For example, the mesh stiffness formulae in the ISO standard 6336 stem from Weber's analytical formulae which were modified to bring the values in closer agreement with the experimental results. Another important simplification brought by the ISO formulae is that the mesh stiffness per unit of contact length  $k_0$  is considered as approximately constant so that the following approximation can be introduced:

$$\int_{L(t,\mathbf{q})} k(M) dM \cong k_0 \int_{L(t,\mathbf{q})} dM = k_0 L(t,\mathbf{q})$$
(24)

where  $L(t,\mathbf{q})$  is the time-varying (possibly non-linear) contact length.

#### 4.2 Contact length variations for external spur and helical gears

Considering involute profiles, the contact lines in the base plane are inclined by the base helix angle  $\beta_b$  (Figure 8) which is nil for spur gears. All contact lines are spaced by integer multiples of the apparent base pitch  $Pb_a$  and, when the pinion and the gear rotate, they all undergo a translation in the **X** direction at a speed equal to  $Rb_1 \Omega_1$ .

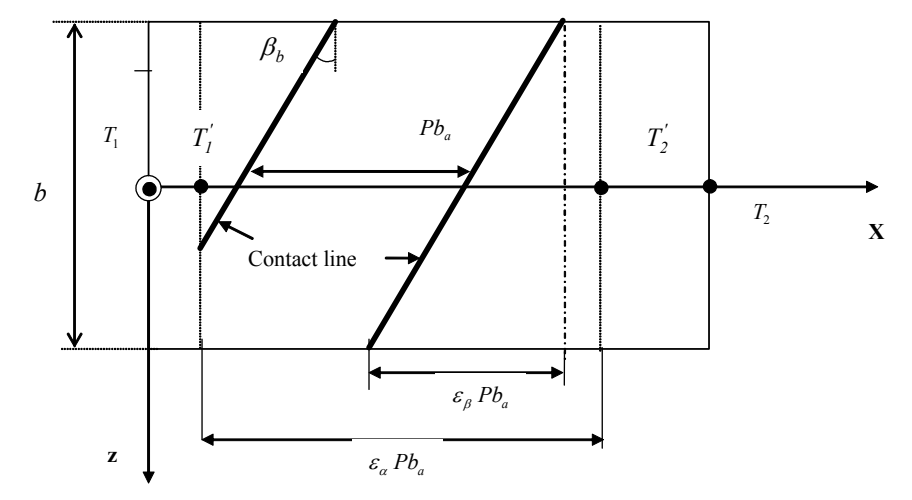


Fig. 8. Base plane and contact lines (b: face width; **Z**: axial direction (direction of the axes of rotation);  $T_1, T_2$ : points of tangency on pinion and gear base circles and  $T_1, T_2$ : limits of the contact area on base plane).

It transpires from this geometrical representation that the total length of contact between the pinion and the gear is likely to vary with time and, based on the simple stiffness equation (24), that mesh stiffness is time-varying and, consequently, contributes to the system excitation via parametric excitations.

The extent of action on the base plane is an important property measured by the contact ratio  $\varepsilon_{\alpha}$  which, in simple terms, represents the 'average number' of tooth pairs in contact (possibly non integer) and is defined by:

$$\varepsilon_{\alpha} = \frac{T_{1}'T_{2}'}{Pb_{a}} = \frac{\sqrt{Ra_{1}^{2} - Rb_{1}^{2}} + \sqrt{Ra_{2}^{2} - Rb_{2}^{2}} - E\sin\alpha_{p}}{\pi m\cos\alpha_{p}}$$
(25-1)

with  $Ra_1, Ra_2$ : external radius of pinion, of gear;  $Rb_1, Rb_2$ : base radius of pinion, of gear;  $E = \|O_1 \vec{O}_2\|$ : centre distance

In the case of helical gears, the overlap due to the helix is taken into account by introducing the overlap ratio  $\varepsilon_{\beta}$  defined as:

$$\varepsilon_{\beta} = \frac{b \tan \beta_b}{P b_a} = \frac{1}{\pi} \frac{b}{m} \frac{\tan \beta_b}{\cos \alpha_p}$$
 (25-2)

and the sum  $\varepsilon = \varepsilon_{\alpha} + \varepsilon_{\beta}$  is defined as the total contact ratio.

Introducing the dimensionless time  $\tau = \frac{t}{T_m}$  where  $T_m = \frac{Pb_a}{Rb_1\Omega_1}$  is the mesh period i.e. the time needed for a contact line to move by a base pitch on the base plane, a closed form expression of the contact length  $L(\tau)$  for ideal gears is obtained under the form (Maatar & Velex, 1996), (Velex et al., 2011):

$$\frac{L(\tau)}{L_m} = 1 + 2\sum_{k=1}^{\infty} Sinc(k\varepsilon_{\alpha})Sinc(k\varepsilon_{\beta})\cos(\pi k(\varepsilon_{\alpha} + \varepsilon_{\beta} - 2\tau))$$
(26)

with:  $L_m = \varepsilon_\alpha \frac{b}{\cos \beta_b}$ , average contact length

 $Sinc(x) = \frac{\sin(\pi x)}{\pi x}$  is the classic sine cardinal function which is represented in Figure 9.

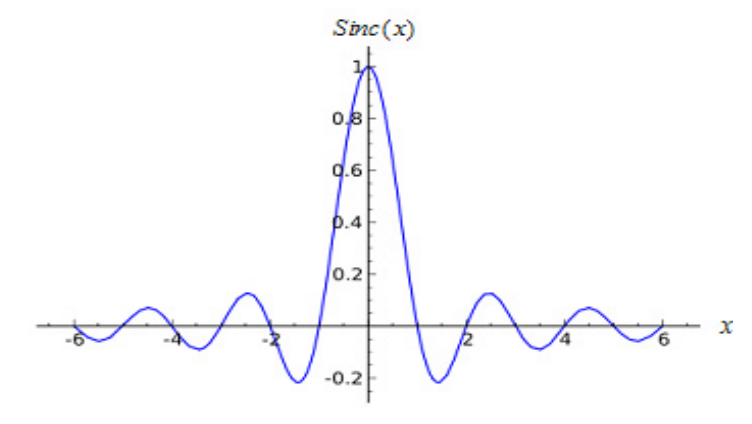


Fig. 9. Evolutions of  $Sinc(x) = \frac{\sin(\pi x)}{\pi x}$ .

The following conclusions can be drawn:

- a. for spur gears,  $\varepsilon_{\beta} = 0$  and  $Sinc(k\varepsilon_{\beta}) = 1$
- b. it can observed that the time-varying part of the contact length disappears when either  $\varepsilon_{\alpha}$  or  $\varepsilon_{\beta}$  is an integer
- c. harmonic analysis is possible by setting k = 1, 2, ... in (27) and it is possible to represent the contact length variations for all possible values of profile and overlap contact ratios on a unique diagram. Figure 10 represents the RMS of contact length variations for a realistic range of contact and overlap ratios. It shows that:
  - contact length variations are significant when  $\varepsilon_{\alpha}$  is below 2 and  $\varepsilon_{\beta}$  below 1
  - contact length is constant when  $\varepsilon_{\alpha}=2$  ( $\varepsilon_{\alpha}=1$  has to avoided for a continuous motion transfer) and /or  $\varepsilon_{\beta}=1$
  - for overlap ratios  $\varepsilon_{\beta}$  above 1, contact length variations are very limited.

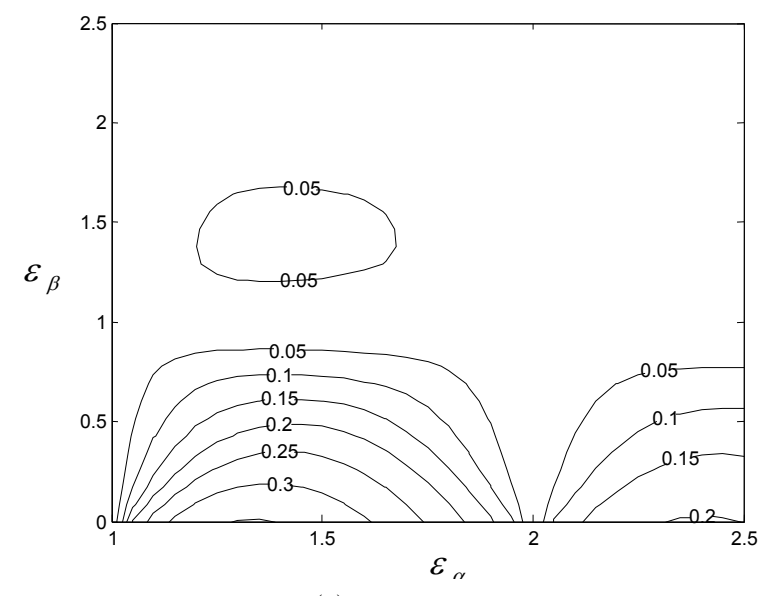


Fig. 10. Contour plot of the R.M.S. of  $L(\tau)/L_m$  for a range of profile and transverse contact ratios.

#### 4.3 Approximate expressions - Orders of magnitude

Mesh stiffness can be determined using the Finite Elements Method but it is interesting to have orders of magnitude or approximate values at the design stage. For solid gears made of steel, an order of magnitude of the mesh stiffness per unit of contact length  $k_0$  is  $\cong 1.3 \, 10^{10} \, \text{N/m}^2$ . More accurate expressions can be derived from the ISO 6336 standard which, for solid gears, gives:

$$k_0 \cong \cos \beta \frac{0.8}{q} \tag{27}$$

with

 $\beta$ : helix angle (on pitch cylinder)

$$q = C_1 + \frac{C_2}{Zn_1} + \frac{C_3}{Zn_2} + C_4x_1 + C_5\frac{x_1}{Zn_1} + C_6x_2 + C_7\frac{x_2}{Zn_2} + C_8x_1^2 + C_9x_2^2$$

coefficients  $C_1,...,C_9$  have been tabulated and are listed in Table 1 below

 $Zn_i = \frac{Z_i}{\cos^3 \beta}$ , i = 1,2 are the number of teeth of the equivalent virtual spur pinion (i = 1) and gear (i = 2).

 $x_i$ , i = 1, 2, are the profile shift coefficients on pinion(i = 1) and gear(i = 2)

$C_1$	$C_2$	$C_3$	$C_4$	$C_5$	$C_6$	$C_7$	$C_8$	$C_9$
0,04723	0,15551	0,25791	-0,00635	-0,11654	-0,00193	-0,24188	0,00529	0,00182

Table 1. Tabulated coefficients for mesh stiffness calculations according to ISO 6336.

# 5. Equations of motion - Dynamic behaviour

#### 5.1 Differential system

The equations of motion for undamped systems are derived by assembling all the elemental matrices and forcing term vectors associated with the gears but also the supporting members (shafts, bearings, casing, etc.) leading to a parametrically excited non-linear differential system of the form:

$$[\mathbf{M}]\ddot{\mathbf{X}} + [\mathbf{K}(t, \mathbf{X})]\mathbf{X} = \mathbf{F}_0 + \mathbf{F}_1(t, \mathbf{X}, \delta e(M)) + \mathbf{F}_2(t, \dot{\Omega}_{1,2})$$
(28)

where X is the total DOF vector, [M] and [K(t,X)] are the global mass and stiffness matrices. Note that, because of the contact conditions between the teeth, the stiffness matrix can be non-linear (partial or total contact losses may occur depending on shape deviations and speed regimes).  $F_0$  comprises the constant nominal torques;  $F_1(t,X,\delta e(M))$  includes the contributions of shape deviations (errors, shape modifications, etc.);  $F_2(t,\dot{\Omega}_{1,2})$  represents the inertial effects due to unsteady rotational speeds

#### 5.2 Linear behaviour - Modal analysis

Considering linear (or quasi-linear) behaviour, the differential system can be re-written as:

$$[\mathbf{M}]\ddot{\mathbf{X}} + [\mathbf{K}(t)]\mathbf{X} = \mathbf{F}_{0}(t) + \mathbf{F}_{1}(t, \delta e(M)) + \mathbf{F}_{2}(t, \dot{\Omega}_{1,2})$$
(29)

The time variations in the stiffness matrix  $[\mathbf{K}(t)]$  are caused by the meshing and, using the formulation based on structural vectors, the constant and time-varying components can be separated as:

$$\left[\mathbf{K}(\mathbf{t})\right] = \left[\mathbf{K}_{0}\right] + \int_{L(\mathbf{t})} k(M) \overline{\mathbf{V}}(\mathbf{M}) \overline{\mathbf{V}}(\mathbf{M})^{T} dM$$
(30)

where  $\overline{V}(M)$  is the extended structural vector: structural vector completed by zeros to the total number of DOF of the model

Using an averaged structural vector as in (18):

$$\overline{\mathbf{V}}_0 = \frac{1}{T_m} \int_0^{T_m} \overline{\mathbf{V}}(M) dt \tag{31}$$

(30) can be simplified as:

$$\left[\mathbf{K}(\mathbf{t})\right] = \left[\mathbf{K}_{0}\right] + \int_{L(t)} k(M) dM \, \overline{\mathbf{V}}_{0} \, \overline{\mathbf{V}}_{0}^{T} = \left[\mathbf{K}_{0}\right] + k_{m}(t) \, \overline{\mathbf{V}}_{0} \, \overline{\mathbf{V}}_{0}^{T}$$
(32)

The separation of the average and time-varying contributions in the mesh stiffness function as  $k(t) = k_m(1 + \alpha \varphi(t))$  leads to the following state equations:

$$[\mathbf{M}]\ddot{\mathbf{X}} + [\mathbf{K}_0] + k_m (1 + \alpha \varphi(t)) \overline{\mathbf{V}}_0 \overline{\mathbf{V}}_0^T] \mathbf{X} = \mathbf{F}_0 + \mathbf{F}_1(t, \delta e(M)) + \mathbf{F}_2(t, \dot{\Omega}_{1,2})$$
(33)

For most gears,  $\alpha$  is usually a small parameter ( $\alpha << 1$ ) and an asymptotic expansion of the solution can be sought as a straightforward expansion of the form:

$$\mathbf{X} = \mathbf{X}_0 + \alpha \mathbf{X}_1 + \alpha^2 \mathbf{X}_2 + \dots \tag{34}$$

which, when re-injected into (33) and after identifying like order terms leads to the following series of constant coefficient differential systems:

Main order:

$$[\mathbf{M}]\ddot{\mathbf{X}}_0 + [\mathbf{K}_0] + k_m \overline{\mathbf{V}}_0 \overline{\mathbf{V}}_0^T ]\mathbf{X}_0 = \mathbf{F}_0 + \mathbf{F}_1(t, \delta e(M)) + \mathbf{F}_2(t, \dot{\Omega}_{1,2})$$
(35-1)

 $\ell^{\it th}$  order:

$$[\mathbf{M}]\ddot{\mathbf{X}}_{\ell} + [\mathbf{K}_0] + k_m \overline{\mathbf{V}}_0 \overline{\mathbf{V}}_0^T] \mathbf{X}_{\ell} = -k_m \varphi(t) \overline{\mathbf{V}}_0 \overline{\mathbf{V}}_0^T \mathbf{X}_{\ell-1}$$
(35-2)

Interestingly, the left-hand sides of all the differential systems are identical and the analysis of the eigenvalues and corresponding eigenvectors of the homogeneous systems will provide useful information on the dynamic behaviour of the geared systems under consideration (critical speeds, modeshapes).

The following system is considered (the influence of damping on critical speeds being ignored):

$$[\mathbf{M}]\ddot{\mathbf{X}}_{\ell} + [\mathbf{K}_{0}] + k_{m}\overline{\mathbf{V}}_{0}\overline{\mathbf{V}}_{0}^{\mathrm{T}}]\mathbf{X}_{\ell} = \mathbf{0}$$
(36)

from which the eigenvalues and eigenvectors are determined. The technical problems associated with the solution of (36) are not examined here and the reader may refer to specialised textbooks. It is further assumed that a set of real eigenvalues  $\omega_p$  and real orthogonal eigenvectors  $\Phi_p$  have been determined which, to a great extent, control the gear set dynamic behaviour.

Focusing on dynamic tooth loads, it is interesting to introduce the percentage of modal strain energy stored in the gear mesh which, for a given pair  $(\omega_v, \Phi_P)$ , is defined as:

$$\rho_{p} = k_{m} \frac{\mathbf{\Phi}_{p}^{T} \bar{\mathbf{V}}_{0} \bar{\mathbf{V}}_{0}^{T} \mathbf{\Phi}_{p}}{\mathbf{\Phi}_{p}^{T} [\mathbf{K}_{0}] + k_{m} \bar{\mathbf{V}}_{0} \bar{\mathbf{V}}_{0}^{T} ] \mathbf{\Phi}_{p}} = v_{\Phi p}^{2} \frac{k_{m}}{k_{\Phi p}}$$
(37)

with  $v_{\Phi p} = \mathbf{\Phi}_{p}^{T} \mathbf{\bar{V}} = \mathbf{\bar{V}}^{T} \mathbf{\Phi}_{p}$ 

 $k_m, k_{\Phi v}$ : average mesh stiffness and modal stiffness associated with  $(\omega_v, \Phi_v)$ 

It as been shown (Velex & Berthe., 1989) that  $\rho_p$  is a reliable indicator of the severity of one frequency with regard to the pinion-gear mesh and it can be used to identify the potentially critical speeds  $\omega_p$  for tooth loading which are those with the largest percentages of modal strain energy in the tooth mesh. If the only excitations are those generated by the meshing (the mesh frequency is  $Z_1\Omega_1$ ), the tooth critical speeds can be expressed in terms of pinion speed as:

$$\Omega_1 = \omega_n / kZ_1$$
  $k = 1, 2, ...$  (38)

Based on the contact length variations and on the transmission error spectrum, the relative severity of the excitations can be anticipated.

*Remark:* The critical frequencies are supposed to be constant over the speed range (gyroscopic effects are neglected). Note that some variations can appear with the evolution of the torque versus speed (a change in the torque or load can modify the average mesh stiffness especially for modified teeth).

For the one DOF tosional model in Figure 4, there is a single critical frequency  $\omega = \sqrt{k_m/\hat{m}}$  whose expression can be developed for solid gears of identical face width leading to:

$$\Omega_1 \cong \frac{\Lambda}{k} \frac{\cos \alpha_p}{MZ_1^2} \sqrt{\frac{b}{B}} \sqrt{\cos \beta_b} \sqrt{\varepsilon_\alpha} \sqrt{1 + u^2}$$
(39)

where k = 1, 2, ... represents the harmonic order;  $\Lambda = \sqrt{\frac{8k_0}{\pi \rho}}$  ( $\rho$  is the density), for steel gears

 $\Lambda \cong 210^3 \ ms^{-1}$ ; M is the module (in meter); B is the pinion or gear thickness (supposed identical); b is the effective contact width (which can be shorter than B because of chamfers for example);  $u = \frac{Z_1}{Z_2}$ , speed ratio.

#### 5.3 Dynamic response

#### 5.3.1 The problem of damping

Energy dissipation is present in all geared systems and the amount of damping largely controls the amplification at critical speeds. Unfortunately, the prediction of damping is still a challenge and, most of the time; it is adjusted in order to fit with experimental evidence. Two classical procedures are frequently employed:

 a. the assumption of proportional damping (Rayleigh's damping) which, in this case, leads to:

$$[\mathbf{C}] = a[\mathbf{M}] + b[\mathbf{K}_0] + k_m \overline{\mathbf{V}}_0 \overline{\mathbf{V}}_0^T$$
(40)

with: *a,b*, two constants to be adjusted from experimental results

b. the use of (a limited number of) modal damping factors  $\varsigma_v$ :

The damping matrix is supposed to be orthogonal with respect to the mode-shapes of the undamped system with the averaged stiffness matrix such that:

$$\mathbf{\Phi}_{\mathbf{p}}^{T}[\mathbf{C}]\mathbf{\Phi}_{\mathbf{p}} = 2\varsigma_{P}\sqrt{k_{\Phi p} m_{\Phi p}}$$
(41-1)

$$\mathbf{\Phi}_{\mathbf{p}}^{T}[\mathbf{C}]\mathbf{\Phi}_{\mathbf{q}} = 0 \tag{41-2}$$

with:  $\varsigma_p$ : modal damping factor associated with mode p

 $k_{\Phi p}$ ,  $m_{\Phi p}$ : modal stiffness and mass associated with mode p

or introducing the modal damping matrix  $[C_{\Phi}]$ :

$$[\mathbf{C}_{\Phi}] = diag(2\varsigma_{P}\sqrt{k_{\Phi p} m_{\Phi p}}), \ p = 1, N \bmod$$
(41-3)

Following Graig (1981), the damping matrix can be deduced by a truncated summation on a limited number of modes *Nr* leading to the formula:

$$[\mathbf{C}] = \sum_{p=1}^{Nr} \frac{2\varsigma_p \,\omega_p}{m_{\phi_{pp}}} \left( [\mathbf{M}] \mathbf{\Phi}_p \right) \left( [\mathbf{M}] \mathbf{\Phi}_p \right)^T \tag{42}$$

with: 
$$\omega_p = \sqrt{\frac{k_{\Phi p}}{m_{\Phi p}}}$$

Regardless of the technique employed, it should be stressed that both (41) and (42) depend on estimated or measured modal damping factors  $\varsigma_p$  for which the data in the literature is rather sparse. It seems that  $0.02 \le \varsigma_p \le 0.1$  corresponds to the range of variation for modes with significant percentages of strain energy in the meshing teeth. The methods also rely on the assumption of orthogonal mode shapes which is realistic when the modal density (number of modes per frequency range) is moderate so that inter-modal couplings can be neglected.

#### 5.3.2 Linear response

Based on the previous developments, the linear response of gears to mesh parametric excitations can be qualitatively assessed. Response peaks are to be expected at all tooth critical speeds and every sub-harmonic of these critical speeds because mesh stiffness time

variations may exhibit several harmonics with significant amplitudes. Figure 11, taken from Cai and Hayashi (1994), is a clear example of such typical dynamic response curves when the gear dynamic behaviour is dominated by one major tooth frequency  $\omega_n$  (and can be simulated by using the classic one DOF model). The amplifications associated with each peak depends on i) the excitation amplitude (Eq. (27) can provide some information on the amplitude associated with each mesh frequency harmonic) and ii) the level of damping for this frequency. For more complex gear sets, interactions between several frequencies can happen but, as far as the author is aware, the number of frequencies exhibiting a significant percentage of modal strain energy in the tooth mesh seems very limited (frequently less than 5) thus making it possible to anticipate the potential dangerous frequency coincidences for tooth durability.

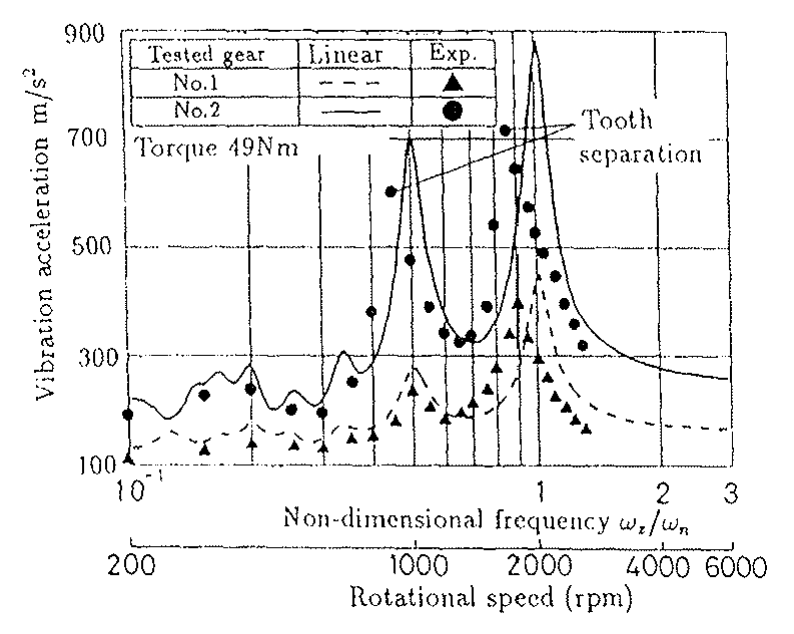


Fig. 11. Examples of dynamic response curves (Cay & Hayashi, 1994).

#### 5.3.3 Contact condition - Contact losses and shocks

Only compressive contact forces can exist on tooth flanks and using (11), this imposes the following unilateral condition in case of contact at point *M*:

$$\mathbf{dF}_{1/2}(\mathbf{M}) \cdot \mathbf{n}_1 = k(M)\Delta(M)dM > 0 \tag{43}$$

or, more simply, a positive mesh deflection  $\Delta(M)$ .

If  $\Delta(M) \le 0$ , the contact at M is lost (permanently or temporarily) and the associated contact force is nil. These constraints can be incorporated in the contact force expression by

introducing the unit Heaviside step function H(x) such that H(x)=1 if x>0 and H(x)=0 otherwise. Finally, one obtains:

$$\mathbf{dF}_{1/2}(\mathbf{M}) = k(M)\Delta(M)H(\Delta(M))dM\,\mathbf{n}_1\tag{44}$$

It can observed that contact losses are related to the sign of  $\Delta(M) \cong \mathbf{V}_0^T \mathbf{X} - \delta e(M)$ , from which, it can be deduced that two cases have to be considered:

- a.  $\delta e(M)$  is larger than the normal approach  $\mathbf{V}_0^T\mathbf{X}$  which, typically, corresponds to large amplitudes of tooth modifications reducing the actual contact patterns, to spalls on the flanks (pitting) where contact can be lost, etc.
- b. the amplitude of the dynamic displacement **X** is sufficiently large so that the teeth can separate (**X** is periodic and can become negative in some part of the cycle).

Momentary contact losses can therefore occur when vibration amplitudes are sufficiently large; they are followed by a sequence of free flight within the tooth clearance until the teeth collide either on the driving flanks or on the back of the teeth (back strike). Such shocks are particularly noisy (rattle noise) and should be avoided whenever possible. Analytical investigations are possible using harmonic balance methods and approximations of H(x) (Singh et al., 1989), (Comparin & Singh, 1989), (Kahraman & Singh, 1990), (Kahraman & Singh, 1991), and numerical integrations can be performed by time-step schemes (Runge-Kutta, Newmark, etc.). The most important conclusions are:

a. contact losses move the tooth critical frequencies towards the lower speeds (softening effect) which means that predictions based on a purely linear approach might be irrelevant. The phenomenon can be observed in Fig. 11 where the experimental peaks are at lower speed than those predicted by the linear theory.

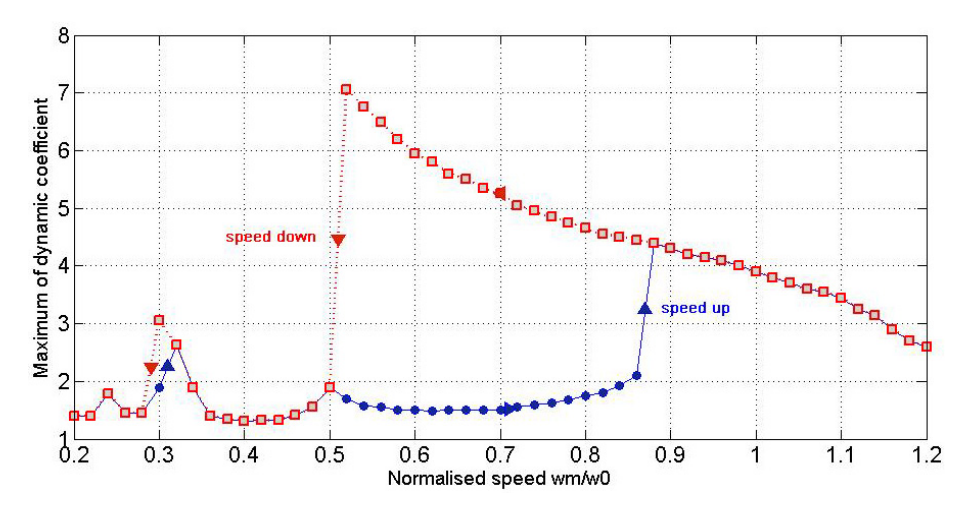


Fig. 12. Dynamic response curves by numerical simulations – Amplitude jumps – Influence of the initial conditions (speed up vs speed down), 2% of the critical damping, Spur gears  $Z_1 = 30$ ,  $Z_2 = 45$ , M = 2mm, standard tooth proportions.

- b. When contact losses occur, response curves exhibit amplitude jumps (sudden amplitude variations for a small speed variation),
- c. Because of a possibly strong sensitivity to initial conditions, several solutions may exist depending on the kinematic conditions i.e., speed is either increased or decreased
- d. damping reduces the importance of the frequency shift and the magnification at critical tooth frequency.

These phenomena are illustrated in the response curves in Figure 12.

#### 6. Transmission errors

#### 6.1 Definitions

The concept of transmission error (*TE*) was first introduced by Harris (1958) in relation to the study of gear dynamic tooth forces. He realised that, for high speed applications, the problem was one of continuous vibrations rather than a series of impacts as had been thought before. Harris showed that the measure of departure from perfect motion transfer between two gears (which is the definition of *TE*) was strongly correlated with excitations and dynamic responses. *TE* is classically defined as the deviation in the position of the driven gear (for any given position of the driving gear), relative to the position that the driven gear would occupy if both gears were geometrically perfect and rigid.

NB: The concept embodies both rigid-body and elastic displacements which can sometimes be confusing.

Figure 13 illustrates the concept of transmission error which (either at no-load or under load) can be expressed as angular deviations usually measured (calculated) on the driven member (gear) or as distances on the base plane.

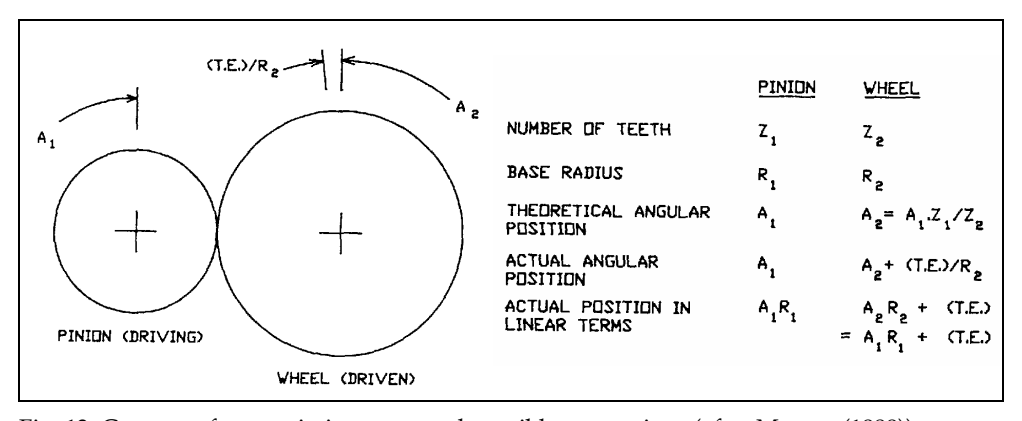


Fig. 13. Concept of transmission error and possible expressions (after Munro, (1989)).

Figures 14 and 15 show typical quasi-static *T.E.* traces for spur and helical gears respectively. The dominant features are a cyclic variation at tooth frequency (mesh frequency) and higher harmonics combined with a longer term error repeating over one revolution of one or both gears.

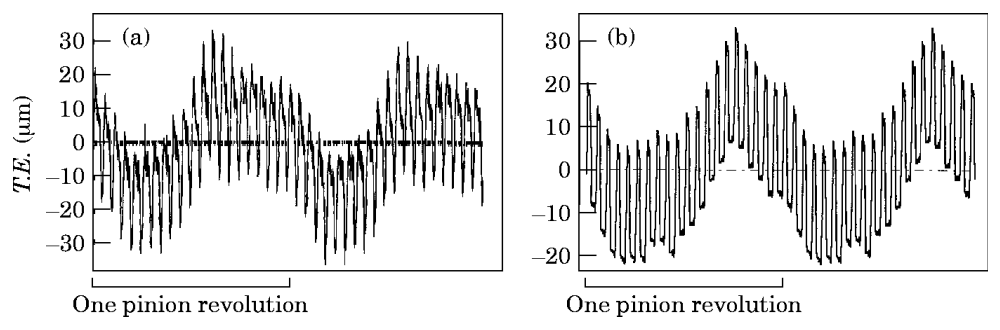


Fig. 14. Examples of quasi-static T.E. measurements and simulations – Spur gear (Velex and Maatar, 1996).

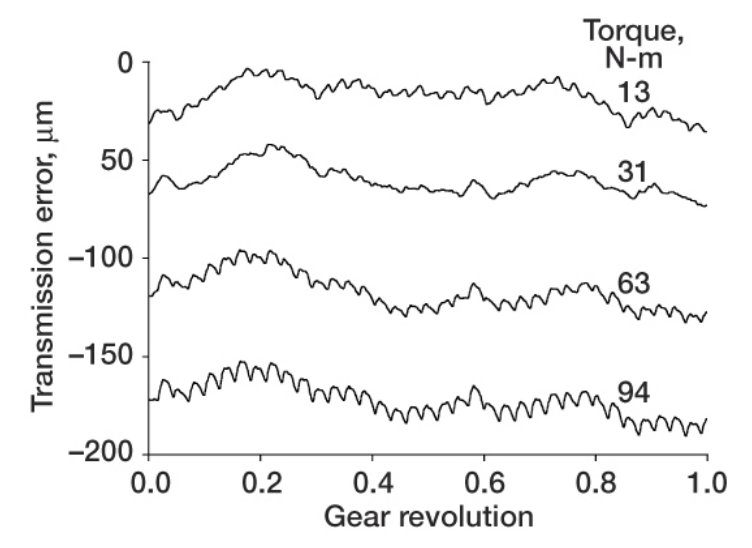


Fig. 15. T.E. measurements at various loads – Helical gear example. NASA measurements from www.grc.nasa.gov/WWW/RT2001/5000/5950oswald1.html.

# 6.2 No-load transmission error (NLTE)

No-load *T.E.* (*NLTE*) has already been introduced in (2); it can be linked to the results of gear testing equipment (single flank gear tester) and is representative of geometrical deviations. From a mathematical point of view, *NLTE* is derived by integrating (2) and is expressed as:

$$NLTE = -\frac{E_{MAX}(t)}{\cos \beta_b} \tag{45}$$

#### 6.3 Transmission errors under load

The concept of transmission error under load (TE) is clear when using the classic single degree of freedom torsional model (as Harris did) since it directly relies on the angles of

torsion of the pinion and the gear. For other models (even purely torsional ones), the definition of *TE* is ambiguous or at least not intrinsic because it depends on the chosen cross-sections (or nodes) of reference for measuring or calculating deviations between actual and perfect rotation transfers from the pinion to the gear. Following Velex and Ajmi (2006), transmission error can be defined by extrapolating the usual experimental practice based on encoders or accelerometers, i.e., from the actual total angles of rotation, either measured or calculated at one section of reference on the pinion shaft (subscript *I*) and on the gear shaft (subscript *II*). *TE* as a displacement on the base plane reads therefore:

$$TE = Rb_1 \left[ \int_0^t \Omega_1 d\xi + \theta_I \right] + Rb_2 \left[ \int_0^t \Omega_2 d\xi + \theta_{II} \right] = Rb_1 \theta_I + Rb_2 \theta_{II} + NLTE$$
 (46)

with  $\xi$ , a dummy integration variable and  $\theta_I$ ,  $\theta_{II}$ , the torsional perturbations with respect to rigid-body rotations (degrees of freedom) at node I on the pinion shaft and at node II on the gear shaft.

Introducing a projection vector  $\mathbf{W}$  of components  $Rb_1$  and  $Rb_2$  at the positions corresponding to the torsional degrees of freedom at nodes I and II and with zeros elsewhere, transmission error under load can finally be expressed as:

$$TE = \mathbf{W}^{\mathsf{T}} \mathbf{X} + NLTE \tag{47-1}$$

which, for the one DOF model, reduces to:

$$TE = x + NLTE (47-2)$$

#### 6.4 Equations of motion in terms of transmission errors

For the sake of clarity the developments are conducted on the one-DOF torsional model. Assuming that the dynamic contact conditions are the same as those at very low speed, one obtains from (21) the following equation for quasi-static conditions (i.e., when  $\Omega_1$  shrinks to zero):

$$k(t,x)x_S = F_t + \zeta \cos \beta_b \int_{L(t,x)} k(M) \delta e(M) dM$$
 (48)

which, re-injected in the dynamic equation (21), gives:

$$\widehat{m}\ddot{x} + k(t,x)x = k(t,x)x_S - \kappa \frac{d^2}{dt^2}(NLTE)$$
(49)

From (47-2), quasi-static transmission error under load can be introduced such that  $x_S = TE_S - NLTE$  and the equation of motion is transformed into:

$$\widehat{m}\ddot{x} + k(t,x)x = k(t,x)[TE_S - NLTE] - \kappa \frac{d^2}{dt^2}(NLTE)$$
(50)

An alternative form of interest can be derived by introducing the dynamic displacement  $x_D$  defined by  $x = x_S + x_D$  as:

$$\widehat{m}\ddot{x}_{D} + k(t,x)x_{D} = -\widehat{m}\frac{d^{2}}{dt^{2}}(TE_{S}) + (\widehat{m} - \kappa)\frac{d^{2}}{dt^{2}}(NLTE)$$
(51)

The theory for 3D models is more complicated mainly because there is no one to one correspondence between transmission error and the degree of freedom vector. It can be demonstrated (Velex and Ajmi, 2006) that, under the same conditions as for the one DOF model, the corresponding differential system is:

$$[\mathbf{M}]\ddot{\mathbf{X}}_{D} + [\mathbf{K}(t, \mathbf{X})]\mathbf{X}_{D} \cong -[\mathbf{M}]\hat{\mathbf{D}}\frac{d^{2}}{dt^{2}}(TE_{S}) + \left[\frac{1}{Rb_{2}}\mathbf{I}_{P} + [\mathbf{M}]\hat{\mathbf{D}}\right]\frac{d^{2}}{dt^{2}}(NLTE)$$
(52)

where  $\hat{\mathbf{D}} = k_m \cos \beta_b \lceil \overline{\mathbf{K}} \rceil^{-1} \overline{\mathbf{V}}$ ,  $\mathbf{X}_D = \mathbf{X} - \mathbf{X}_S$ , dynamic displacement vector

#### 6.5 Practical consequences

From (51) and (52), it appears that the excitations in geared systems are mainly controlled by the fluctuations of the quasi-static transmission error and those of the no-load transmission error as long as the contact conditions on the teeth are close to the quasi-static conditions (this hypothesis is not verified in the presence of amplitude jumps and shocks). The typical frequency contents of *NLTE* mostly comprise low-frequency component associated with run-out, eccentricities whose contributions to the second-order time-derivative of NLTE can be neglected. It can therefore be postulated that the mesh excitations are dominated by  $\frac{d^2}{dt^2}(TE_s)$ . This point has a considerable practical importance as it shows that reducing the dynamic response amplitudes is, to a certain extent, equivalent to reducing the fluctuations of  $TE_s$ . Profile and lead modifications are one way to reach this objective. Equation (50) stresses the fact that, when total displacements have to be determined, the forcing terms are proportional to the product of the mesh stiffness and the difference between  $TE_s$  and NLTE (and not  $TE_s$ !). It has been demonstrated by Velex et al. (2011) that a unique dimensionless equation for quasi-static transmission error independent of the number of degrees of freedom can be derived under the form:

$$\cos \beta_b \hat{k}(t, \mathbf{X_s}) TE_s^*(t) = 1 - \int_{L(t, \mathbf{X_s})} \hat{k}(M) e^*(M) dM$$
(53)

with  $\hat{A} = \frac{A}{k_m}$ ,  $A^* = \frac{A}{\delta_m}$ , for any generic variable A (normalization with respect to the average mesh stiffness and the average static deflection).

Assuming that the mesh stiffness per unit of contact length is approximately constant (see section 2-5), analytical expressions for symmetric profile modifications (identical on pinion and gear tooth tips as defined in Fig. 16) rendering  $TE_s(t)$  constant (hence cancelling most of the excitations in the gear system) valid for spur and helical gears with  $\varepsilon_{\alpha} \le 2$  can be found under the form:

$$E = \frac{\Gamma \Lambda}{2\Gamma - 1 + \frac{1}{\varepsilon_{\alpha}}} \tag{54}$$

submitted to the condition  $\Gamma \ge \frac{\varepsilon_{\alpha} - 1}{2\varepsilon_{\alpha}}$ 

with E: tip relief amplitude;  $\Gamma$ : dimensionless extent of modification (such that the length of modification on the base plane is  $\Gamma \varepsilon_{\alpha} Pb_{a}$ ) and  $\Lambda = \frac{Cm}{Rb_{1}b\,k_{0}}$ : deflection of reference.

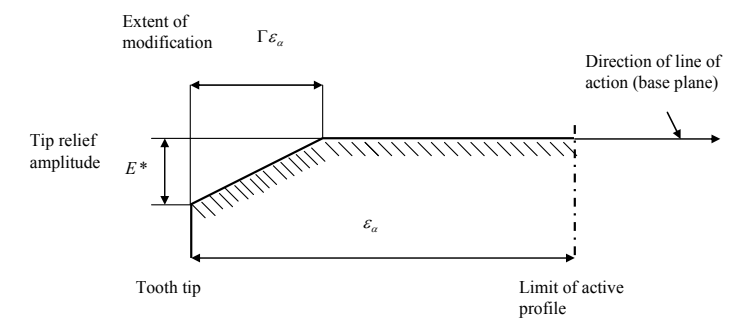


Fig. 16. Definition of profile relief parameters

Based on these theoretical results, it can be shown that quasi-static transmission error fluctuations for ideal gears with profile relief depend on a very limited number of parameters: i) the profile and lead contact ratios which account for gear geometry and ii) the normalised depth and extent of modification. These findings, even though approximate, suggest that rather general performance diagrams can be constructed which all exhibit a zone of minimum TE variations defined by (54) as illustrated in Figure 17 (Velex et al., 2011). It is to be noticed that similar results have been obtained by a number of authors using very different models (Velex & Maatar, 1996), (Sundaresan et al., 1991), (Komori et al., 2003), etc.

The dynamic factor defined as the maximum dynamic tooth load to the maximum static tooth load ratio is another important factor in terms of stress and reliability. Here again, an approximate expression can be derived from (51-52) by using the same asymptotic expansion as in (34) and keeping first-order terms only (Velex & Ajmi, 2007). Assuming that  $TE_S$  and NLTE are periodic functions of a period equal to one pinion revolution; all forcing terms can be decomposed into a Fourier series of the form:

$$-\left[\mathbf{M}\right]\hat{\mathbf{D}}\frac{d^{2}}{dt^{2}}\left(TE_{S}\right)+\left[\frac{1}{Rb_{2}}\mathbf{I}_{\mathbf{P}}+\left[\mathbf{M}\right]\hat{\mathbf{D}}\right]\frac{d^{2}}{dt^{2}}\left(NLTE\right)=-\Omega_{1}^{2}\sum_{n\geq1}n^{2}\left[A\star_{n}\sin n\Omega_{1}t+B\star_{n}\cos n\Omega_{1}t\right]$$
(55)

and an approximate expression of the dimensionless dynamic tooth load can be derived under the form:

$$r(t) = \frac{F_D(t)}{F_S} \cong 1 + \sum_p \sqrt{\rho_p \hat{k}_{\Phi p}} Y_{pn}(t)$$
(56)

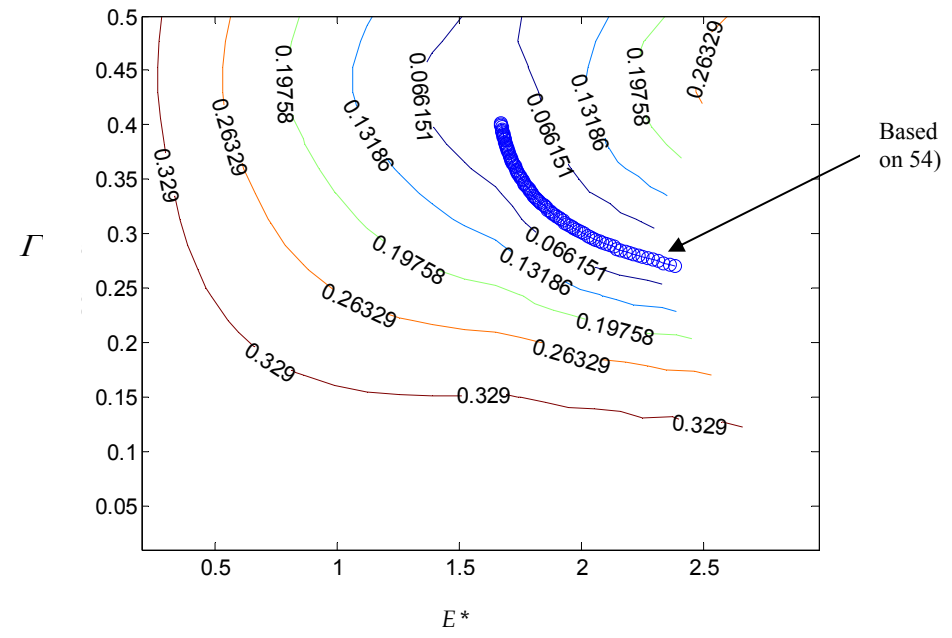


Fig. 17. Example of performance diagram: contour lines of the RMS of quasi-static transmission error under load - Spur gear  $\varepsilon_{\alpha}$  = 1.67.

with

$$\begin{aligned} \mathbf{Y}_{pn}\left(t\right) &= \sum_{n\geq 1} \frac{\overline{A} *_{n} \left[ \left(\boldsymbol{\varpi}_{pn}\right)^{2} - 1 \right] + 2\overline{B} *_{n} \varsigma_{p}\left(\boldsymbol{\varpi}_{pn}\right)}{\left[ \left(\boldsymbol{\varpi}_{pn}\right)^{2} - 1 \right]^{2} + 4\varsigma_{p}^{2}\left(\boldsymbol{\varpi}_{pn}\right)^{2}} \sin n\Omega_{1}t + \frac{\overline{B} *_{n} \left[ \left(\boldsymbol{\varpi}_{pn}\right)^{2} - 1 \right] - 2\overline{A} *_{n} \varsigma_{p}\left(\boldsymbol{\varpi}_{pn}\right)}{\left[ \left(\boldsymbol{\varpi}_{pn}\right)^{2} - 1 \right]^{2} + 4\varsigma_{p}^{2}\left(\boldsymbol{\varpi}_{pn}\right)^{2}} \cos n\Omega_{1}t \\ \boldsymbol{\varpi}_{pn} &= \frac{\boldsymbol{\varpi}_{p}}{n\Omega_{1}} \end{aligned}$$

Equation (56) makes it possible to estimate dynamic tooth loads with minimum computational effort provided that the modal properties of the system with averaged stiffness matrix and the spectrum of  $TE_s$  (predominantly) are known. One can notice that the individual contribution of a given mode is directly related to its percentage of strain energy in the meshing teeth and to the ratio of its modal stiffness to the average mesh stiffness. These properties can be used for identifying the usually limited number of critical mode shapes and frequencies with respect to tooth contact loads. They may also serve to test the structural modifications aimed at avoiding critical loading conditions over a range of speeds. It is worth noting that, since  $\alpha$  is supposed to be a small parameter, the proposed methodology is more suited for helical gears.

#### 7. Towards continuous models

### 7.1 Pinion, gear distortions

In the case of wide-faced gears, gear body deflections (especially those of the pinion) cannot be neglected and the torsion/bending distortions must be modelled since they can strongly affect the contact conditions between the teeth. For solid gears, one of the simplest approaches consists in modelling gear bodies by two node shaft finite elements in bending, torsion and traction as described in Ajmi and Velex (2005) which are connected to the same mesh interface model as that described in section 3 and Fig. 6. Assuming that any transverse section of the pinion or gear body originally plane remains plane after deformation (a fundamental hypothesis in Strength of Materials), gear bodies can then be sliced into elemental discs and infinitesimal gear elements using the same principles as those presented in section 2. The degrees of freedom of every infinitesimal gear element are expressed by using the shape functions of the two-node, six DOFs per node shaft element. By so doing, all the auxiliary DOFs attributed at every infinitesimal pinion and gear are condensed in terms of the degrees of freedom of the shaft nodes leading to a (global) gear element with 24 DOFs.

# 7.2 Thin-rimmed applications

The approach in 6.1 is valid for solid gears but is irrelevant for deformable structures such as thin-rimmed gears in aeronautical applications for example where the displacement field cannot be approximated by simple polynomial functions as is the case for shafts. Most of the attempts rely on the Finite Element Method applied to 2D cases (Parker et al., 2000), (Kahraman et al., 2003) but actual 3D dynamic calculations are still challenging and do not lend themselves to extensive parameter analyses often required at the design stage. An

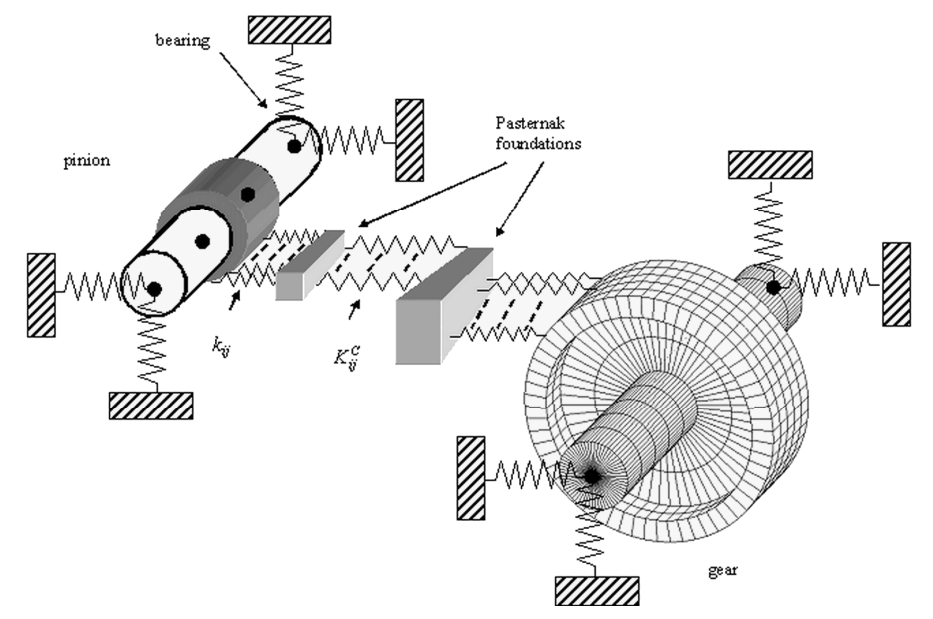


Fig. 18. Example of hybrid model used in gear dynamics (Bettaieb et al., 2007).

alternative to these time-consuming methods is to use hybrid FE/lumped models as described by Bettaieb et al, (2007). Figure 18 shows an example of such a model which combines i) shaft elements for the pinion shaft and pinion body, ii) lumped parameter elements for the bearings and finally iii) a FE model of the gear + shaft assembly which is sub-structured and connected to the pinion by a time-varying, non-linear Pasternak foundation model for the mesh stiffness. The computational time is reduced but the modelling issues at the interfaces between the various sub-models are not simple.

#### 8. Conclusion

A systematic formulation has been presented which leads to the definition of gear elements with all 6 rigid-body degrees-of-freedom and time-varying, possibly non-linear, mesh stiffness functions. Based on some simplifications, a number of original analytical results have been derived which illustrate the basic phenomena encountered in gear dynamics. Such results provide approximate quantitative information on tooth critical frequencies and mesh excitations held to be useful at the design stage.

Gear vibration analysis may be said to have started in the late 50's and covers a broad range of research topics and applications which cannot all be dealt with in this chapter: multimesh gears, power losses and friction, bearing-shaft-gear interactions, etc. to name but a few. Gearing forms part of traditional mechanics and one obvious drawback of this long standing presence is a definite sense of déjà vu and the consequent temptation to construe that, from a research perspective, gear behaviour is perfectly understood and no longer worthy of study (Velex & Singh, 2010). At the same time, there is general agreement that although gears have been around for centuries, they will undoubtedly survive long into the 21st century in all kinds of machinery and vehicles.

Looking into the future of gear dynamics, the characterisation of damping in geared sets is a priority since this controls the dynamic load and stress amplitudes to a considerable extent. Interestingly, the urgent need for a better understanding and modelling of damping in gears was the final conclusion of the classic paper by Gregory et al. (1963-64). Almost half a century later, new findings in this area are very limited with the exception of the results of Li & Kahraman (2011) and this point certainly remains topical. A plethora of dynamic models can be found in the literature often relying on widely different hypotheses. In contrast, experimental results are rather sparse and there is certainly an urgent need for validated models beyond the classic results of Munro (1962), Gregory et al. (1963), Kubo (1978), Küçükay (1984 &87), Choy et al. (1989), Cai & Hayashi (1994), Kahraman & Blankenship (1997), Baud & Velex (2002), Kubur et al. (2004), etc. especially for complex multi-mesh systems. Finally, the study of gear dynamics and noise requires multi-scale, multi-disciplinary approaches embracing non-linear vibrations, tribology, fluid dynamics etc. The implications of this are clear; far greater flexibility will be needed, thus breaking down the traditional boundaries separating mechanical engineering, the science of materials and chemistry.

#### 9. References

Ajmi, M. & Velex, P. (2005). A model for simulating the dynamic behaviour of solid wide-faced spur and helical gear, *Mechanisms and Machine Theory*, vol. 40, n°2, (February 2005), pp. 173-190. ISSN: 0094 -114X.

- Attia, A. Y. (1964). Deflection of Spur Gear Teeth Cut in Thin Rims, *Journal of Engineering for Industry*, vol. 86, (November 1964), pp. 333-342. ISSN: 0022-0817.
- Baud, S. & Velex, P. (2002). Static and dynamic tooth loading in spur and helical geared systems—experiments and model validation, *Journal of Mechanical Design*, vol.124, n° 2, (June 2002), pp. 334–346. ISSN: 1050-0472
- Bettaieb, N.M.; Velex, P. & Ajmi, M. (2007). A static and dynamic model of geared transmissions by combining substructures and elastic foundations Applications to thin-rimmed gears, *Journal of Mechanical Design*, vol.119, n°2, (February 2007), pp. 184-195, ISSN: 1050-0472
- Cai, Y. & Hayashi, T. (1994). The linear approximated equation of vibration of a pair of spur gears (theory and experiment), *Journal of Mechanical Design*, Vol. 116, n°2, (June 1994), pp. 558-565, ISSN: 1050-0472
- Choy F.K., Townsend, D.P. & Oswald F.B. (1989). Experimental and analytical evaluation of dynamic load vibration of a 2240-kW (3000 Hp) rotorcraft transmission, *Journal of the Franklin Institute*, vol. 326, n°5, pp. 721-735, ISSN: 0016-0032.
- Comparin, R.J & Singh, R.(1989). Non-linear frequency response characteristics of an impact pair, *Journal of Sound and Vibration*, vol. 134, n°2, (October 1989), pp. 259–290, ISSN: 0022-460X
- Cornell, R.W. (1981). Compliance and stress sensitivity of spur gear teeth, *Journal of Mechanical Design*, Vol. 103, n°2, (April 1981), pp. 447-460, ISSN: 1050-0472
- Craig, R. R. (1981). Fundamentals of structural dynamics, John Wiley, ISBN: 13: 978-0-471-43044-5, New-York
- Gregory, R. W.;S. L. Harris, S. L. & Munro, R. G. (1963). Torsional motion of a pair of spur gears. *ARCHIVE: Proceedings of the Institution of Mechanical Engineers, Conference Proceedings*, Vol. 178, n° 3J, pp. 166-173, ISSN: 0367-8849
- Haddad, C. D. (1991). The elastic analysis of load distribution in wide-faced helical gears, PhD dissertation, University of Newcastle, UK.
- Harris, S. L. (1958). Dynamic loads on the teeth of spur gears, *ARCHIVE: Proceedings of the Institution of Mechanical Engineers*, Vol. 172, (1958), pp. 87-112. ISSN: 0020-3483.
- Kahraman, A. & Singh, R. (1990). Non-linear dynamics of spur gears, *Journal of Sound and Vibration*, Vol. 142, n°1, (October 1990), pp. 49-75, ISSN: 0022-460X.
- Kahraman, A. & Singh, R. (1991). Interactions between time-varying mesh stiffness and clearance non-linearities in a geared system, *Journal of Sound and Vibration*, Vol. 146, n°1, (April 1991), pp. 135-156, ISSN: 0022-460X.
- Kahraman, A. & Blankenship, G.W. (1997). Experiments on nonlinear dynamic behaviour of an oscillator with clearance and periodically time-varying parameters, *Journal of Applied Mechanics*, vol. 64, n°1, (March 1997), pp. 217-227, ISSN: 0021-8936.
- Kahraman, A; Kharazi, A. A. & Umrani, M. (2003). A deformable body dynamic analysis of planetary gears with thin rims, *Journal of Sound and Vibration*, Vol. 262, n°3, (Mai 2003), pp. 752-768, ISSN: 0022-460X.
- Komori, M.; Kubo, A. & Suzuki, Y. (2003). Simultaneous optimization of tooth flank form of involute helical gears in terms of both vibration and load carrying capacity, *JSME International Journal*, *Series C*, vol. 46, n° 4, pp. 1572-1581.
- Kubo, A. (1978). Stress condition, vibrational exciting force and contact pattern of helical gears with manufacturing and alignment errors, *Journal of Mechanical Design*, Vol. 100, n°1, (1978), pp. 77-84, ISSN: 1050-0472.

- Kubur, M., Kahraman, A., Zini, D. M. & Kienzle, K. (2004). Dynamic analysis of multi-shaft helical gear transmission by finite elements: model and experiment, *Journal of Vibration and Acoustics*, vol. 126, n°3, (July 2004), pp. 398-407, ISSN: 1048-9002.
- Küçükay, F. (1984). Dynamic behaviour of high-speed gears, *Proceedings of the 3rd International Conference on Vibrations in Rotating Machinery*, York, September 1984, pp. 81-90.
- Küçükay, F. (1987). Dynamik der Zahnradgetriebe. Modelle, Verfahren, Verhalten, Springer Verlag, ISBN 3-540-17111-8, Berlin.
- Lalanne, M. & Ferraris, G. (1998). *Rotordynamics Prediction in Engineering (2nd edition)*, John Wiley, New-York.
- Li, S. & Kahraman, A. (2011). A spur gear mesh interface damping model based on elastohydrodynamic contact behaviour, *International Journal of Powertrains*, vol. 1, n°1, (2011), pp. 4-21, ISSN: 1742-4267.
- Lundberg, G. (1939). Elastische Berührung zweier Halbraüme, Forschung auf dem Gebiete des Ingenieurwesen, vol. 10, n°5, (September-October 1939), pp. 201–211.
- Maatar, M. &Velex, P. (1996). An analytical expression of the time-varying contact length in perfect cylindrical gears-Some possible applications in gear dynamics, *Journal of Mechanical Design*, Vol. 118, n°4, (December 1996), pp. 586-589, ISSN: 1050-0472.
- Munro, R.G., (1962). The dynamic behaviour of spur gears. PhD dissertation, University of Cambridge, UK.
- Munro, R.G. (1989). The DC component of gear transmission error, *Proceedings of the 1989 ASME International Power Transmission and Gearing Conference*, Chicago, April 1989, pp. 467-470.
- O'Donnell, W. J. (1960). The Additional Deflection of a Cantilever Due to the Elasticity of the Support, *Journal of Applied Mechanics*, vol. 27 (September 1960), pp. 461-464. ISSN: 0021-8936
- O'Donnell, W. J. (1963). Stresses and Deflections in Built-In Beams, *Journal of Engineering for Industry*, vol. 85 (August 1963), pp. 265-273. ISSN: 0022-0817.
- Ozgüven, H.N. & Houser, D.R. (1988). Mathematical models used in gear dynamics—A review, *Journal of Sound and Vibration*, Vol. 121, n°3, (March 1988), pp. 383–411, ISSN: 0022-460X.
- Palmgren, A. (1959). Ball and roller bearing engineering (3rd edition), S.H. Burbank & Co, Philadelphia, USA.
- Parker, R. G.; Vijayakar, S. M. & Imajo, T. (2000). Non-linear dynamic response of a spur gear pair: modelling and experimental comparisons. *Journal of Sound and Vibration*, Vol. 237, n°3, (October 2000), pp. 435-455, ISSN: 0022-460X.
- Sainsot, P.; Velex, P. & Duverger, O. (2004). Contribution of gear body to tooth deflections-A new bidimensional analytical formula, *Journal of Mechanical Design*, vol. 126, n°4, (July 2004), pp. 748-752, ISSN: 1050-0472.
- Seager, D. L., (1967). Some elastic effects in helical gear teeth, PhD dissertation, University of Cambridge, UK.
- Singh, R.; Xie, H. & Comparin R.J. (1989). Analysis of automotive neutral gear rattle, *Journal of Sound and Vibration*, vol. 131, n° 2, (June 1989), pp. 177–196. ISSN: 0022-460X.
- Sundaresan, S.; Ishii, K. & Houser, D. R. (1991). A Procedure Using Manufacturing Variance to Design Gears With Minimum Transmission Error, *Journal of Mechanical Design*, vol. 113, n°3, (September 1991), pp. 318-325, ISSN: 1050-0472.

- Velex, P. & Berthe, D. (1989). Dynamic tooth loads on geared train, *Proceedings of the*1989 *ASME International Power Transmission and Gearing Conference*, Chicago, April 1989, pp. 447–454.
- Velex, P.& Maatar, M. (1996). A mathematical model for analyzing the influence of shape deviations and mounting errors on gear dynamics. *Journal of Sound and Vibration*, Vol. 191, n°5, (April 1996), pp. 629-660, ISSN: 0022-460X.
- Velex, P. & Ajmi, M. (2006). On the modelling of excitations in geared systems by transmissions errors, *Journal of Sound and Vibration*, Vol. 290, n° 3-5, (March 2006), pp. 882-909, ISSN 0022-460X.
- Velex, P. & Ajmi, M. (2007). Dynamic tooth loads and quasi-static transmission errors in helical gears Approximate dynamic factor formulae, *Mechanism and Machine Theory*, vol. 42, n° 11, (November 2007), pp. 1512-1526, ISSN: 0094-114X.
- Velex, P. & Singh, A. (2010). Top gear, (Guest Editorial) *Journal of Mechanical Design*, vol. 132, n°6, (June 2010), 2 p., ISSN: 1050-0472.
- Velex, P.; Bruyère, J. & Houser, D. R. (2011). Some analytical results on transmission errors in narrow-faced spur and helical gears Influence of profile modifications, *Journal of Mechanical Design*, Vol. 133, n°3, (March 2011), 11 p., ISSN: 1050-0472.
- Weber, C. & Banaschek, K. (1953). Formänderung und Profilrücknahme bei Gerad-und Schrägverzahnten Antriebstechnik, Heft 11, F. Vieweg und Sohn, Braunschweig, Germany.

# The Role of the Gearbox in an Automatic Machine

Hermes Giberti<sup>1</sup>, Simone Cinquemani<sup>1</sup> and Giovanni Legnani<sup>2</sup>

<sup>1</sup>Politecnico di Milano

<sup>2</sup>Università degli studi di Brescia

Italy

#### 1. Introduction

A *machine* is a system realized by many parts with different functions, linked each other to reach a defined task. Depending on the task, a classification of machines equipped with moving parts can be done. In particular, one can distinguish:

- Drive machines (*motors*): these machines deliver mechanical power from other forms of energy. If their purpose is simply to make placements or generate forces/torques, they are called *actuators*.
- Working machines (users): these machines absorb mechanical power to accomplish a specific task (machine tools, transportation, agricultural machinery, textile machinery, machine packaging, etc.).
- Mechanical transmissions: these machines transmit mechanical power by appropriately
  changing values of torques and speed. Mechanical transmissions are generally made up
  of *mechanisms* that have been studied (mainly from the point of kinematic view) to connect
  motors and users.

The combination of a motor, a transmission and a mechanical user is the simplest form of machine.

In servo-actuated machines, the choice of the electric motor required to handle a dynamic load, is closely related to the choice of the transmission Giberti et al. (2011).

The choice of the transmission plays an important role in ensuring the performance of the machine. It must be carried out to meet the limitations imposed by the motor working range and it is subjected to a large number of constraints depending on the motor, through its rotor inertia  $J_M$  or its mechanical speed and on the speed reducer, through its transmission ratio  $\tau$ , its mechanical efficiency  $\eta$  and its moment of inertia  $J_T$ .

This chapter critically analyzes the role of the transmission on the performance of an automatic machine and clarifies the strategies to choose this component. In particular, it is treated the general case of coupled dynamic addressing the problem of inertia matching and presenting a methodology based on a graphical approach to the choice of the transmission.

The identification of a suitable coupling between motor and transmission for a given load has been addressed by several authors proposing different methods of selection. The most common used procedure are described in Pasch et al. (1984), Van de Straete et al. (1998), Van de Straete et al. (1999), Roos et al. (2006). In these procedures, the transmission is

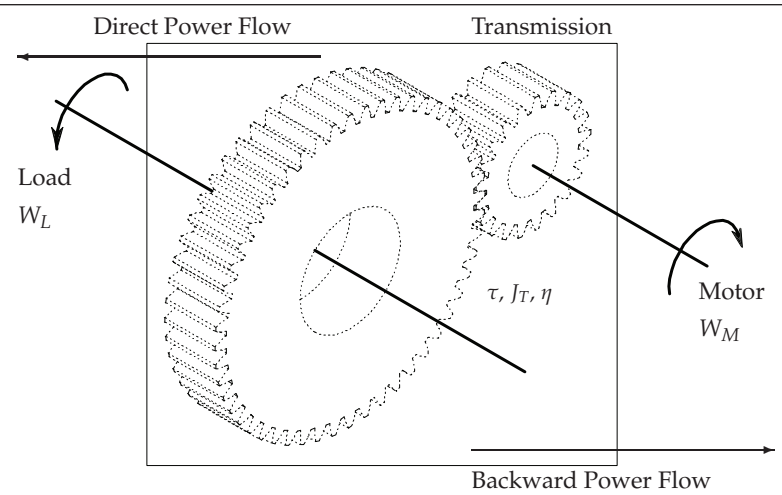


Fig. 1. A scheme of a simple transmission

approximated to an ideal system in which power losses are neglected, as the effects of the transmission inertia. Only after the motor and the reducer are selected, the transmission mechanical efficiency and inertia are considered to check the validity of the choice. Naturally, if the check gives a negative result, a new motor and a new transmission should be selected and the entire procedure has to be performed again. Differently, in Giberti et al. (2010a) the effects of transmission efficiency and inertia are considered since the beginning.

This chapter is structured as follows. Paragraph 2 gives an overview of main features of a mechanical transmission, while Par.3 describes the functioning of a generic machine when a given load is applied. Paragraph 4 describes the conditions, in terms of useful transmission ratios, for which a motor-load combination is feasible. Paragraph 5 gives the guidelines for the selection of both the gearbox and the electric motor, neglecting the effects of the transmission mechanical efficiency and inertia. Theoretical aspects are supported by a practical industrial case. Paragraphs 6 and 7 extend results previously reached considering the effects of the transmission mechanical efficiency and inertia. Finally conclusions are drawn in paragraph 8.

All the symbols used through the chapter are defined in Par.9.

### 2. The transmission

To evaluate the effect of the transmission in a motor-load coupling, the transmission can be considered as a black box in which the mechanical power flows (Figures 1, 2, 4). The mechanical power is the product of a torque (extensive factor) for an angular speed (intensive factor).

A mechanical transmission is a mechanism whose aim is:

- 1. to transmit power
- 2. to adapt the speed required by the load
- 3. to adapt the torque.

and it is characterized by a transmission ratio  $\tau$  and a mechanical efficiency  $\eta$ .

Conventional mechanical transmissions with a constant ratio involve the use of *friction wheels*, *gear*, *belt* or *chains*. The choice of the most suitable transmission for a given application depends on many factors such as dimensions, power, speed, gear ratio, motor and load characteristics, cost, maintenance requirements. Table 1 gives an overview of the most common applications of mechanical transmissions.

	Power max		Dimensions	Cost	Efficienc	
	(kW)	minimu	n			bearings
Friction	1/6	20	low	medium	0.90	high
wheels						J
Spur gear	750	1/6	low	high	0.96	low
Helical gears	50000	1/10	low	high	0.98	low
Worm gears	300	1/100	low	high	0.80	medium
Belt	200	1/6	high	low	0.95	high
Trapezoidal	350	1/6	medium	low	0.95	high
belt						
Toothed belt	100	1/6	medium	low	0.90	low
Linkages	200	1/6	medium	medium	0.90	low

Table 1. Typical characteristics of mechanical transmissions.

#### 2.1 The transmission ratio

The *transmission ratio*  $\tau$  is defined as:

$$\tau = \frac{\omega_{out}}{\omega_{in}} \tag{1}$$

where  $\omega_{in}$  and  $\omega_{out}$  are the angular velocity of the input and the output shafts respectively. This value characterizes the transmissions. If  $\tau < 1$  the gearbox is a *speed reducer*, while if  $\tau > 1$  it is a *speed multiplier*.

The mechanical transmission on the market can be subdivided into three main categories: transmissions with constant ratio  $\tau$ , transmissions with variable ratio  $\tau$  and transmissions that change the kind of movement (for example from linear to rotational).

Since it is generally easier to produce mechanical power with small torques at high speeds, the transmission performs the task of changing the distribution of power between its extensive and intensive factors to match the characteristics of the load.

It is possible to define the term  $\mu$  as the *multiplication factor of force (or torque)*:

$$\mu = \frac{T_{out}}{T_{in}} \tag{2}$$

where  $T_{in}$ , and  $T_{out}$  are respectively the torque upstream and downstream the transmission.

# 2.2 The mechanical efficiency

If the power losses in the transmission can be considered as negligible, it results:

$$\mu = \frac{1}{\tau}.\tag{3}$$

However, a more realistic model of the transmission has to take into account the inevitable loss of power to evaluate how it affects the correct sizing of the motor-reducer coupling and the resulting performance of the machine.

In general, transmissions are very complex, as the factors responsible for the losses of power. In this chapter they are taken into account just considering the transmission mechanical efficiency  $\eta$  defined as the ratio between the power outgoing from the transmission ( $W_{out}$ ) and the incoming one ( $W_{in}$ ), or through the extensive factors ( $T_{in}$ ,  $T_{out}$ ) and the intensive ones ( $\omega_{in}$ ,  $\omega_{out}$ ) of the power itself:

$$\eta = \frac{W_{out}}{W_{in}} = \frac{T_{out}}{T_{in}} \frac{\omega_{out}}{\omega_{in}} = \mu \tau \le 1$$
 (4)

The loss of power within the transmission leads to a reduction of available torque downstream of the transmission. Indeed, if the coefficient of multiplication of forces for an ideal transmission is  $\mu = \tau^{-1}$ , when  $\eta \neq 1$  it becomes  $\mu' < \mu$ , thus leading to a consequent reduction of the transmitted torque  $(T'_{out} < T_{out})$ .

Let's define  $W_M$  and  $W_L$  respectively as the power upstream and downstream of the transmission. When the power flows from the motor to the load the machine is said to work with *direct power flow*, otherwise, the functioning is said to be *backward*. Depending on the machine functioning mode, the transmission power losses are described by two different mechanical efficiency values  $\eta_d$  and  $\eta_r$ , where:

$$\eta_d = \frac{W_L}{W_M}$$
 (direct power flow)  $\eta_r = \frac{W_M}{W_L}$  (backward power flow). (5)

# 3. A single d.o.f. machine

An automatic machine is a system, usually complex, able to fulfill a particular task. Regardless of the type of machine, it may be divided into simpler subsystems, each able to operate only one degree of freedom and summarized by the three key elements: motor, transmission and load (Fig. 2).

### 3.1 The load and the servo-motor

The power supplied by the motor depends on the external load applied  $T_L$  and on the inertia acting on the system  $J_L\dot{\omega}_L$ . Since different patterns of speed  $\omega_L$  and acceleration  $\dot{\omega}_L$  generate different loads, the choice of a proper law of motion is the first project parameter that should be taken into account when sizing the motor-reducer unit. For this purpose, specific texts are recommended (Ruggieri et al. (1986), Melchiorri (2000)).

Once the law of motion has been defined, all the characteristics of the load are known.

Electric motor, and among these brushless motors, are the most widespread electrical actuators in the automation field, and their working range can be approximately subdivided into a *continuous* working zone (delimited by the motor rated torque) and a *dynamic* zone (delimited by the maximum motor torque  $T_{M,max}$ ). A typical shape of the working zones is displayed in Fig.3. Usually the motor rated torque decreases slowly with the motor speed  $\omega_M$  from  $T_{M,N_c}$  to  $T_{M,N}$ . To simplify the rated torque trend and to take a cautious approach, it's usually considered constant and equal to  $T_{M,N}$  up to the maximum allowed motor speed

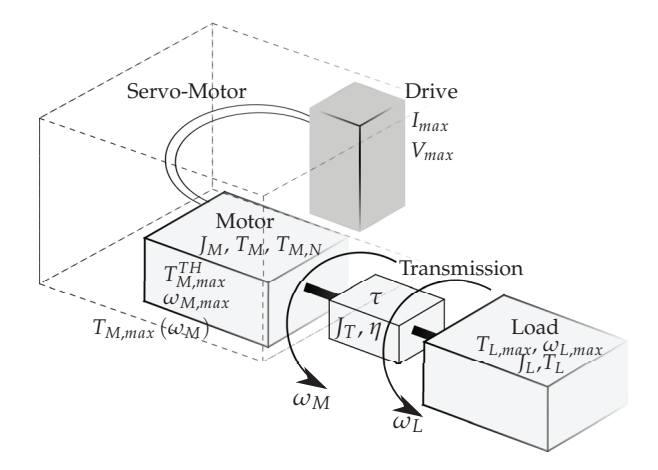


Fig. 2. Scheme of a generic machine actuated by an electric motor

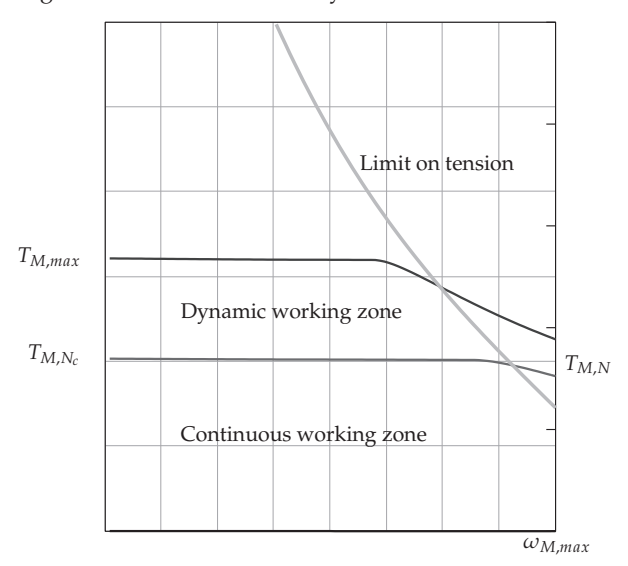


Fig. 3. An example of a speed/torque curve of a common brushless motor

 $\omega_{M,max}$ , whereas  $T_{M,max}$  decreases from a certain value of  $\omega_M$ . The nominal motor torque  $T_{M,N}$ , which is specified by the manufacturer in the catalogs, is defined as the torque that can be supplied by the motor for an infinite time, without overheating. Conversely, the trend of the maximum torque  $T_{M,max}$  is very complex and depends on many factors. For this reason it is difficult to express it with an equation.

### 3.2 Conditions to the right coupling between motor and load

Frequently in industrial applications, the machine task is cyclical with period  $t_a$  much smaller than the motor thermal time constant. Once the task has been defined, a motor-task

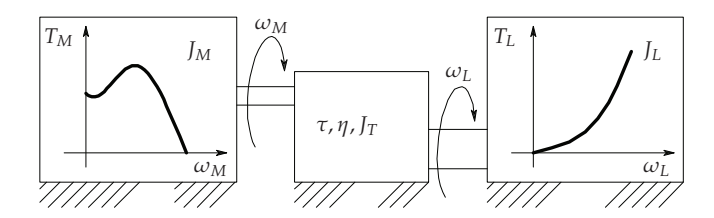


Fig. 4. Scheme of a generic single degree of freedom machine

combination is feasible if there exists a transmission ratio such that:

1. the maximum speed required from the motor is smaller than the maximum speed achievable ( $\omega_{M,max}$ );

$$\omega_{M} \le \omega_{M,max}$$
 (6)

2. a certain p-norm  $^1$  of the motor torque  $||T_M(t)||_p$  is smaller than a corresponding motor specific limit  $T_p$ . The norms that have most physical meaning for motor torques are Van de Straete et al. (1998):

$$||T_M(t)||_2 = T_{rms} = \left(\frac{1}{t_a} \int_0^{t_a} T_M^2(t) dt\right)^{\frac{1}{2}}$$
 (7)

$$||T_M(t,\omega)||_{\infty} = T_{Max}(\omega) = \max |T_M(t,\omega)| \quad 0 \le t \le t_a$$
(8)

Since the motor torque is proportional to the current, 2-norm is a measure of mean square current through the windings and it should be limited by the nominal torque  $T_{M,N}$  to avoid overheat. The  $\infty$ -norm is a measure of peak current and its limit is the maximum torque that can be exerted  $T_{M,max}$ . These limits translate into:

$$T_{rms} \le T_{M,N} \tag{9}$$

$$T_{Max}(\omega) \le T_{M,max}(\omega) \quad \forall \omega$$
 (10)

where  $T_{M,max}$  depends on  $\omega$  as shown in Fig. 3.

While the terms on the right of inequalities (6), (9), (10) are characteristics of each motor,  $\omega_M$ ,  $T_{rms}$  and  $T_{Max}$  depend on the load and on the mechanical features of the motor and the speed reducer.

#### 3.3 Mathematical model of a machine

The machine functioning can be described as an instantaneous balance of power. In the case of direct power flow it can be expressed as:

$$\eta_d \left( \frac{T_M}{\tau} - \frac{J_M \dot{\omega}_L}{\tau^2} \right) = T_L + (J_L + J_T) \dot{\omega}_L \tag{11}$$

$$||f(t)||_p = \left(\frac{1}{t_a} \int_0^{t_a} f^p(t) dt\right)^{\frac{1}{p}}$$

<sup>&</sup>lt;sup>1</sup> In general, the *p*-norm  $\|\cdot\|_p$  of a time function f(t) over the period  $t_a$  is defined as:

while in backward power flow it is:

$$\left(\frac{T_M}{\tau} - \frac{J_M \dot{\omega}_L}{\tau^2}\right) = \eta_r \left[T_L + (J_L + J_T) \dot{\omega}_L\right]$$
(12)

Equations (11), (12) can be written as:

$$T_{M,d} = \frac{\tau T_L^*}{\eta_d} + J_M \frac{\dot{\omega}_L}{\tau} \tag{13}$$

$$T_{M,r} = \tau T_L^* \eta_r + J_M \frac{\dot{\omega}_L}{\tau} \tag{14}$$

where:

$$T_{I}^{*} = T_{L} + (J_{L} + J_{T}) \dot{\omega}_{L} \tag{15}$$

is the total torque applied to the outgoing transmission shaft.

To unify these different operating conditions, a general mechanical efficiency function is introduced by Legnani et al. (2002). It is defined as:

$$\eta = \begin{cases} \eta_d & \text{(direct power flow)} \\ 1/\eta_r & \text{(backward power flow)} \end{cases}$$
(16)

where  $\eta$ ,  $\eta_d$  and  $\eta_r$  are constants.

In the case of backward power flow it results  $\eta > 1$ . Note that this does not correspond to a power gain, but it is simply an expedient for unifying the equations of the two working conditions (direct/backward power flow). In fact, in this case, the effective efficiency is  $\eta_d = 1/\eta < 1$ .

# 4. Selecting the transmission

Conditions (6), (9), (10) can be expressed, for each motor, as constraints on acceptable transmission ratios. However, each transmission is characterized not only by its reduction ratio, but also by its mechanical efficiency and its moment of inertia. This chapter analyzes how these factors affect the conditions (6), (9), (10) and how they reduce the range of suitable transmission ratios for a given motor.

### 4.1 Limit on the maximum achievable speed

Since each motor has a maximum achievable speed  $\omega_{M,max}$ , a *limit transmission ratio*  $\tau_{kin}$  can be defined as the minimum transmission ratio below which the system cannot reach the requested speed:

$$\tau_{kin} = \frac{\omega_{L,max}}{\omega_{M,max}} \tag{17}$$

The condition of maximum speed imposed by the system can be rewritten in terms of minimum gear ratio  $\tau_{kin}$  to guarantee the required performance. Eq.(6) becomes:

$$\tau \geq \tau_{kin}$$
 (18)

## 4.2 Limit on the root mean square torque

When the direction of power flow during a working cycle is mainly direct or mainly backward, using the notation introduced in eq. (16), the root mean square torque can be expressed as:

$$T_{rms}^{2} = \int_{0}^{t_{a}} \frac{T_{M}^{2}}{t_{a}} dt = \int_{0}^{t_{a}} \frac{1}{t_{a}} \left( \frac{\tau T_{L}^{*}}{\eta} + J_{M} \frac{\dot{\omega_{L}}}{\tau} \right)^{2} dt$$
 (19)

Developing the term in brackets and using the properties of the sum of integrals, it is possible to split the previous equation into the following terms:

$$\int_{0}^{t_{a}} \frac{1}{t_{a}} \left(\frac{\tau T_{L}^{*}}{\eta}\right)^{2} dt = \frac{T_{L,rms}^{*2} \tau^{2}}{\eta^{2}}$$

$$\int_{0}^{t_{a}} \frac{1}{t_{a}} \left(J_{M} \frac{\dot{\omega}_{L}}{\tau}\right)^{2} dt = \frac{J_{M}^{*}}{\tau^{2}} \dot{\omega}_{L,rms}^{2}$$

$$\int_{0}^{t_{a}} \frac{1}{t_{a}} \left(\frac{2T_{L}^{*} J_{M} \dot{\omega}_{L}}{\eta}\right)^{2} dt = 2\frac{J_{M}}{\eta} \left(T_{L}^{*} \dot{\omega}_{L}\right)_{mean}$$
(20)

In cases in which the power flow changes during the cycle it is not possible to choose the proper value of  $\eta$  and eq.(19) is no longer valid. In this circumstance, any individual working cycle must be analyzed to check if one of the two conditions (eq.(11) or eq.(12)) can be reasonably adopted. For example, in the case of purely inertial load ( $T_L = 0$ ) it is<sup>2</sup>:

$$|T_{M,d}| \ge |T_{M,r}| \tag{21}$$

and the equation for direct power flow can be prudentially adopted. Same considerations can be done when the load is mainly resistant (limited inertia). For all these cases, the condition of eq.(9) becomes:

$$\frac{T_{M,N}^2}{I_M} \ge \frac{\tau^2}{I_M} \frac{T_{L,rms}^{*2}}{n^2} + J_M \frac{\dot{\omega}_{L,rms}^2}{\tau^2} + 2 \frac{(T_L^* \dot{\omega}_L)_{mean}}{n}$$
(22)

### 4.2.1 The accelerating factor and the load factor

Considering eq.(22) two terms can be introduced: the accelerating factor Legnani et al. (2002)

$$\alpha = \frac{T_{M,N}^2}{I_M} \tag{23}$$

$$T_I^* = (J_L + J_T) \dot{\omega}_L$$

Then eq.(21) becomes:

$$\left(\frac{\tau\left(J_{L}+J_{T}\right)}{\eta_{d}}+\frac{J_{M}}{\tau}\right)\left|\dot{\omega}_{L}\right|\geq\left(\tau\left(J_{L}+J_{T}\right)\eta_{r}+\frac{J_{M}}{\tau}\right)\left|\dot{\omega}_{L}\right|$$

and thus:

$$\frac{1}{n_d} \ge \eta_r$$

which is always true since both  $\eta_d$  and  $\eta_r$  are defined as positive and smaller than 1.

<sup>&</sup>lt;sup>2</sup> For purely inertial load eq.(15) can be written as:

that characterizes the performance of a motor Giberti et al. (2010b), and the load factor:

$$\beta = 2 \left[ \dot{\omega}_{L,rms} T_{L,rms}^* + (\dot{\omega}_L T_L^*)_{mean} \right] \tag{24}$$

defining the performance required by the task. The unit of measurement of both factors is W/s.

Coefficient  $\alpha$  is exclusively defined by parameters related to the motor and therefore it does not depend on the machine task. It can be calculated for each motor using the information collected in the manufacturers' catalogs. On the other hand, coefficient  $\beta$  depends only on the working conditions (applied load and law of motion) and it is a term that defines the power rate required by the system.

# 4.2.2 Range of suitable transmission ratios

Introducing  $\alpha$  and  $\beta$ , equation (22) becomes:

$$\alpha \ge \frac{\beta}{\eta} + \left[ \frac{T_{L,rms}^*}{\eta} \left( \frac{\tau}{\sqrt{J_M}} \right) - \dot{\omega}_{L,rms} \left( \frac{\sqrt{J_M}}{\tau} \right) \right]^2 \tag{25}$$

Since the term in brackets is always positive, or null, the load factor  $\beta$  represents the minimum value of the right hand side of equation (25). It means that the motor accelerating factor  $\alpha$  must be sufficiently greater than the load factor  $\beta/\eta$ , so that inequality (22) is verified. This check is a first criterion for discarding some motors. If  $\alpha > \beta/\eta$ , a range of useful transmission ratio exists and can be obtained by solving the biquadratic inequality:

$$\left(\frac{T_{L,rms}^*}{\eta^2 J_M}\right) \tau^4 + \left(\frac{\beta}{\eta} - \alpha - 2\frac{T_{L,rms}^*}{\eta} \dot{\omega}_{L,rms}\right) \tau^2 + J_M \dot{\omega}_{L,rms}^2 \le 0$$
(26)

Inequality (26) has 4 different real solutions for  $\tau$ . As the direction of the rotation is not of interest, only the positive values of  $\tau$  are considered. A range of suitable transmission ratios is included between a minimum  $\tau_{min}$  and a maximum gear ratio  $\tau_{max}$  for which the condition in equation (9) is verified:

$$\tau_{min}, \tau_{max} = \eta \sqrt{J_M} \frac{\sqrt{\alpha - \frac{\beta}{\eta} + \frac{4\dot{\omega}_{L,rms} T_{L,rms}^*}{\eta}} \pm \sqrt{\alpha - \frac{\beta}{\eta}}}{2T_{L,rms}^*}$$
(27)

$$\tau_{min} \le \tau \le \tau_{max} \tag{28}$$

>From equation 27 it is evident that a solution exists only if  $\alpha \ge \frac{\beta}{\eta}$ .

# 4.2.3 The optimum transmission ratio

The constraint imposed by equation (25) becomes less onerous when a suitable transmission is selected, with a transmission ratio  $\tau$  that annuls the terms in brackets. This value of  $\tau$  is called *optimum transmission ratio*. Considering an ideal transmission ( $\eta = 1$ ,  $J_T = 0 \, kgm^2$ ) one gets:

$$\tau = \tau_{opt} = \sqrt{\frac{J_M \dot{\omega}_{L,rms}}{T_{L,rms}^*}} \tag{29}$$

that, for a purely inertial load ( $T_L = 0$ ), coincides with the value introduced in Pasch et al. (1984):

$$\tau' = \sqrt{\frac{J_M}{J_L}} \tag{30}$$

The choice of the optimum transmission ratio allows system acceleration to be maximized (supplying the same motor torque) or to minimize the torque supplied by the motor (at the same acceleration).

For real transmissions, eq.(29) takes the general form:

$$\tau = \tau_{opt,\eta} = \sqrt{\frac{J_M \dot{\omega}_{L,rms}}{T_{L,rms}^*} \eta} = \tau_{opt} \sqrt{\eta}$$
(31)

showing the dependence of the optimum transmission ratios on the mechanical efficiency  $\eta$ . Eq. (31) shows how the optimization of the performance of the motor-reducer unit through the concept of inertia matching is considerably affected by the mechanical efficiency. In the following (par. 6.3) this effect will be graphically shown.

## 4.3 Limit on the motor maximum torque

As shown in Fig.3, each motor can supply a maximum torque  $T_{M,max}(\omega_M)$  that depends on the speed  $\omega_M$ . However this relationship cannot be easily described by a simple equation. As a result, it is difficult to express condition (10) as a range of suitable transmission ratios.

Moreover the maximum torque that can be exerted depends on the maximum current supplied by the drive system. For this reason, these conditions will be checked only once the motor and the transmission have been chosen. It has to be:

$$T_{M,max}(\omega_M) \ge \max \left| \frac{\tau T_L}{\eta} + \left( \frac{J_M + J_T}{\tau} + \frac{J_L \tau}{\eta} \right) \dot{\omega}_L \right| \quad \forall \omega.$$
 (32)

This test can be easily performed by superimposing the motor torque  $T_M(\omega_M)$  on the motor torque/speed curve.

#### 4.4 Checks

Once the transmission has been chosen, it is important to check the operating conditions imposed by the machine task satisfy the limits imposed by the manufacturers. Main limits concern:

- the maximum achievable speed;
- the maximum torque applicable on the outcoming shaft;
- the nominal torque applicable on the outcoming shaft;
- the maximum permissible acceleration torque during cyclic operation (over 1000/h) using the load factor.

There is no a standard procedure for checking the transmission. Each manufacturer, according to his experience and to the type of transmission produced, generally proposes an empirical procedure to check the right functioning of his products.

These verifications can be carried out by collecting information from catalogs.

### 5. Ideal transmission

If both the inertia of the transmission and the power losses are negligible, the gearbox can be considered as ideal ( $J_T = 0 \text{ kgm}^2$ ,  $\eta = 1$ ). In this cases the problem is easier and the equations describing the dynamical behavior of the machine and the corresponding operating conditions can be simplified.

The limit on the maximum achievable speed remains the same (6), since it arises from kinematic relationships, while limits on the root mean square torque (7) and maximum torque (8) are simplified. Inequality (22) can be written as:

$$\frac{T_{M,N}^2}{J_M} \ge \tau^2 \frac{T_{L,rms}^{*2}}{J_M} + J_M \frac{\dot{\omega}_{L,rms}^2}{\tau^2} + 2(T_L^* \dot{\omega}_L)_{mean}.$$
 (33)

whose solutions are between

$$\tau_{min}, \tau_{max} = \frac{\sqrt{J_M}}{2T_{Lrms}^*} \left[ \sqrt{\alpha - \beta + 4\dot{\omega}_{L,rms}} T_{L,rms}^* \pm \sqrt{\alpha - \beta} \right]. \tag{34}$$

Accordingly, the condition on the maximum torque can be expressed as:

$$T_{M,max}(\omega_M) \ge \max \left| \tau T_L + \left( \frac{J_M}{\tau} + J_L \tau \right) \dot{\omega}_L \right| \quad \forall \omega.$$
 (35)

# 5.1 Selection of gearbox and motor

The main steps to select the gear-motor are:

- **STEP 1:** Creation of a database containing all the commercially available motors and reducers useful for the application. For each motor the accelerating factor  $(\alpha_i)$  must be calculated. Once the database has been completed it can be re-used and updated each time a new motor-reducer unit selection is needed.
- **STEP 2:** Calculation of the load factor  $\beta$ , on the basis of the features of the load  $(T_I^*)$ .
- **STEP 3:** Preliminary choice of useful motors: all the available motors can be shown on a graph where the accelerating factors of available motors are compared with the load factor. All the motors for which  $\alpha < \beta$  can be immediately rejected because they cannot supply sufficient torque, while the others are admitted to the next selection phase. Figure 7 is related to the industrial example discussed in par.5.2 and displays with circles the acceleration factors  $\alpha_i$  of the analyzed motors, while the horizontal line represents the load factor  $\beta$ .
- **STEP 4:** Identification of the ranges of useful transmission ratios for each motor preliminarily selected in step 3. For these motors a new graph can be produced displaying for each motor the value of the transmission ratios  $\tau_{max}$ ,  $\tau_{min}$ ,  $\tau_{opt}$  and  $\tau_{M,lim}$ . The graph is generally drawn using a logarithmic scale for the y-axis, so  $\tau_{opt}$  is always the midpoint of the adoptable transmission ratios range. In fact:

$$\tau_{opt}^2 = \tau_{min}\tau_{max} \quad \Leftrightarrow \quad \log \tau_{opt} = \frac{\log \tau_{min} + \log \tau_{max}}{2} \tag{36}$$

A motor is acceptable if there is at least a transmission ratio  $\tau$  for which equations (18, 28) are verified. These motors are highlighted by a vertical line on the graph. Figure 8 is related to the same industrial example and shows the useful transmission ratios for each motor preliminarily selected.

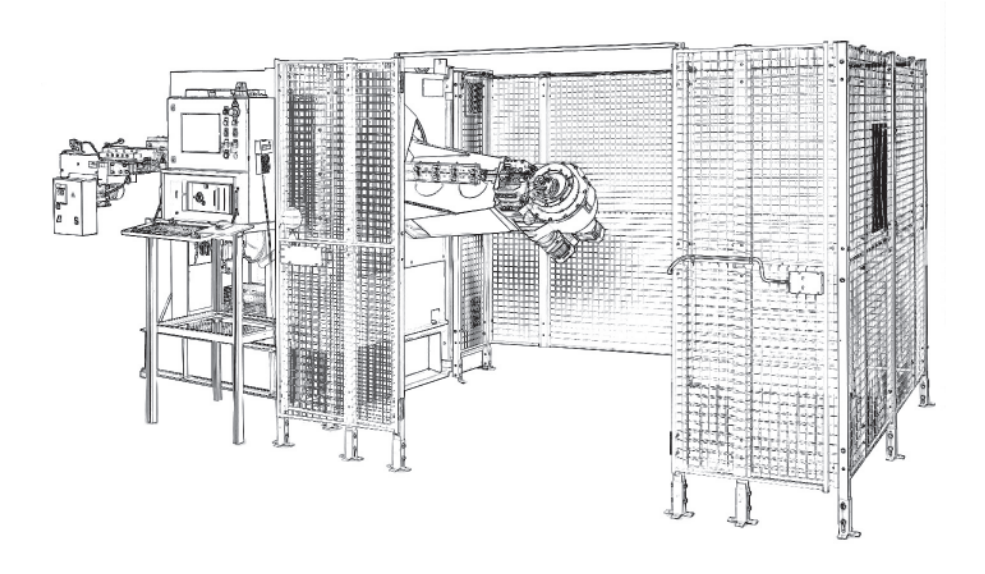


Fig. 5. CNC wire bending machine

**STEP 5:** Identification of the useful commercial speed reducers: the speed reducers available are represented by horizontal lines. If one of them intersects the vertical line of a motor, this indicates that the motor can supply the required torque if that specific speed reducer is selected. Table 2 sums up the acceptable combinations of motors and speed reducers for the case shown in figure 8. These motors and reducers are admitted to the final selection phase.

**STEP 6:** Optimization of the selected alternatives: the selection can be completed using different criteria such as economy, overall dimensions, space availability or any other depending on the specific needs.

STEP 7: Checks (see Sec.4.4).

# 5.2 Example

Fig. 5 shows a CNC wire bending machine. The system automatically performs the task of bending in the plane, or three-dimensionally, a wire (or tape) giving it the desired geometry. The machine operation is simple: semi-finished material is stored in a hank and is gradually unrolled by the unwinding unit. The straightened wire is guided along a conduit to the machine's bending unit, which consists of a rotating arm on which one or more bending heads are mounted. Each head is positioned in space by a rotation of the arm around the axis along which the wire is guided in order to shape it in all directions 6.

The production capacity of the machine is related to the functionality of the heads, while bending productivity depends strongly on arm speed, which allows the heads to reach the position required for bending. The design of the system actuating the rotating arm (selection of motor and speed reducer) is therefore one of the keys to obtaining high performance.

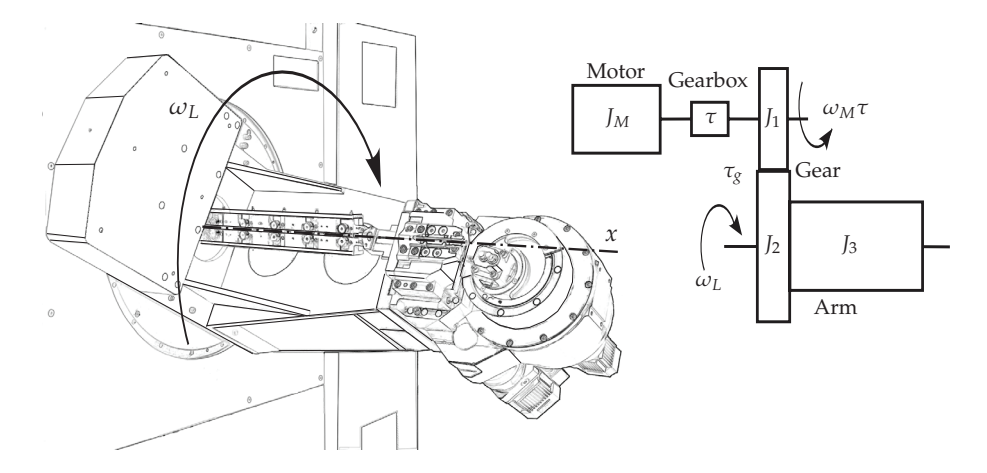


Fig. 6. The moving arm and mechanical system layout

Consider now only the bending unit: the motor, with its moment of inertia  $J_M$ , is connected through a planetary reducer with transmission ratio  $\tau$  to a pair of gear wheels that transmits the rotation to the arm.

The pair of gear wheels has a ratio  $\tau_2 = 1/5$  which is dictated by the overall dimension of the gearbox and cannot be modified. Putting  $J_1 = 0.0076$  [kgm²],  $J_2 = 1.9700$  [kgm²] and  $J_3 = 26.5$  [kgm²] respectively as the moment of inertia referred to the axes of rotation of the two wheels and of the arm, the comprehensive moment of inertia referred to the output shaft of the planetary gear is:

$$J_L = J_1 + (J_2 + J_3)\tau_2^2 = 1.1464 \text{ [kgm}^2]$$

Since the load is purely inertial<sup>3</sup>, the load factor can easily be calculated as:

$$\beta = 4J_L \dot{\omega}_{L,rms}^2 \tag{37}$$

where  $\dot{\omega}_{L,rms}$  is a function of the law of motion used. The choice of the law of motion depends on the kind of operation requested and, in the most extreme case, it consists of a rotation of  $h=180^\circ$  in  $t_a=0.6$  [s]. After this, a stop of  $t_s=0.2$  [s] before the next rotation is normally scheduled.

The value of  $\dot{\omega}_{L,rms}$  can be expressed through the mean square acceleration coefficient ( $c_{a,rms}$ ) using the equation:

$$\dot{\omega}_{L,rms} = c_{a,rms} \frac{h}{t_a^2} \frac{1}{\tau_2} \sqrt{\frac{t_a}{t_a + t_s}}$$

As is known (Van de Straete et al., 1999), the minimum mean square acceleration law of motion is the cubic equation whose coefficient is  $c_{rms} = 2\sqrt{3}$ . Moreover, this law of motion has the advantage of higher accelerations, and therefore high inertial torques, corresponding to low velocities. Substituting numerical values in eq.(37) one gets:  $\beta = 7.8573 \cdot 10^4$  [W/s].

<sup>&</sup>lt;sup>3</sup> In the selecting phase frictions are not considered.

Considering the same law of motion, maximum acceleration and maximum speed can easily be obtained by:

$$\dot{\omega}_{L,max} = c_a \frac{h}{t_a^2} \frac{1}{\tau_2} \simeq 261.8 \,[\text{rad/s}^2]; \ \omega_{L,max} = c_v \frac{h}{t_a} \frac{1}{\tau_2} \simeq 39.3 \,[\text{rad/s}]$$
 (38)

where  $c_a = 6$  and  $c_v = 1.5$ .

Knowing the load factor  $\beta$  and after selecting the motors and transmissions available from catalogs, the graph shown in Fig.7 can be plotted. Available motors for this application are synchronous sinusoidal brushless motors<sup>4</sup>. Manufacturer's catalogs give information on motor inertia, maximum and nominal torque. A first selection of suitable motors can be performed. Motors whose accelerating factor  $\alpha_i$  is lower than the load factor  $\beta$  can be discarded.

For all the accepted motors a new graph can be produced. It displays, for each motor, the corresponding minimum and maximum transmission ratios and the optimum and the minimum kinematic transmission ratios.

They can be obtained using the simplified expression for the purely inertial load case:

$$\tau_{min}, \tau_{max} = \frac{\sqrt{J_M}}{2T_{L\,rms}^*} \left[ \sqrt{\alpha} \pm \sqrt{\alpha - \beta} \right]. \tag{39}$$

and eq.(29),(17). Commercial transmissions considered for the selection are planetary reducers<sup>5</sup>.

The graph in Fig.8 shows all the available couplings between the motors and transmissions considered. Three of the eleven motors (M1, M2 e M7) are immediately discarded, since their accelerating factors  $\alpha$  are too small compared with the load factor  $\beta$ . Motors M3, M4, M5, and M6 are eliminated because their maximum speed is too low. Suitable motors are M8, M9, M10 and M11. The selection can be completed evaluating the corresponding available commercial speed reducers whose ratio is within the acceptable range. Motor M8 is discarded since no transmission can be coupled to it. Suitable pairings are shown in Tab.2.

Motor	Speed reducer
M9	$\tau = 1/10,  \tau = 1/7$
M10	$\tau = 1/5, \tau = 1/4$
M11	$\tau = 1/5, \tau = 1/4, \tau = 1/3$

Table 2. Combination of suitable motors and speed reducers for the industrial example discussed in par.5.2

The final selection can be performed using the criterion of cost: the cheapest solution is motor M9 and a reducer with a transmission ratio  $\tau = 1/10$ . The main features of the selected motor<sup>6</sup> and transmission<sup>7</sup> are shown in table 3.

<sup>&</sup>lt;sup>4</sup> Produced by "Mavilor", http://www.mavilor.es/.

<sup>&</sup>lt;sup>5</sup> produced by "Wittenstein", http://www.wittenstein.it/.

<sup>&</sup>lt;sup>6</sup> Model Mavilor BLS 144.

<sup>&</sup>lt;sup>7</sup> Model Alpha SP+140.

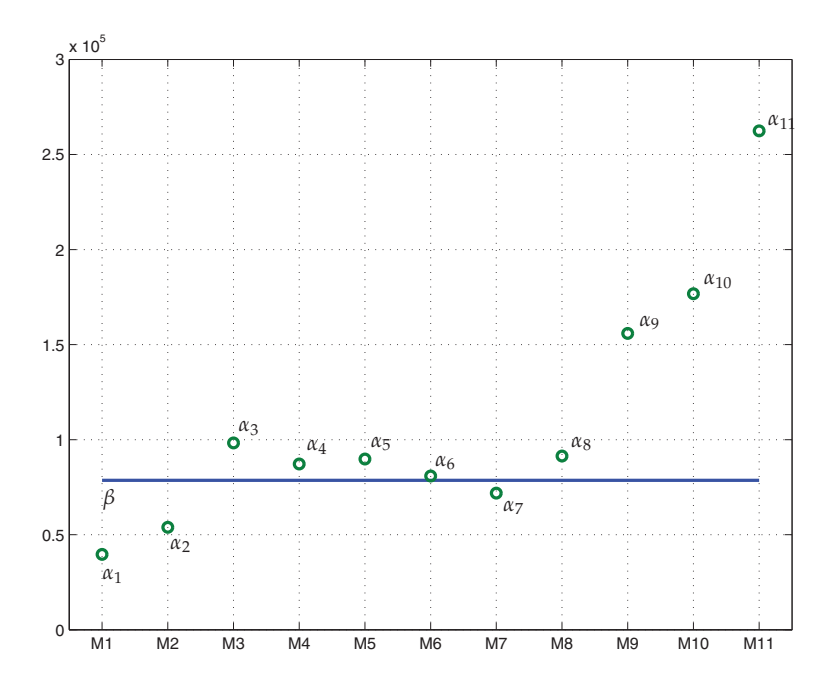


Fig. 7. A first selection of suitable motors

Motor M9		
moment of inertia	$J_M = 0.0046  [\text{kgm}^2]$	
nominal torque	$T_{M,N} = 26.7 [Nm]$	
maximum Torque	$T_{M,max}^{TH} = 132 [Nm]$	
maximum achievable speed		
Speed reducer $\tau = 1/10$		
moment of inertia	$J_T = 5.8 \cdot 10^{-4}  [\text{kgm}^2]$	
nominal torque	$T_{T,N} = 220  [\text{Nm}]$	
maximum Torque	$T_{T,max} = 480 [Nm]$	
maximum endurable speed	$\omega_{T,max} = 4000 [\text{rpm}]$	
nominal speed	$\omega_{T,N} = 2600  [\text{rpm}]$	
mechanical efficiency	$\eta = 0.97$	

Table 3. Main features of selected motor and transmission

Figure 9 shows the required motor torque as a function of speed during the working cycle. It has been calculated considering the inertia of both the motor and the gearbox and the mechanical efficiency of the transmission. Since the mechanical efficiency of the speed reducer in backward power flow mode is not available, it is assumed to be equal to that in direct power flow. To verify the condition on the maximum torque reported in eq.(32), the curve has to be contained within the dynamic working field. Note how the maximum torque achieved by the motor is limited by the drive associated with it. From Fig.9 it is possible to check that the condition on the maximum torque is verified.

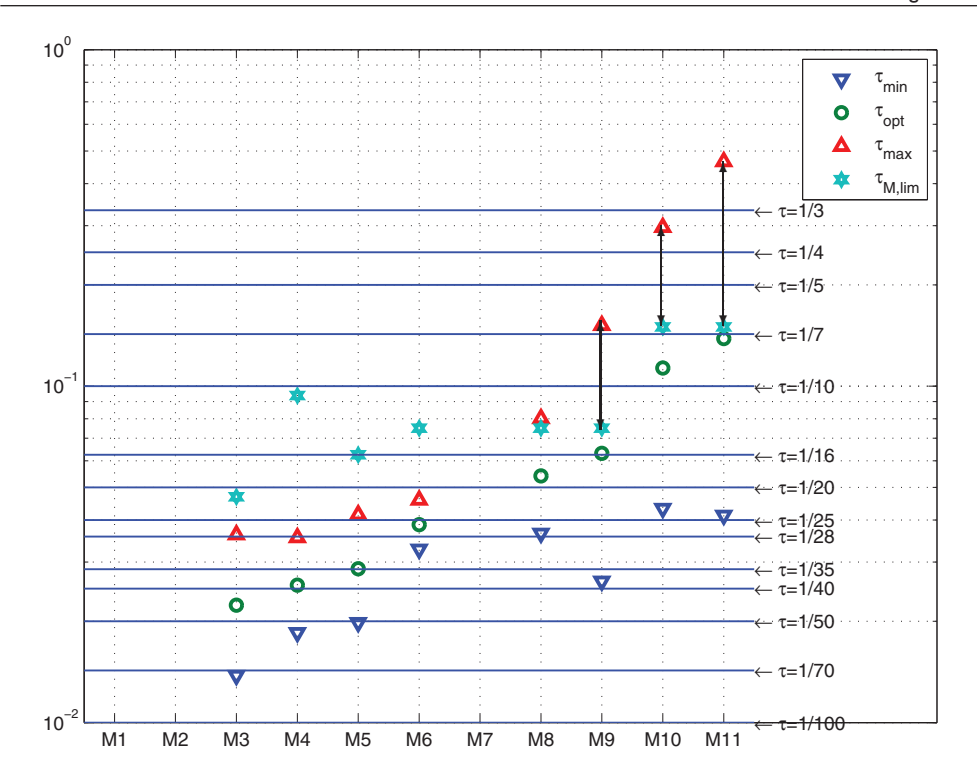


Fig. 8. Overview of available motor-reducer couplings

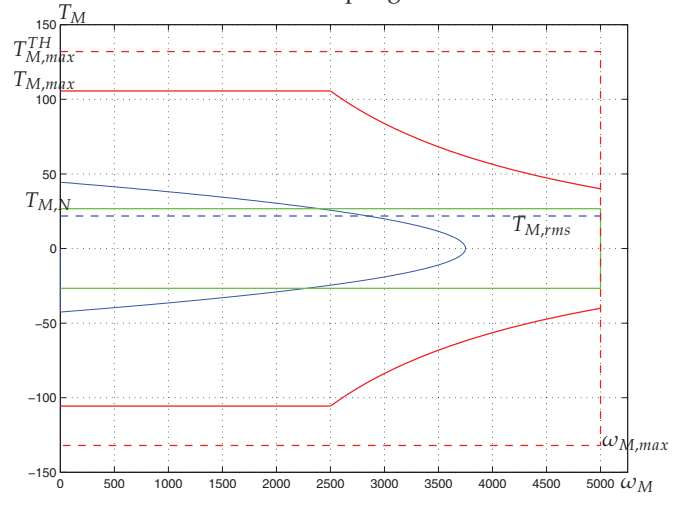


Fig. 9. Checkouts on maximum and nominal torque.

The motor root mean square torque can now be updated, considering the inertia of the transmission and its mechanical efficiency.

Finally, checks should be carried out on the reducers following the manufacturer's guidelines. In this case they mainly consist of verifying that both the maximum and the nominal torque applied to the transmission incoming shaft are lower than the corresponding limits shown in the catalog ( $T_{T,max}$ ,  $T_{T,N}$ ).

$$T_{max} \simeq 300[Nm] < T_{T,max} = 480[Nm]$$
  
 $T_{D} \simeq 150[Nm] < T_{T,N} = 220[Nm]$ 

In addition, the maximum and the mean angular speed of the incoming shaft have to be lower than the corresponding limits on velocity ( $\omega_{T,max}$ ,  $\omega_{T,N}$ ).

$$n_{max,rid} \simeq 3750[rpm] < \omega_{T,max} = 4000[rpm]$$
  
 $n_{mean,rid} \simeq 1873[rpm] < \omega_{T,N} = 2600[rpm]$ 

The selected motor-transmission pairing satisfies all the checks and provides margins for both the motor ( $\approx 20\%$  on the nominal torque) and the reducer.

### 6. Real transmission

For machines working with direct power flow, a decrease of the performance of the transmission that corresponds to an increase in the power dissipation may result in a motor overhead which makes it non longer adequate.

## 6.1 The mechanical efficiency limit

A motor which is able to perform the task planned in ideal conditions ( $\eta=1$ ), when coupled with a transmission characterized by poor efficiency, could be discarded. Referring to equation (27), once  $\beta$  is known, a minimum transmission mechanical efficiency exists, for each motor, below which  $\tau_{min}$  and  $\tau_{max}$  are undefined. The limit value is called the transmission *mechanical efficiency limit* and it is defined as the ratio between the load factor and the accelerating factor:

$$\eta \ge \eta_{lim} = \frac{\beta}{\alpha} \tag{40}$$

This parameter gives to the designer a fundamental indication: if the task required by the machine is known (and thus the load factor can be calculated), for each motor there is a minimum value of the transmission mechanical efficiency below which the system can not work. This limit is not present in the case of backward power flow functioning.

# 6.2 Restriction of the range of useful transmission ratios

For each selectable motor it is possible to graphically represent the trend of both the minimum and maximum transmission ratios. Combining equations (27) and (40), the two functions  $\tau_{min}$  and  $\tau_{max}$  are respectively defined as:

$$\tau_{min}, \tau_{max} = \begin{cases} \eta \sqrt{J_M} \frac{\sqrt{\alpha - \frac{\beta}{\eta} + \frac{4\dot{\omega}_{L,rms} T_{L,rms}^*}{\eta}} \pm \sqrt{\alpha - \frac{\beta}{\eta}}}{2T_{L,rms}^*} & \text{if } \eta \ge \eta_{lim} \\ \text{undefined} & \text{if } \eta < \eta_{lim} \end{cases}$$

$$(41)$$

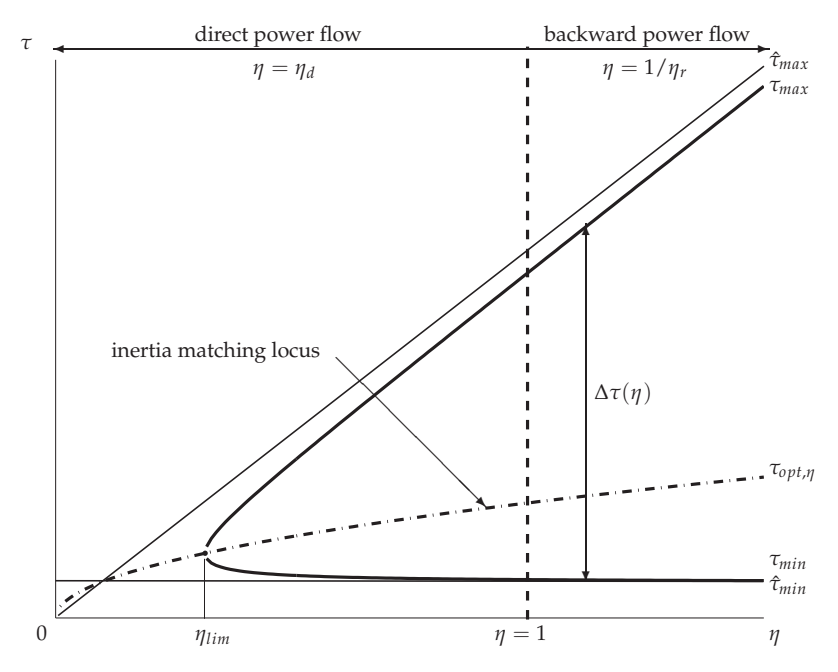


Fig. 10. Trends of  $\tau_{min}$  and  $\tau_{max}$  as functions of mechanical efficiency (using the notation introduced in eq. (16)), for a certain motor.

For each motor it is possible to plot  $\tau_{min}$  and  $\tau_{max}$  as functions of the mechanical efficiency, highlighting a region in the plane  $\eta\tau$  satisfying the condition on the root mean square torque (Fig.10). Depending on the machine functioning mode (direct or backward power flow) the left side or the right side of the graph should be taken into account. On the same graph the trends of the optimum transmission ratio  $\tau_{opt,\eta}$  and the breadth  $\Delta\tau$  of the range of useful transmission ratios is shown. Note that the range grows monotonically with the difference between the accelerating and load factors. In particular, the range breadth is:

$$\Delta \tau(\eta) = \frac{\sqrt{J_{\rm M}}}{T_{L,rms}^*} \eta \sqrt{\alpha - \frac{\beta}{\eta}}$$
(42)

and decreases appreciably with the transmission mechanical efficiency. However, while the limit on the maximum transmission ratio  $\tau_{max}$  varies considerably, the minimum transmission ratio  $\tau_{min}$  remains almost constant. This behavior is clearly visible in the  $\eta\tau$  graph which plots the asymptotes of the two functions (Fig. 10) described respectively by:

$$\hat{\tau}_{max} = \frac{T_{M,N}}{T_{L,rms}^*} \eta \qquad \qquad \hat{\tau}_{min} = \frac{J_M}{T_{M,N}} \dot{\omega}_{L,rms}$$
 (43)

It is interesting to observe that, while  $\hat{\tau}_{max}$  depends on the reducer,  $\hat{\tau}_{min}$  depends only on the chosen motor and on the law of motion defined by the task. This is because the transmission ratio  $\tau$  is so small that the effect of the load is negligible compared to the inertia of the motor.

The power supplied, therefore, is used just to accelerate the motor itself. Note that, for values of  $\eta > 1$ , that is backward power flow functioning, the range of suitable transmission ratios is wider than in the case of direct power flow functioning, which is the most restrictive working mode. For this reason, in all cases where the direction of power flow is not mainly either direct or backward, the first functioning mode can be considered as a precautionary hypothesis on the root mean square torque and the left side of the  $\eta \tau$  graph ( $\eta < 1$ ) can be used.

## 6.3 The extra-power rate factor

Inequality (25) can be written as:

$$\alpha \ge \frac{\beta}{\eta} + \gamma(\tau, \eta, J_M) \tag{44}$$

where:

$$\gamma(\tau, \eta, J_M) = \left[ \frac{T_{L,rms}^*}{\eta} \left( \frac{\tau}{\sqrt{J_M}} \right) - \dot{\omega}_{L,rms} \left( \frac{\sqrt{J_M}}{\tau} \right) \right]^2 \tag{45}$$

The term  $\gamma$  is called the *extra-power rate factor* and represents the additional power rate that the system requires if the transmission ratio is different from the optimum ( $\tau \neq \tau_{opt}$ ).

Figure 11 shows the trends of the terms of the  $\gamma$  function when the transmission efficiency changes. Note that, when the transmission ratio is equal to the optimum ( $\tau = \tau_{opt}$ ), the curve  $\gamma$  reaches a minimum. For this value the convexity of the function is small and, even for large variations of the transmission ratio, the extra-power rate factor appears to be contained in eq.(44).

With the mechanical efficiency decreasing, two effects take place: first the optimum transmission ratio decreases, moving on the left of the graph, secondly the convexity of the curve  $\gamma$  is more pronounced and the system is more sensitive to changes in  $\tau$  with respect to the optimum. For transmissions characterized by poor mechanical efficiency, in the case of the direct power flow mode, the choice of a gear ratio different from the optimum significantly affects the choice of the motor.

# 6.4 Effect of the transmission inertia

The inclusion of the transmission inevitably changes the moment of inertia of the system. With  $J_T$  as the moment of inertia of the speed reducer, referred to its outgoing shaft, the resistive torque is generally given by eq.(15). Entering this new value in eq.(24), the load factor can be updated. This change makes the system different from that previously studied with the direct consequence that the limit on the mean square torque can no longer be satisfied.

In particular, for the  $i^{th}$  transmission, characterized by a moment of inertia  $J_{T,i}$ , the limits on the transmission ratio to satisfy the root mean square torque condition can be expressed as  $\tau_{min,i}$  and  $\tau_{max,i}$ . Let's consider, as example, a machine task characterized by a constant resistant load ( $T_L = \cos t$ ). Figure 12 shows how the range of suitable transmission ratios is reduced when the inertia of the transmission increases. The same reduction can be observed in the  $\eta \tau$  graph (Fig. 13) for a purely inertial load. Note that, even for the moment of inertia, there is a limit value beyond which, for a given motor, there is no suitable transmission ratio.

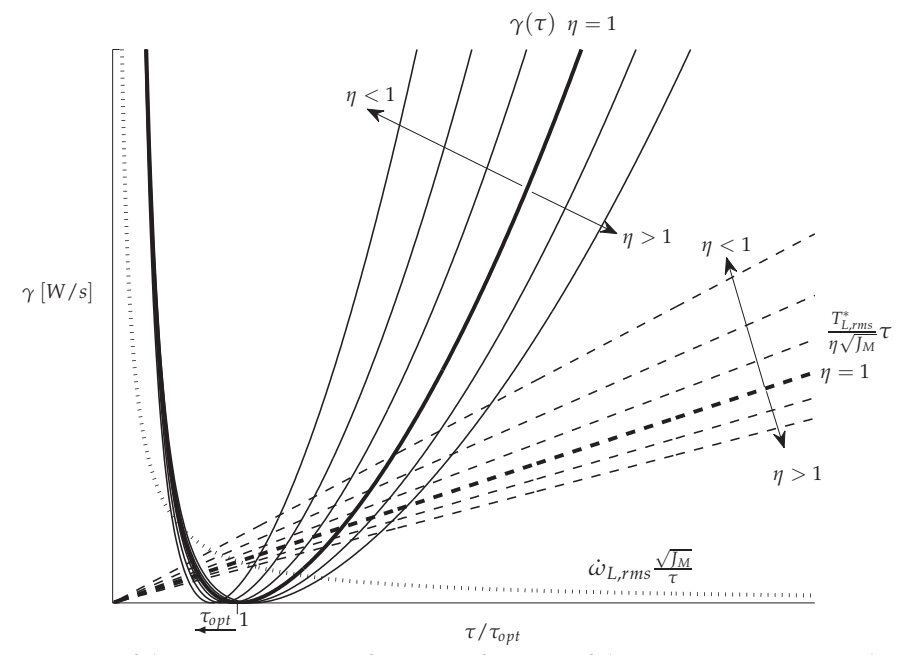


Fig. 11. Variation of the extra-power rate factor as a function of the transmission ratio and mechanical efficiency.

# 7. Guidelines for the motor-reducer selection

The theoretical steps presented can be summarized by a series of graphs for evaluating the effect of the transmission on the choice of the motor that make the selection process easy to use.

Firstly, to ensure the condition on the root mean square torque it should be verified that the accelerating factor  $\alpha$  of each available motor is greater than the limit  $\beta/\eta$ . However, since the transmission has not yet been selected and thus its efficiency and inertia are still unknown, it is possible to perform only a first selection of acceptable motors, eliminating those for which  $\alpha < \beta$ .

For each selectable motor a  $\eta\tau$  graph can be plotted (Fig. 14), with the limits on the transmission ratio defined by equations (18), (28). Since these functions depend on the transmission moment of inertia, such limits are plotted for each available transmission.

Available transmissions can be inserted in the  $\eta\tau$  graph (there is an example in Fig. 14) using their coordinates ( $\eta_{di}$ ,  $\tau_i$ ) and ( $\eta_{ri}$ ,  $\tau_i$ ) which can easily be found in manufacturers' catalogs. Each speed reducer appears twice: to the left of the dashed line for direct power flow, to the right for backward power flow.

Remember that for tasks characterized by mainly backward power flow, only the transmissions on the right half plane should be considered ( $\eta > 1$ ). For all other cases only the transmissions on the left half plane ( $\eta < 1$ ) should be taken into account.

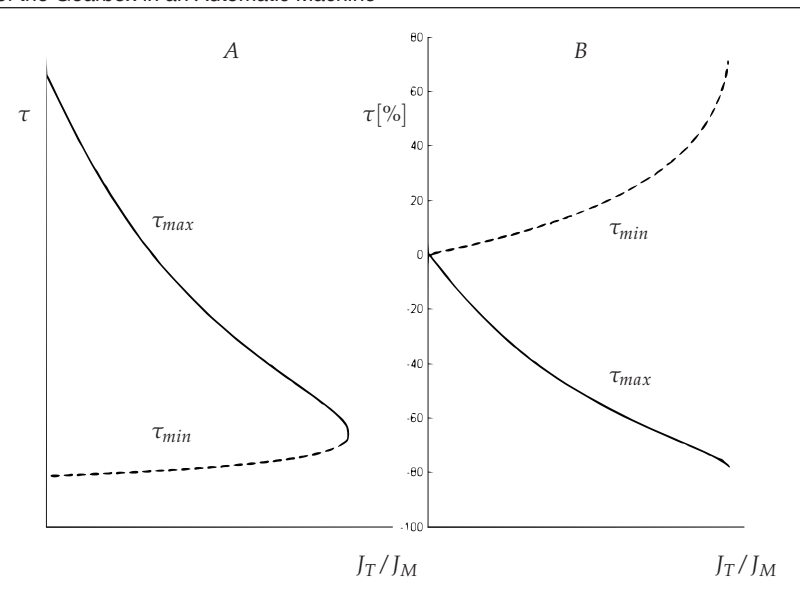


Fig. 12. A - reduction of range of useful transmission ratio as function of  $J_T/J_M$  (for  $T_L = \cos t$ ); B - percentage change of maximum and minimum transmission ratios as function of  $J_T/J_M$  (for  $T_L = \cos t$ ).

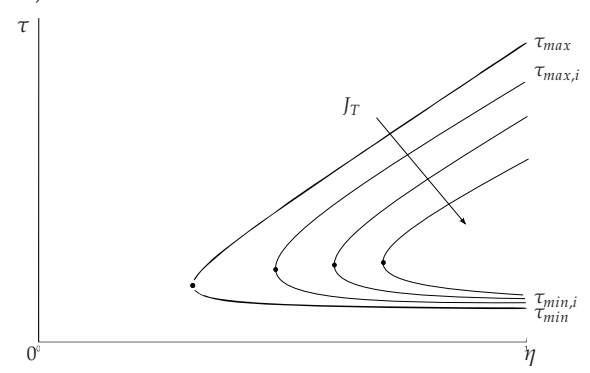


Fig. 13. Effect of the transmission moment of inertia on the  $\eta \tau$  graph (for  $T_L = \cos t$ ).

The  $i^{th}$  speed reducer is acceptable if it lies inside the area limited by the limit transmission ratio  $(\tau_{kin})$  and the corresponding maximum and minimum ratios  $(\tau_{max,i}, \tau_{min,i})$ . These reducers are highlighted on the graph with the symbol  $\odot$ , unacceptable ones with  $\otimes$ 

Table 4 resumes all the alternatives both for the direct and backward power flow modes.

Note that, for the direct power flow mode, transmissions which would be acceptable with normal selection procedures, are now discarded (e.g. transmission  $T_2$  because of insufficient efficiency, reducer  $T_4$  because of its excessively high moment of inertia).

Moreover it is evident that, for the motor considered, there are no acceptable transmissions with a ratio equal to the optimum. More generally it could happen that a motor, while meeting

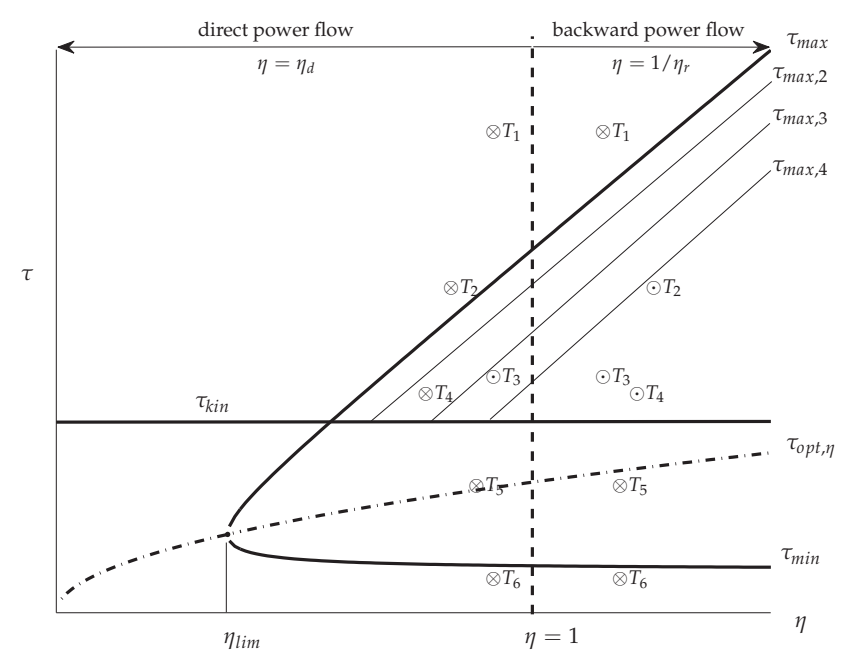


Fig. 14. Graph  $\eta\tau$  for the selection of the speed reducer for a specific motor: ( $\odot$  acceptable transmission,  $\otimes$  unacceptable transmission)

Transmission	Direct P.F.	Cause	Backward P.F.	Cause
$T_1$	unaccept.	$\tau_1 > \tau_{max}$	unaccept.	$\tau_1 > \tau_{max}$
$T_2$	unaccept.	$\tau_2 > \tau_{max}$	accept.	_
$T_3$	accept.		accept.	
$T_4$	unaccept.	$ au_4 >  au_{max,4}$	accept.	
$T_5$	unaccept.	$ au_5 <  au_{kin}$	unaccept.	$ au_5 <  au_{kin}$
$T_6$	unaccept.	$\tau_6 < \tau_{kin} \wedge \tau_6 < \tau_{min}$	unaccept.	$\tau_6 < \tau_{kin} \wedge \tau_6 < \tau_{min}$

Table 4. Overview of acceptable and unacceptable transmissions for the example in Fig. 14

all the constraints mentioned, may have a range of acceptable gear ratios within which there is no reducer commercially available. For this reason it cannot be chosen.

The choice of the motor-reducer unit is made easy by comparing the  $\eta\tau$  graphs for each selectable motor.

The resulting graphs give an overview of all the possible pairings of motors and transmissions that satisfy the original conditions. They allow the best solution to be selected from the available alternatives, in terms of cost, weight and dimensions, or other criteria considered important according to the application.

Once the motor and the transmission have been selected and all their mechanical properties are known, the final checks can be performed.

### 8. Conclusions

The correct choice of the motor-reducer unit is a key factor in automation applications. Such a selection has to be made taking into account the mechanical constraints of the components, in particular the operating ranges of the drive system and the mechanical features of the transmission. The paper investigates the effects of these constraints on the correct choice of the motor-reducer unit at the theoretical level and illustrated a method for its selection that allows the best available combination to be chosen using a practical approach to the problem.

It identifies the influence of the transmission's mechanical efficiency and inertia on the coupling between motor and reducer itself, showing how they affect the optimum solution. The procedure, based on the production of a chart containing all the information needed for the correct sizing of the system, sums up all the possible solutions and allows them to be quickly compared to find the best one.

### 9. Nomenclature

Symbol	Description
$T_M$	motor torque
$J_{M}$	motor moment of inertia
$T_{M,N}$	motor nominal torque
$T_{M,max}$	motor maximum torque
$\omega_M$ , $\dot{\omega}_M$	motor angular speed and acceleration
$T_L$	load torque
$J_L$	load moment of inertia
$T_L^*$	generalized load torque
$T_{L,rms}^*$	generalized load root mean square torque
$T_L^*$ $T_{L,rms}^*$ $T_{L,max}$	load maximum torque
$\omega_L, \dot{\omega}_L$	load angular speed and acceleration
$\dot{\omega}_{L,rms}$	load root mean square acceleration
$t_a$	cycle time
$\tau = \omega_L/\omega_M$	transmission ratio
$ au_{opt}$	optimal transmission ratio
η	transmission mechanical efficiency
$\eta_d$	transmission mechanical efficiency (direct power flow)
$\eta_r$	transmission mechanical efficiency (backward power flow)
$J_T$	transmission moment of inertia
α	accelerating factor
β	load factor
$\gamma$	extra-power rate factor
$\tau_{min}$ , $\tau_{max}$	minimum and maximum acceptable transmission ratio
$ au_{kin}$	minimum kinematic transmission ratio
$\omega_{M,max}$	maximum speed achievable by the motor
$\omega_{L,max}$	maximum speed achieved by the load
$W_M$	motor side power
$W_L$	load side power

### 10. References

- Pasch, K.A., Seering, W.P., "On the Drive Systems for High-Performance Machines", Transactions of ASME, 106, 102-108 (1984).
- Cusimano, G., "A Procedure for a Suitable Selection of Laws of Motion and Electric Drive Systems Under Inertial Loads", *Mechanism and Machine Theory* 38, 519-533 (2003)
- Chen, D.Z., Tsai, L.W., "The Generalized Principle of Inertia Match for Geared Robotic Mechanism", Proc. IEEE International Conference on Robotics and Automation, 1282-1286 (1991)
- Van de Straete, H.J, Degezelle, P., De Shutter, J., Belmans, R., "Servo Motor Selection Criterion for Mechatronic Application", *IEEE/ASME Transaction on Mechatronics* 3, 43-50 (1998).
- Van de Straete, H.J, De Shutter, J., Belmans, R., "An Efficient Procedure for Checking Performance Limits in Servo Drive Selection and Optimization", *IEEE/ASME Transaction on Mechatronics* 4, 378-386 (1999)
- Van de Straete, H.J, De Shutter, J., Leuven, K.U., "Optimal Variable Transmission Ratio and Trajectory for an Inertial Load With Respect to Servo Motor Size", *Transaction of the ASME* 121, 544-551 (1999)
- Giberti, H, Cinquemani, S., Legnani, G., "A Practical Approach for the Selection of the Motor-Reducer Unit in Electric Drive Systems" *Mechanics Based Design of Structures and Machines*, Vol. 39, Issue 3, 303-319 (2011)
- Giberti, H, Cinquemani, S., Legnani, G., "Effects of transmission mechanical characteristics on the choice of a motor-reducer", *Mechatronics* Vol. 20, Issue 5, 604-610 (2010)
- Giberti, H, Cinquemani, "On Brushless Motors Continuous Duty Power Rate", ASME 2010 10th Biennial Conference on Engineering Systems Design and Analysis, ESDA 2010, Istanbul, Turkey, 12-14 July (2010).
- Legnani, G., Tiboni, M., Adamini, R., "Meccanica degli Azionamenti", Ed. Esculapio, Italy, (2002)
- Roos, F., Johansson, H., Wikander, J., "Optimal Selection of Motor and Gearhead in Mechatronic Application", *Mechatronics* 16, 63-72 (2006)
- Magnani P.L., Ruggieri G. Meccanismi per Macchine Automatiche, UTET, Italy (1986) Melchiorri C., Traiettorie per azionamenti elettrici, Esculapio, Italy (2000)